Title

THE EFFECT OF CONDENSATION IN THE BOUNDARY LAYER ON MASS TRANSFER FROM A ROTATING DISK

Author

Omberg, Ronald P.

Publication Date

1969-10-01

UCRL-18577

c. 2

THE EFFECT OF CONDENSATION IN THE BOUNDARY LAYER ON MASS TRANSFER FROM A ROTATING DISK

Ronald P. Omberg
(Ph. D. Thesis)

October 1969

AEC Contract No. W-7405-eng-48

LAWRENCE RADIATION LABORATORY
UNIVERSITY of CALIFORNIA BERKELEY

UCRL-18577 c. 2

DISCLAIMER

TABLE OF CONTENTS

APPENDICES

THE EFFECT OF CONDENSATION IN THE BOUNDARY LAYER ON MASS TRANSFER FROM A ROTATING DISK

Ronald P. Omberg

Inorganic Materials Research Division, Lawrence Radiation Laboratory,
Department of Nuclear Engineering, College of Engineering
University of California, Berkeley, California

ABSTRACT

The vaporization rate of a hot solid into a cold gas may be increased above the diffusion-limited value if condensation occurs in the boundary layer. This phenomenon was analyzed by combining the microscopic balance equations of nucleation kinetics with the boundary layer conservation equations. The equations were derived for rotating disk hydrodynamics and calculations made for the vaporization of iron into cold argon. The vaporization rate of the rotating disk was computed, and the structure of the nucleation zone in the boundary layer surrounding the disk was examined.

The vaporization rate was measured experimentally for a hot rotating disk of chromium vaporizing into a cold helium environment. The data showed that condensation enhancement of the vaporization rate does in fact occur. The vaporization rate proceeded, within the error bounds of the measurement, from the condensation-free value to the bulk equilibrium condensation value as the temperature was increased.

The measured rates were compared with the theoretical rates calculated with the above model. The theoretical rates were always considerably lower than the measured rates. It is felt that better agreement between experiment and theory could be obtained with a nucleation kinetic model which gives a larger nucleation rate for a given supersaturation.

ACKNOWLEDGEMENTS

A thesis is not entirely an individual effort. The advice and counsel of others is an essential ingredient of good research. In particular, I would like to express my appreciation to the following people:

Professor Donald R. Olander who was always available for consultation and whose very excellent advice and guidance contributed heavily to this work.

Dr. Wigbert Siekhaus whose expertise in spark-cutting and polishing metal surfaces greatly facilitated the fabrication of the chromium disks.

Dr. Paul Concus for his interest, discussions and suggestions pertaining to the numerical solution of the droplet equations.

Professors Chang-Lin Tien and Lawrence M. Grossman for their comments while reading this dissertation and for serving on the thesis committee.

The Oak Ridge Institute of Nuclear Studies and the National Science Foundation whose financial support made this graduate study possible. This work was also supported in part by the United States Atomic Energy Commission.

And finally my wife, Lillian, for her remarkable typing and editorial talents while preparing the rough draft of this work and also for her patience and encouragement during the course of this graduate study.

NOMENCLATURE

A_g - Surface area of a drop of size g (cm^2)

A_{th} - Thermal accommodation coefficient

b - Parameter in the evaporation coefficient (dyne-cm)

c_g - Concentration of drops of size g ($drops/cm^3$)

c_p - Specific heat at constant pressure (cal/cm-°K)

c_w - Monomer mass fraction at the wall (ρ_v/ρ)

D - Binary diffusion coefficient (cm^2/sec)

D_g - Binary diffusion coefficient for a drop of size g (cm^2/sec)

f - Monomer concentration ($atoms/cm^3$)

F - Dimensionless radial gas velocity ($u/r\omega$)

g - Number of atoms per drop

G - Dimensionless angular gas velocity ($v/r\omega$)

H - Dimensionless axial gas velocity ($w/\sqrt{\nu_\infty \omega}$)

$\hat{H}$ - Dimensionless axial gas velocity ($\rho/\rho_\infty \dfrac{w}{\sqrt{\lambda \nu_\infty \omega}}$)

i - Set of all drops existing in the i^{th} group

J_g - Droplet current in g-space, i.e., the net rate at which drops of size g-1 grow to size g ($drops/cm^3$-sec)

j - Mass flux of monomer (gm/cm^2-sec)

k - Thermal conductivity (cal/cm-sec-°K), or Boltzman's constant ($1.38 \cdot 10^{-16}$ ergs/°K)

k_T - Thermal diffusion ratio

ℓ - Average value of the latent heat of vaporization per molecule (ergs/molecule)

m - Mass of a vaporized atom (gm)

M - Molecular weight

n - Molar concentration (moles/cm^3)

N - Atom density (atoms/cm^3)

p - Total pressure of the gas (dyne/cm^2)

p_v - Partial pressure of the monomer in the gas (dyne/cm^2)

$p_{v,eq}$ - Equilibrium vapor pressure of the monomer (dyne/cm^2)

P - Dimensionless total pressure ($p/\mu_\infty \omega$)

Pr - Prandtl number ($\mu\, c_p/k$)

r - Radial distance from the center of the disk (cm)

r_g - Radius of a drop of size g atoms (cm)

R - Dimensionless value of a thermal diffusion integral

S - Supersaturation ($p_v/p_{v,eq}$)

S_l - Volumetric source of monomer (atoms/cm^3-sec)

Sc - Schmidt number (ν/D)

Sc_g - Schmidt number for drops of size g (ν/D_g)

S_v - Volumetric source of monomer (gm/cm^3-sec)

S_g - Volumetric source of drop of size g (drops/cm^3-sec)

T - Temperature (°K)

u - Radial component of the gas velocity (cm/sec).

U - Dimensionless monomer concentration function ($\rho_w f/f_w \rho$)

v - Angular component of the gas velocity (cm/sec)

V_g - Dimensionless concentration of drops of size g($\rho_w c_g/f_w \rho$)

V_i - Average dimensionless concentration of drops in the i^{th} group

w - Axial component of the gas velocity (cm/sec)

x - Dimensionless axial distance

$$\left(x = \frac{1}{\sqrt{\lambda_f}} \sqrt{\frac{\omega}{\nu_\infty}} \int_0^z \frac{\rho}{\rho_\infty}\, dz \right)$$

X	-Mole fraction
z	-Axial distance from the disk (cm)

Subscripts

b	- Denotes a local property of the inert gas
eq	- Denotes a thermodynamic equilibrium value
f	- Property evaluated at the film temperature
g	- Property of a drop of size g atoms
v	- Property of the monomer
w	- Property at the wall, i.e., the disk surface
∞	- Property at infinity

Greek Letters

α_g -Vaporization coefficient for drop of size g (atoms/cm^2-sec)

α_g^+ -Dimensionless vaporization coefficient for drops of size g ($A_g \alpha_g / \omega$)

α_T -Thermal diffusion factor

β -Rate at which atoms of a gas cross a unit area per cm^2 per sec

β_g^+ -Dimensionless condensation coefficient for a drop of size g ($A_g \beta_g / \omega$)

γ -Surface tension (dyne/cm)

ϵ -Total emissivity

η -Dimensionless axial distance $\left(\sqrt{\frac{\omega}{\nu_\infty}}\, z\right)$

θ -Dimensionless temperature $\frac{T - T_\infty}{T_w - T_\infty}$

λ -Dimensionless density viscosity parameter $\frac{\rho\mu}{\rho_\infty \mu_\infty}$ or mean free path in the gas.

μ -Dynamic viscosity (gm/cm-sec)

ν -Kinematic viscosity (cm^2/sec)

ξ -Dimensionless axial distance $\left(\sqrt{\frac{\omega}{\nu_\infty}} \int_0^z \frac{\rho}{\rho_\infty}\, dz\right)$

ρ_v -Density of the monomer (gm/cm^3)

ρ -Density of the gas (gm/cm^3)

σ -Stephan-Boltzman constant ($1.35 \cdot 10^{-12}$ cal/sec-cm^2-$^\circ K^4$)

ω -Angular velocity (rad/sec)

PART I - THEORETICAL

A. Introduction

The vaporization rate of a hot surface into a cold gas environment may be substantially increased above the diffusion-limited value if the vaporizing species condenses in the thermal boundary layer. When condensation does occur, the diffusing molecules combine to form drops in accordance with the laws of nucleation kinetics. The creation of drops produces a sink in the ordinary convective-diffusion process which depresses the vapor pressure profile and causes an increase in the gradient at the wall. Hence, a larger vaporization rate is obtained.

A knowledge of the process of nucleation and condensation in the boundary has application in the area of nuclear engineering. For example if an isotopic power source in outer space were to re-enter a planet's atmosphere, it is desirable to have this source vaporize completely at the highest possible altitude. An exact calculation of the vaporization rate of the falling body is possible only if the effect of condensation in the boundary layer is known.

Turkdogan[1] has investigated this enhancement in the vaporization rate for molten iron spheres in helium. He used the concept of the "critical supersaturation" from classical infinite-medium nucleation kinetics to determine the iron vapor pressure profile in the condensing region of the boundary layer. The supersaturation is the ratio of the partial pressure of the iron vapor to the equilibrium vapor pressure over a plane surface. Classical nucleation kinetics show that for supersaturations above a "critical" value condensation takes place at an extremely rapid rate while for saturations below the critical value condensation takes place at an extremely slow rate.[2-8] In Turkdogan's analysis, the boundary

layer is divided into two distinct zones: a condensate-free region close to the vaporizing surface in which the supersaturation is less than the critical value and an outer portion in which sufficient condensation occurs to maintain the supersaturation at the critical value corresponding to the local gas temperature. The profile between the condensation zone and the wall was assumed to be linear, as in the stagnant film model of ordinary mass transfer. The theoretical results agreed qualitatively with a limited amount of rough experimental data taken by Turkdogan and Mills,[9] which indicates the enhancement to be approximately a factor of three.

With the additional assumption that the logarithm of the critical supersaturation was a linear function of reciprocal temperature, Rosner[10] developed a set of analytical relationships to describe Turkdogan's model.

The major assumptions of the critical supersaturation approach are:

1) Mass transfer is based upon the stagnant film model. In particular, drops formed in the outer condensing region of the boundary layer are not convected into the wall region, which is assumed to be free of drops larger than the critical size.

2) The location of the nucleation zone is determined by a critical supersaturation value obtained from the infinite-medium solution of the nucleation kinetics equation for an arbitrarily selected nucleation rate.

3) The drop temperature is equal to the local gas temperature. Thermal radiation from the hot wall to the drop is neglected.

4) Diffusion of the drops is neglected. Only the vapor species (the "monomer") diffuses. Elenbaas[11] has shown that if drops do not penetrate the outer edge of the boundary layer, drop diffusion eliminates enhancement

of the vaporization rate in the stagnant film model.

Epstein and Rosner[12] have examined the validity of the second assumption of the critical supersaturation model by simultaneously solving the classical nucleation equations (the infinite medium solutions) with the conservation equations for a stagnant film mass transfer situation. Their analysis contains a convective term caused by the interfacial velocity which transports drops away from the vaporizing surface. As a result, drops leave the outer edge of the film and acceleration of the vaporization rate occurs. For this stagnant film model, Epstein and Rosner suggest that drop diffusion is unimportant.

Epstein and Rosner did find that nucleation currents in their boundary layer were on the order of 10^{10} to 10^{14} drops/cm^3-sec rather than 1 drop/cm^3-sec. The current of 1 drop/cm^3-sec was used to define the critical supersaturation in cloud chambers[2-8] and had previously been used to define the critical supersaturation in boundary layers.[9,10] This definition was used in cloud chambers because 1 drop/cm^3-sec is a drop current which is easily countable by visual techniques. Its use to define the critical supersaturation in boundary layers was simply an ad hoc assumption. The actual nucleation current in a boundary layer is determined by a mass balance between the drops and the vapor.

The approach of Epstein and Rosner is similar to that used in analysis of condensation in expansion nozzles.[13,14] Droplets are nucleated at rates dependent upon local supersaturation in accordance with classical nucleation theory. These embryos are convected along flow streamlines and grow by absorbing vapor from the surrounding gas phase. This method is Lagrangian in flavor, since the characteristics of the drop population at any point in the one-dimensional flow field are determined by integration

of the growth history of the drops from their upstream nucleation point. In mass transfer problems, this approach is convenient if the direction of mass transfer and the flow streamlines coincide, as is the case in the stagnant film model analyzed by Epstein and Rosner. However, for many flow geometries, the streamlines may be complicated curves while the concentration of the transferring species depends only on one distance coordinate. Such is the case for example for a rotating disk, where the streamlines execute spiral motion of increasing amplitude as the fluid moves towards the disk. The concentration, however, is a function only of axial location. In this instance, it is obviously desirable to avoid integrating along streamlines.

Consequently, the present analysis utilizes an Eulerian approach, in which mass conservation of the vapor species (termed the "monomer") and of different size drops is applied in a fixed control volume in the flow field. In this analysis, the source term in the drop conservation equations and the sink term in the monomer equation are derived from the microscopic balance equations of nucleation kinetics. The effect of thermal radiation from the wall on drop temperature is included by a heat balance on the drops.

With this approach, the final results of classical nucleation kinetics are not directly used to modify the mass transfer problem. Rather, by integrating the microscopic (kinetic theory) rate equations into the drop conservation equations, an internally consistent description of the drop convection-diffusion-condensation process is obtained.

The equations were solved for the rotating disk flow geometry, which is one of the few fluid-mechanical systems which has an exact solution for the continuity, momentum, and the energy equations.[15,16] This means

that the velocities and temperature in the monomer and drop conservation equations can be determined from first principles; the correlations or approximations needed to solve other hydrodynamic systems are not required. The monomer and drop equations for the rotating disk reduce to one-dimensional forms which simplifies numerical solutions. Experimental verification of the theory is possible, since rotating disks can be operated as high as 2000°K.[35]

This work extends the previous work in the following manner.

1. The diffusion and convection of drops in the boundary layer is considered in a rigorous manner; the assumption of a stagnant film is not required.

2. The microscopic rate equations of the nucleation kinetics are combined directly with the drop conservation equations to obtain from first principles a description of the convection-diffusion-condensation process.

3. The nucleation rate is not arbitrarily selected but is determined by a microscopic mass balance between the monomer and the drops.

4. The effect of thermal radiation from the hot wall to the drops is considered.

5. The experimental data were obtained with a rotating disk system which is known to be a precise experimental tool.[16,32,35,38]

6. The data taken in this work show very little scatter; this is in contrast to previous data[9] which scatter widely and hence give only qualitative estimate of condensation.

B. Problem Formulation

Consider a hot rotating disk of infinite extent surrounded by a cold inert gas (Fig. 0). The disk is at constant temperature T_w and rotates with angular velocity ω. The gas far from the disk is at temperature T_∞. Since the disk is spinning, it induces angular and radial velocities in the boundary layer. The gas adjacent to the surface flows radially outward and by continuity the gas far above the surface flows downward. The molecules of the vaporizing substance diffuse out from the disk into the laminar boundary layer, the thickness of which can be shown to be the same at all radial positions. If the conditions in the boundary layer are conducive to drop formation, molecules may combine to form a droplet nucleus, or more probably, may combine with an existing drop by colliding with it. The drops thus formed are convected with the bulk fluid (and also diffuse) while growing or evaporating. It is assumed in this development that the disk vaporizes monatomically.

Net motion of the drops relative to the bulk gas velocity is neglected, i.e. gravitational and centrifugal forces on the drops are assumed negligible compared to drag forces exerted by the gas flow. This assumption is reasonable if very large drops are not formed; the limits on drop size required to neglect these forces are shown in Appendix A.

Only "dilute" systems are considered. While no precise concentration level separating "dilute" and "concentrated" mixtures is possible, the term "dilute" implies neglect of:

1) Interfacial velocity.
2) Property variations due to concentration changes in the boundary layer.
3) The effect of heat release due to condensation on the boundary layer energy equation.

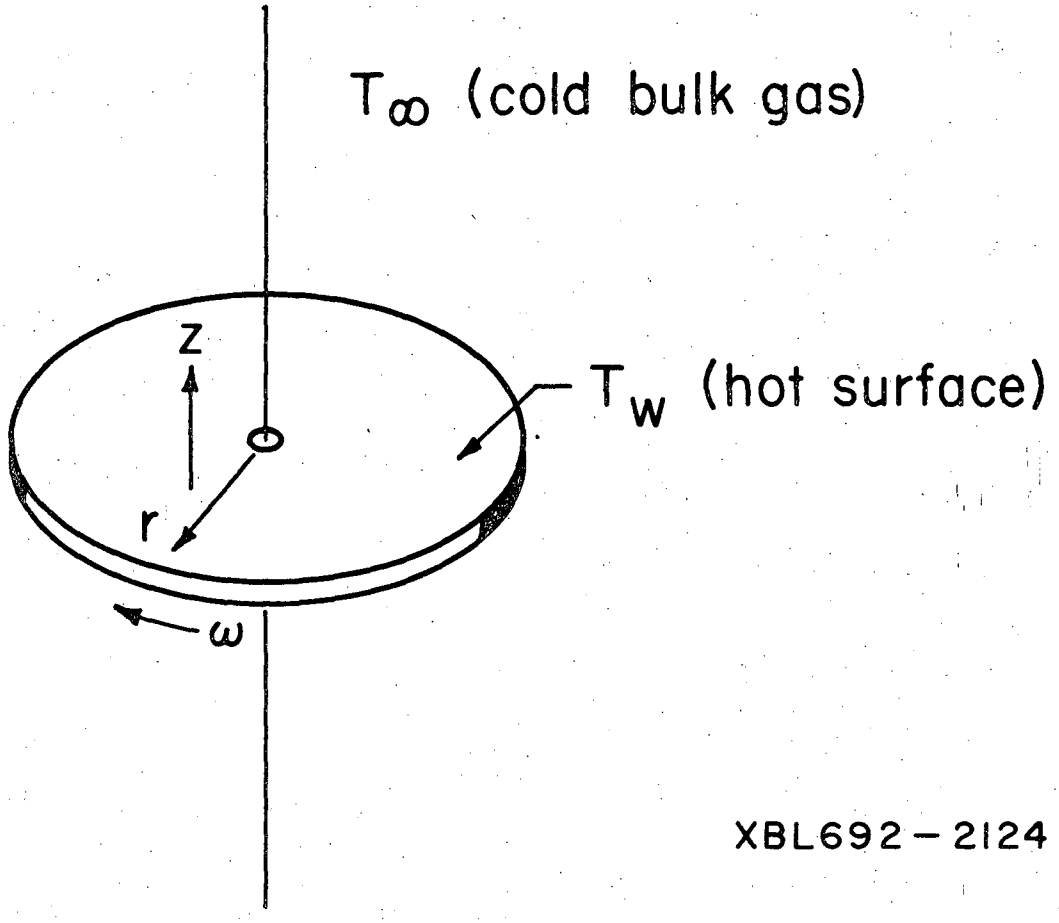

Fig. 0

Most metal-inert gas systems, because of the low vapor pressure of the metal, are dilute; the methanol-air mixture considered by Epstein and Rosner[12] is not.

The effect of restrictions (1)-(3) above is to uncouple the momentum and energy equations from the material conservations equations. The momentum and energy euqations, however, are still coupled to each other because of the temperature-induced physical property variations (viscosity, density and therma conductivity) in the boundary layer. This problem, however, can be solved independently of the material conservation equations.

Figure 1 shows the difference between the isothermal vaporization case and the non-isothermal vaporization case. In the isothermal case, condensation enhancement cannot occur because the vapor pressure in the boundary layer is at all points below the equilibrium value. In the non-isothermal case, the decrease in the temperature through the boundary layer produces a rapid decrease in the equilibrium vapor pressure. This is because the equilibrium vapor pressure is a strong function of temperature. The result is that the equilibrium vapor pressure profile may fall below the no-condensation vapor pressure profile and so condensation occurs. The vapor pressure profile with condensation must at all times lie between the no-condensation profile and the equilibrium profile, however, its exact position in this region determined by a mass balance between the drops and the monomer.

1. The Conservation Equations

The equations describing conservation of mass, energy, and vapor (or monomer)[15,17] are

continuity: $$\frac{1}{r}\frac{\partial}{\partial r}(\rho r u) + \frac{\partial}{\partial z}(\rho w) = 0 \qquad (1)$$

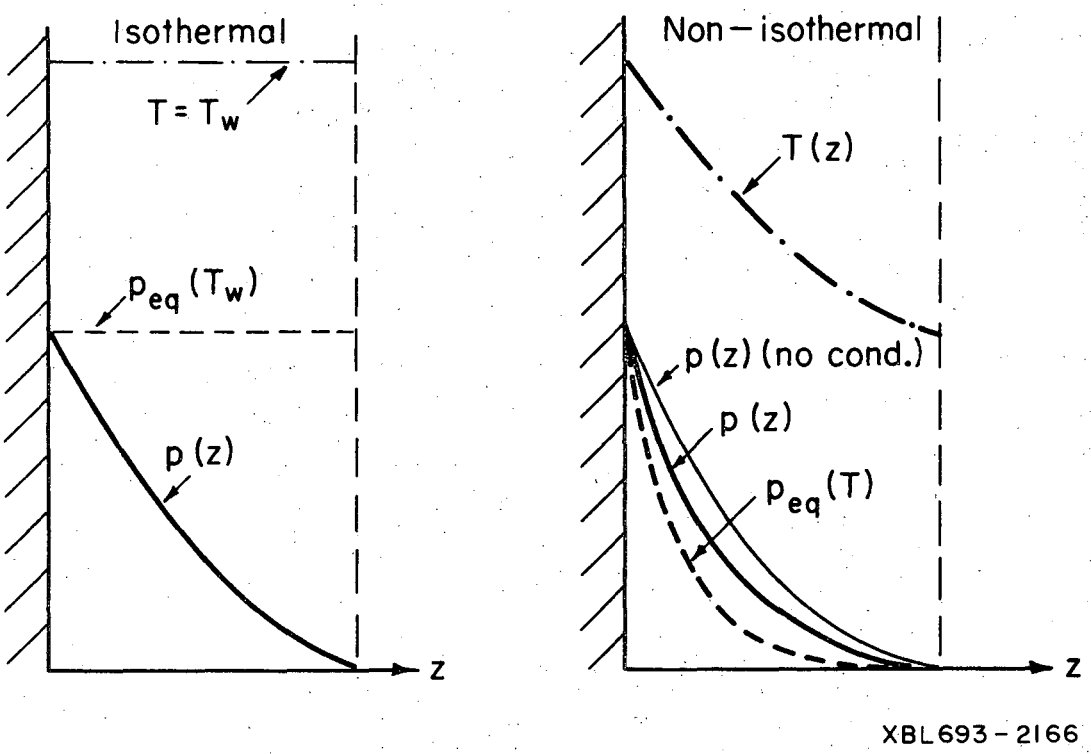
Isothermal
T = Tw
peq (Tw)
p (z)
z
Non – isothermal
T (z)
p (z) (no cond.)
p (z)
peq (T)
z
XBL693 - 2166

Fig. 1

r-momentum:

$$\rho\left(u\ \frac{\partial u}{\partial r} - \frac{v^2}{r} + w\ \frac{\partial u}{\partial r}\right) = -\frac{\partial p}{\partial r} + \frac{\partial}{\partial r}\left\{\mu\left[2\ \frac{\partial u}{\partial r} - \frac{2}{3}\left(\frac{1}{r}\frac{\partial}{\partial r}(ru) + \frac{\partial w}{\partial z}\right)\right]\right\} + \frac{\partial}{\partial z}\left[\left(\frac{\partial u}{\partial z} + \frac{\partial w}{\partial r}\right) + \frac{2\mu}{r}\left(\frac{\partial u}{\partial r} - \frac{u}{r}\right)\right] \quad (2)$$

ϕ-momentum:

$$\rho\left(u\ \frac{\partial v}{\partial r} + \frac{uv}{r} + w\ \frac{\partial v}{\partial z}\right) = \frac{\partial}{\partial r}\left[\mu\left(\frac{\partial v}{\partial r} - \frac{v}{r}\right) + \frac{\partial}{\partial z}\left(\mu\ \frac{\partial v}{\partial z}\right) + \frac{2\mu}{r}\left(\frac{\partial v}{\partial r} - \frac{v}{r}\right)\right] \quad (3)$$

z-momentum:

$$\rho\left(u\ \frac{\partial w}{\partial r} + w\ \frac{\partial w}{\partial r}\right) = -\frac{\partial p}{\partial z} + \frac{\partial}{\partial z}\left\{\mu\left[2\ \frac{\partial w}{\partial z} - \frac{2}{3}\left(\frac{1}{r}\ \frac{\partial}{\partial r}(ru) + \frac{\partial w}{\partial z}\right)\right]\right\} + \frac{1}{r}\ \frac{\partial}{\partial r}\left[\mu r\left(\frac{\partial u}{\partial r} + \frac{\partial w}{\partial z}\right)\right] \quad (4)$$

energy:

$$\rho\ c_p\left(u\ \frac{\partial T}{\partial r} + w\ \frac{\partial T}{\partial z}\right) = \frac{\partial}{\partial r}\left(k\ \frac{\partial T}{\partial r}\right) + \frac{k}{r}\ \frac{\partial T}{\partial r} + \frac{\partial}{\partial z}\left(k\ \frac{\partial T}{\partial z}\right) \quad (5)$$

vapor (monomer):

$$\frac{1}{r}\ \frac{\partial}{\partial r}\ (r\ u\ \rho_v) + \frac{\partial}{\partial z}\ (w\rho_v) = \frac{\partial}{\partial r}\left(\rho\ D\ \frac{\partial}{\partial r}\ (\rho_v/\rho)\right) + \rho\ \frac{D}{r}\ \frac{\partial}{\partial r}\ (\rho_v/\rho) + \frac{\partial}{\partial z}\left(\rho\ D\ \frac{\partial}{\partial z}\ (\rho_v/\rho)\right) + S_v \quad (6)$$

with boundary conditions:

at $z = 0$

$$u = 0,\ v = r\omega,\ w = 0,\ T = T_w,\ \rho_v = \rho_{v,eq}(T_w) \quad (7)$$

as $z \to \infty$

$$u = 0,\ v = 0,\ \rho = \rho_\infty,\ T = T_\infty,\ \rho_v = 0$$

Equation (1) is the hydrodynamic continuity equation for the flowing gas; Eqs. (2), (3), and (4) are the hydrodynamic momentum equations for the r, ϕ and z directions, respectively; Eq. (5) is the energy equation for the gas; the Eq. (6) is the convective-diffusion equation for the monomer. The notation is as follows: u, v, and w are the velocity components of the gas in the r, ϕ and z directions, respectively; ρ is the gas density; μ is the dynamic viscosity; p is the total pressure; c_p is the specific

heat at constant pressure; k is the thermal conductivity; and T is the temperature of the gas. The density of the monomer in gm/cm^3 is ρ_v, D is the binary diffusion coefficient for the monomer in the inert gas, and S_v is the volumetric source of monomer in gm/cm^3-sec.

The convective-diffusion equation, Eq. (6), states that the rate at which monomer is convected out of a unit volume is equal to the rate at which it diffuses into the unit volume plus the rate at which it is produced in the unit volume. The source term is, in fact, negative for in this case monomer is not produced but consumed in the unit volume. The monomer consumed is used to produce the drops and the magnitude of the source term is equal to the total amount of monomer going into drop production in the unit volume. The vapor boundary condition in Eq. (7) utilizes the equilibrium vapor density $\rho_{v,eq}$.*

The conservation equation for drops of size g molecules is:

$$\frac{1}{r}\frac{\partial}{\partial r}(ruc_g) + \frac{\partial}{\partial z}(wc_g) = \frac{\partial}{\partial r}\left(\rho D_g \frac{\partial}{\partial r}(c_g/\rho)\right) + \rho\frac{D_g}{r}\frac{\partial}{\partial r}(c_g/\rho) + \frac{\partial}{\partial z}\rho\left(D_g\frac{\partial}{\partial z}(c_g/\rho)\right) + S_g$$

where c_g is the concentration of drops of size g in $drops/cm^3$; D_g is the binary diffusion coefficient for drops of size g through the inert gas; and S_g is the source of drops of size g in $drops/cm^3$-sec. Like Eq. (6) for the monomer, this equation states that the rate at which drops of size

---

* The mass flux at the wall, even with condensation enhancement, is small compared to the rate at which atoms leave the surface and condense upon it. Hence the surface kinetic limitations characteristic of vacuum vaporization are absent since boundary layer diffusion is by far the slowest step in the overall process and the equilibrium vapor pressure is obtained at the disk surface.

g are convected out of a unit volume is equal to the rate at which they diffuse in plus the rate at which they are produced. One such equation is required for each drop size g considered.

Note that the conservation Eqs. (1)-(8) are written in the variable property form. This is necessary because the temperature differences across a boundary layer required before appreciable condensation occurs are greater than 1000°K for metals.

The droplet diffusion coefficient D_g is given by[18]

$$D_g = C \frac{kT}{6\pi\mu r_g} \tag{9}$$

where r_g is the radius of a drop of size g

$$r_g = \left(\frac{3}{4\pi N} g\right)^{1/3} \tag{10}$$

with N the atom density of the vaporizing species in its bulk liquid state in atoms/cm^3.. The coefficient C is given by

$$C = 1 + \frac{\lambda}{r_g} [1.257 + 0.400 \exp(-1.10\, r_g/\lambda)] \tag{11}$$

with λ the mean free path of the metal atom in the gas,

$$\lambda = \frac{\mu}{\rho} \sqrt{\frac{9\pi m_{gas}}{8kT}} \tag{12}$$

where m_{gas} is the mass of an inert gas atom. For drops smaller than the mean free path, Eq. (9) yields the classical molecular diffusion coefficient and D_g varies as $D/g^{2/3}$. For drops larger than the mean free path, Eq. (9) yields the Stokes-Einstein relation in which D_g varies as $g^{-1/3}$. In the actual calculations, 2/3 power law was used for all drop sizes. This simplification was made because the effect of drops larger than the mean free path on the vaporization rate was very small.

The source term in the energy equation has been neglected. This is because the system considered here is dilute in the condensing species while the temperature gradient across the boundary layer is very large; thus the quantity of vapor condensing in the boundary is not large enough to significantly effect the temperature profile.

2. The Droplet Source Terms

The source term S_g in the droplet Eq. (8) is obtained from the microscopic banace equations of nucleation kinetics.[3,4,6] Consider a distribution of drops of all sizes in a unit volume. Let A_g be the surface area of a drop of size g, β_g the rate at which vapor atoms in the gas condense upon a unit area of a drop of size g per unit time, and α_g the rate at which atoms are evaporated from a drop of size g per unit time. Let J_g be the net rate at which drops pass from size g-1 to size g per cm^3 per second, i.e. the droplet "current" in g-space.* Since the product $\beta_{g-1}A_{g-1}c_{g-1}$ is the rate at which drops of size g-1 grow to size g per cm^3 per second and the product of $\alpha_g A_g c_g$ is the rate at which drops of size g diminish to size g-1 per cm^3 per second, the net rate at which drops of size g-1 grow to size g is given by

$$J_g = \beta_{g-1}A_{g-1}c_{g-1} - \alpha_g A_g c_g \tag{13}$$

The coefficient β_g is given by

$$\beta_g = \frac{p_v}{\sqrt{2\pi mkT}\left(1 + \frac{r_g}{D}\sqrt{\frac{kT}{2\pi m}}\right)} \tag{14}$$

where the Hertz-Knudsen equation has been modified by the factor

$$\frac{1}{1 + \frac{r_g}{D}\sqrt{\frac{kT}{2\pi m}}}$$

to give the correct net transfer rate across the drop-vapor interface for large drops, i.e. drops whose growth rate is limited by diffusion rather

* The droplet current in g-space is analogous to the "slowing down density" of neutrons in energy space, a concept which has been of considerable utility in nuclear reactor calculations.

than kinetics.[19,20] The modification to the Hertz-Knudsen equation is not strictly accurate for drops equal in size to the mean free path. However since few drops of mean free path size or larger should exist, this simplified form was considered adequate. A unit sticking probability was assumed. The mass of vapor molecule is m, p_v is the partial pressure of the diffusing vapor, and k is Boltzman's constant. The evaporation coefficient α_g is given by:[3-5]

$$\alpha_g = \frac{A_{g-1}}{A_g} \frac{p_{v,eq}(T_g) \exp\left(\frac{2b}{3kT_g} g^{-1/3}\right)}{\sqrt{2\pi mkT_g}\left(1 + \frac{r_g}{D}\sqrt{\frac{kT}{2\pi m}}\right)} \quad (15)$$

where $p_{v,eq}$ is the equilibrium vapor pressure at the drop temperature T_g and b is the parameter

$$b = 4\pi\gamma \left(\frac{3}{4\pi N}\right)^{2/3}$$

where γ is the surface tension in dynes/cm and $p_{v,eq}$ is the equilibrium vapor pressure over a plane surface. The exponential term accounts for the increase of the vapor pressure due to the finite radius of curvature of the drop.* The drop temperature T_g is the temperature of a drop composed of g molecules. The surface area A_g in terms of g is:

$$A_g = 4\pi \left(\frac{3}{4\pi m}\right)^{2/3} g^{2/3} \quad (16)$$

Note that α_g has also been modified to give the correct net transfer rate for large drops.

The net rate S_g at which drops of size g are formed per cm^3 per second is equal to the net rate at which drops of size g-1 grow to size g minus the net rate at which drops of size g grow to size g+1, i.e,

$$S_g = J_g - J_{g+1} \quad (17)$$

---

*There is still considerable controversy over the proper form for the coefficient α_g.[21-24] We use the classical form embodied in Eq. (15) because of the agreement between classical nucleation theory and experiment obtained by Katz and Ostermier.

$$= \beta_{g-1} A_{g-1} c_{g-1} - \alpha_g A_g c_g - \beta_g A_g c_g + \alpha_{g+1} A_{g+1} c_{g+1} \qquad (18)$$

At this point, it is appropriate to review the various conditions under which the concepts of drop current and drop source have been applied in other nucleation studies.

1. The balanced equilibrium theory of homogeneous nucleation[2-6] applies to a system with no gradients, no flow, and no means of removing growing drops from the system. These conditions are summarized by the statements: $S_g = 0$ and $J_g = 0$. Because balanced equilibrium theory requires abnormally high concentrations of large drops, the condition of no removal of growing drops must be relaxed for nucleation theory to be applied to real systems.

2. In the unbalanced equilibrium case[2-6] drops are permitted to grow through g-space at a constant rate; large drops are assumed removed from the system by an unspecified mechanism and returned to the vapor phase as monomer. Since this process is considered to be at steady state, and since no concentration gradients or bulk flow exist, it will be referred to as the infinite-medium, steady state case. It is characterized by the requirements: $S_g = 0$, J_g = constant. The source-free condition follows from Eq. (8) if all convective and diffusive terms are set equal to zero. The evaluation of the constant value of J for this case, which is commonly termed the nucleation rate, has been the subject of many studies.[2-7,22] Turkdogan[1] and Epstein and Rosner[12] have utilized the nucleation rate derived from the inifinte-medium, steady state solution in their analyses of condensation effects on mass transfer in stagnant films.

3. The infinite-medium transient case has been studied by various authors.[3,4,6,25,26] The governing equation in this case is $\partial c_g / \partial t = S_g = J_g - J_{g+1}$, which is the unsteady state analog of Eq. (8) for an

infinite medium.

4. The present case may be characterized as the finite-medium steady state because in the finite system, convection and diffusion of the monomer and the drops must be considered.

Using Eq. (18) the drop conservation Eq. (8) becomes:

$$\frac{1}{r}\frac{\partial}{\partial r}(ruc_g) + \frac{\partial}{\partial z}(wc_g) = \frac{\partial}{\partial r}\left(\rho D_g \frac{\partial}{\partial z}(c_g/\rho)\right) + \rho\frac{D_g}{r}\frac{\partial}{\partial r}(c_g/\rho) + \frac{\partial}{\partial z}\left(\rho D_g \frac{\partial}{\partial z}(c_g/\rho)\right) + \beta_{g-1}A_{g-1}c_{g-1} - \alpha_g A_g c_g - \beta_g A_g c_g + \alpha_{g+1} \cdot A_{g+1}c_{g+1} \qquad (19)$$

for $g = g_0, g_0+1, g_0+2, \ldots$ where g_0 is smallest drop size considered.

The value of g_0 in our case varied between 10 atoms and 150 atoms. The results were insensitive to the value used. A g_0 larger than unity must be used for two reasons. First, a standard nucleation theory assumption[2-8,25] is that the bulk properties of the liquid can be used in the calculations even though the drops do not contain many molecules. Clearly this is untenable for drops approaching atomic size. The normal technique,[25] however, is to set g_0 approximately equal to ten or twenty atoms and to assume that the bulk liquid properties apply to all drops greater than this size. The second reason g_0 could not approach unity in that our numerical calculations became unstable at very small g_0. Courtney,[25] used a value of 20 for g_0 in his numerical solution of the infinite medium transient case.

If the monomer Eq. (6) is divided by the mass of the monomer atom m, the result is an equation similar to Eq. (19) in that it conserves drops of size unity. Defining f as the concentration of monomer atoms/cm^3,

$$f = \rho_v/m = p_v/kT \qquad (20)$$

Eq.(6) becomes

$$\frac{1}{r}\frac{\partial}{\partial r}(ruf) + \frac{\partial}{\partial z}(wf) = \frac{\partial}{\partial r}\left(\rho D \frac{\partial}{\partial r}(f/\rho)\right) + \rho \frac{D}{r}\frac{\partial}{\partial r}\left(\frac{f}{\rho}\right) + \frac{\partial}{\partial z}\left(\rho D \frac{\partial}{\partial z}(f/\rho)\right) + S_1 \quad (21)$$

The source term S_1 is in atoms/cm^3-sec.

3. The Monomer Source Term

The monomer equation source term S_1 is found as follows. Multiply Eq. (8) by g and sum the resulting equations for all $g \geq g_0$. When this sum is added to the monomer conservation Eq. (21) the result is a conservation statement for the vaporizing species in any form, drops or monomer. Since the source term in this total species balance must be zero,

$$S_1 = - \sum_{g_0}^{\infty} gS_g \tag{22}$$

The coupling between the monomer and droplet equations can now be seen. The source term in the monomer balance, S_1, depends upon S_g by Eq. (22) and S_g depends upon c_g via Eqs. (13) and (17). The coefficient β_g depends on monomer partial pressure by Eq. (14) which is related to f by Eq. (20).

4. Boundary Conditions on the Drop Conservation Equations

It has been shown by Zeldovich[6] that the source term in Eq. (19) can be approximated by an expression involving the first and second partial derivatives of c_g with respect to g. This is an interesting situation in which the basic physics are expressed in finite difference form whereas the differential form is an approximation. Since machine computation invariably requires approximation of partial derivatives by their finite difference analogs, nothing is gained by transforming Eq. (19) to differential form. However, the fact that the source term in Eq. (19) is equivalent to a second order partial derivative suggests that two boundary conditions on c_g in g-space in addition to the two boundary conditions in z are required to render the problem completely specified. Moreover, the infinite medium problem also requires two boundary conditions in g-space.[4,6]

In the z-direction the boundary conditions are as follows. At the disk-vapor interface, the supersaturation is unity and the droplet concentrations are assumed to be given by the equilibrium model:

$$c_g = f_w \exp\left(-\frac{b}{kT_w} g^{2/3}\right) \quad \text{at } z = 0, \text{ all } g \qquad (23)$$

and in the bulk gas, far from the disk

$$c_g \to 0 \quad \text{as } z \to \infty, \text{ all } g \qquad (24)$$

Consider the development of the g-space boundary condition for the infinite-medium steady state case. Drops of small size spend most of their time oscillating back and forth between large and smaller g while only a few pass on to consitute the current J_g.[4] So for small drops in the steady-state infinite-medium case, J_g, of Eq. (13) is a small difference between two large numbers. Thus since $\beta_{g-1} A_{g-1} c_{g-1} \gg J_g$, $\alpha_g A_g c_g \gg J_g$, then $\beta_{g-1} A_{g-1} c_{g-1} \approx \alpha_g A_g c_g$ which leads to equilibrium values of c_g.

Hence, in the steady-state infinite-medium analysis, one boundary condition is that the solution must approach the equilibrium solution as $g \to 1$. The other is that the solution must approach zero as $g \to \infty$.

In the present analysis, the same boundary conditions could in principle be used. However, at points in the boundary layer where the supersaturation is very large, the critical drop radius of equilibrium theory approaches atomic size. Fitting with equilibrium theory would require either using a very small starting value g_0, which both renders used of Eq. (15) doubtful and makes machine computation subject to instabilities, or matching on the rising part of the equilibrium theory curve, which is unrealistic. Consequently, we have matched our solution with the physically acceptable steady-state infinite-medium solution at g_0. This is equivalent to assuming that at $g = g_0$, $J_g \gg S_g$, $J_{g+1} \gg S_g$, $S_g \approx 0$. Thus by Eq. (17), $J_g \approx J_{g+1} \approx$ constant, which is the basis of the infinite medium solution. Thus the boundary condition for small g is:

$$c_g = J/\beta_g A_g, \quad J = J_g = \text{constant} \tag{25}$$

at $g = g_0$ in the nucleation zone where[4,7]

$$J = \sqrt{\frac{2}{\pi}} \left(\frac{p_{veq}}{kT}\right)^2 \sqrt{\frac{\gamma}{m}} \frac{1}{N} \; S^2 \; \exp\left(-\frac{16\pi}{3}\left(\frac{\gamma}{kT}\right)^3 \; \frac{1}{N^2} \; \frac{1}{(\ln(S))^2}\right) \tag{26}$$

and S is the supersaturation:

$$S = p_v/p_{v,eq} \tag{27}$$

Note that given the partial pressure of the monomer p_v and the surface tension γ, then J follows. Equation (25) is the steady-state infinite-medium solution in a highly supersaturated vapor for drops larger than the critical size, i.e. for $\alpha_g \ll \beta_g$. The matching condition is utilized only in the nucleation zone, i.e. the region of large supersaturation where the critical

drop size approaches unity. Outside the nucleation zone, the concentration of small drops is determined by transport via diffusion and convection from the nucleation zone rather then by local nucleation. This is because the local nucleation rate outside the nucleation zone is very small because of the small supersaturation, and so the concentration of drops due simply to transport is much greater than the concentration due to local nucleation. In fact then, the boundary condition in our problem is determined by solving the diffusion-convection equation for very small drops with a source term such that the drop concentration in the nucleation zone is identical to that given by the steady state infinite medium solution in this zone. In principle, the drop concentration could be matched to the steady state infinite medium solution at all points in the boundary layer if g_0 could be allowed to approach unity. Since this could not be done, the effect of diffusion and convection on drops at the initial starting size g_0 had to be considered in this approximate manner.

The boundary condition for large drops is:

$$c_g \to 0 \quad \text{as} \quad g \to \infty \quad \text{for all } z \tag{28}$$

5. Drop Temperature

Only the temperature of a drop of size g, T_g, remains to be specified for a well-defined problem. Since the drop is in a strong thermal radiation field, it may not be at the temperature of the surrounding gas. A quasi-static energy balance upon the drop gives the following transcendental equation for T_g:

$$\frac{1}{2}\sigma\epsilon T_w^4 A_g + \ell(\beta_g - \alpha_g) A_g = \sigma\epsilon T_g^4 A_g + c_p A_{th} \beta_{gas} (T_g - T) A_g \tag{29}$$

where the first term is the amount of heat radiated from the rotating disk to the drop, the second term is the heat added to the drop by condensation of the vapor on the drop, the third term is the heat radiated from the drop to the surroundings, and the last term is quantity of heat removed by inert gas atoms colliding with the drop. The Stephan-Boltzman constant is σ, ϵ is the emissivity of the disk and the drop, ℓ is the average value of the latent heat per atom, c_p is the average value of the augmented specific heat per atom, A_{th} is the thermal accommodation coefficient, β_{gas} is the rate at which the inert gas atoms cross a unit area per second, and T is the local temperature of the gas. The augmented specific heat is the average specific heat of a sample of molecules crossing a plane surface and is higher than the ordinary specific heat per atom by $\frac{1}{2}$ k.[26]

6. Dimensionless Form of the Basic Equations

The advantage of the rotating disk as a vaporizing surface is that the governing equations can be reduced to one-dimensional forms and exact solutions obtained. Von Karman[27] has shown that the constant-property form of the hydrodynamic Eqs. (1)-(4) can be reduced to a coupled set of ordinary differential equations and Cochran[28] solved the set exactly. Using Von Karman's and Cochran's solutions of the momentum equations, the constant-property form of the energy Eq. (5) was solved exactly by Millsaps and Pohlhausan[29] and Sparrow and Gregg.[30] The solution of the constant-property source-free form of the monomer conservation Eq. (6) then follows by analogy since it is identical in form to the energy equation if the system is dilute and the bulk velocity at the wall is negligible.

A series of transformations can be found which reduce the variable-property hydrodynamic Eqs. (1)-(4) to von Karman's coupled set. In addition the variable property energy Eq. (5) can be reduced to Sparrow and Gregg's ordinary differential equation. These transformations are similar to those used to reduce the variable-property flat plate boundary layer problem to a constant-property one.[31] To use them, one must assume that the Prandtl number, the Schmidt number, and the product $\rho\mu$ are constant throughout the boundary layer. These, however, are very good assumptions; for a 1500°C temperature drop across argon boundary layer these values vary by only about 60%, and the solution evaluated at the film temperature should be very close to the exact variable-property solution.

It will be shown that the variable-property monomer and droplet equations can be reduced to inhomogeneous ordinary differential equations

if the solution can be assumed independent of radius. If the equations were homogeneous, the solutions would then depend on z alone for the solutions of the rotating disk system must be similar with respect to radius and match the boundary conditions at the wall and at infinity, both of which are independent of radius. However, even though the equations are inhomogeneous, the solutions may still depend on z alone because the source terms have no explicit r dependence. The source of one equation is, in fact, determined by the solution of the other equation; it is difficult to see how an r-dependence could arise, for both solutions must be similar with respect to r and both sets of z boundary conditions are independent of r. It will be assumed in this development that there is no r-dependence.

The hydrodynamic and energy Eqs. (1)-(5) were reduced to von Karman's and Millsaps' ordinary differential equations as follows. Assume, as von Karman and Millsaps did, that the solution is similar in the r-direction with

$$u = r\omega F(\eta), \quad v = r\omega G(\eta), \quad w = \sqrt{\omega\nu_\infty}\, H(\eta)$$

$$p = \mu_\infty \omega P(\eta), \quad \frac{T-T_\infty}{T_w-T_\infty} = \theta(\eta) \tag{30}$$

where η is the dimensionless distance

$$\eta = \sqrt{\frac{\omega}{\nu_\infty}}\, z$$

Applying this to Eqs. (1)-(5) gives:

$$2\rho F + \frac{d}{d\eta}(\rho H) = 0 \tag{31}$$

$$\rho\left(F^2 - G^2 + H\frac{dF}{d\eta}\right) = \frac{d}{d\eta}\left(\frac{\mu\rho_\infty}{\mu_\infty}\frac{dF}{d\eta}\right) \tag{32}$$

$$\rho(2FG + H\frac{dG}{d\eta} = \frac{d}{d\eta}\left(\frac{\mu\rho_\infty}{\mu_\infty}\frac{dG}{d\eta}\right) \tag{33}$$

$$\rho\, c_p\, H\frac{d\theta}{d\eta} = \frac{d}{d\eta}\left(\frac{k\rho_\infty}{\mu_\infty}\frac{d\theta}{d\eta}\right) \tag{34}$$

where Eq. (4) has been dropped since its solution yields only the pressure.

To eliminate the property effects, define a new dimensionless distance ξ

$$d\xi = \frac{\rho}{\rho_\infty}\, d\eta\ ,\ \lambda_f = \rho_f\mu_f/\rho_\infty\mu_\infty \tag{35}$$

and regard λ, the specific heat c_p, and the Prandtl number Pr as constants evaluated at the film temperature. Then Eqs. (31)-(34) become:

$$2F + \frac{d}{d\xi}\left(\frac{\rho}{\rho_\infty}H\right) = 0 \tag{36}$$

$$F^2 - G^2 + \frac{\rho}{\rho_\infty}H\frac{dF}{d\xi} = \lambda_f\frac{d^2F}{d\xi^2} \tag{37}$$

$$2FG + \frac{\rho}{\rho_\infty}H\frac{dG}{d\xi} = \lambda_f\frac{d^2G}{d\xi^2} \tag{38}$$

$$\frac{d^2\theta}{d\xi^2} - \frac{\rho}{\rho_\infty}\,Pr_f\,H\,\frac{d\theta}{d\xi} = 0 \tag{39}$$

where the subscript f denotes evaluation at the film temperature. Again defining a new dimensionless distance x

$$x = \frac{1}{\sqrt{\lambda_f}}\,\xi \tag{40}$$

and a new dimensionless z velocity $\hat{H}$

$$\hat{H} = \frac{1}{\sqrt{\lambda_f}} \frac{\rho}{\rho_\infty} H \tag{41}$$

the ordinary differential equations found by von Karman and Millsaps for constant properties are recovered:

$$2F + \frac{d\hat{H}}{dx} = 0 \tag{42}$$

$$F^2 - G^2 + \hat{H} \frac{dF}{dx} = \frac{d^2F}{dx^2} \tag{43}$$

$$2FG + \hat{H} \frac{dG}{dx} = \frac{d^2G}{dx^2} \tag{44}$$

$$\frac{d^2\theta}{dx^2} - Pr_f \hat{H} \frac{d\theta}{dx} = 0 \tag{45}$$

with boundary conditions:

$$\begin{aligned} &F = 0, \quad G = 1, \quad \hat{H} = 0, \quad \theta = 1 \\ &\text{at } x = 0 \\ &F = 0, \quad G = 0, \quad \theta = 0 \\ &\text{at } x \to \infty \end{aligned} \tag{46}$$

The solution to this set of equations is known exactly[15,16] and hence we know the variable-property velocity and temperature profiles in the gas surrounding the rotating disk. In employing these solutions the approximation[32]

$$\hat{H}(x) = -\frac{1}{4} x \tag{47}$$

was used to calculate the condensation-free vaporization rate and the approximation

$$\begin{aligned} &\hat{H} = -\frac{1}{4} x && 0 \leq x \leq x_o \\ &\hat{H}(x) = -H_\infty && x_o \leq x < \infty \\ &H_\infty = 0.866 && x_o = 3.544 \end{aligned} \tag{48}$$

was used in the numerical solution. The effect of this simplification is less than 2% for the Schmidt numbers of this problem.

The reduction of the monomer Eq. (21) and drop Eq. (19) proceed in a similar manner. First assume, in accordance with the similarity arguments given above, that the monomer and droplet concentrations are functions of z alone, i.e.,

$$f = f(z) \qquad c_g = c_g(z) \tag{49}$$

Then if two concentration functions are defined:

$$\bar{U} = f/\rho \qquad \bar{V}_g = c_g/\rho \tag{50}$$

Equations (21) and (19) become, after differentiating the left-hand sides by parts and applying the continuity Eq. (1):

$$\rho w \frac{d\bar{U}}{dz} = \frac{d}{dz}\left(\rho D \frac{d\bar{U}}{dz}\right) - \rho \sum_{g_0}^{\infty} g\left(\beta_{g-1} A_{g-1} \bar{V}_{g-1} - \alpha_g A_g \bar{V}_g - \beta_g A_g \bar{V}_g + \right.$$

$$\left. + \alpha_{g+1} A_{g+1} \bar{V}_{g+1}\right) \tag{51}$$

$$\rho w \frac{d\bar{V}_g}{dz} = \frac{d}{dz}\left(\rho D_g \frac{d}{dz} \bar{V}_g\right) + \rho \beta_{g-1} A_{g-1} \bar{V}_{g-1} - \alpha_g A_g \bar{V}_g - \beta_g A_g \bar{V}_g +$$

$$+ \alpha_{g+1} A_{g+1} \bar{V}_{g+1}) \tag{52}$$

where the source term S_1 has been written explicitly in terms of $\bar{V}_g$ using Eqs. (13), (17), and (22). Applying the dimensionless parameters, variables, and functions defined for the hydrodynamic and energy equations in an identical manner gives:

$$\hat{H}\frac{d\bar{U}}{dx} = \frac{1}{Sc_f}\frac{d^2\bar{U}}{dx^2} - \frac{1}{\omega}\sum_{g_0}^{\infty} g(\beta_{g-1}A_{g-1}\bar{V}_{g-1} - \alpha_g A_g \bar{V}_g - \beta_g A_g \bar{V}_g + \alpha_{g+1} A_{g+1} \bar{V}_{g+1}) \tag{53}$$

$$\hat{H}\frac{d\bar{V}_g}{dx} = \frac{1}{Sc_{g_f}}\frac{d^2\bar{V}_g}{dx^2} + \frac{1}{\omega}(\beta_{g-1}A_{g-1}\bar{V}_{g-1} - \alpha_g A_g \bar{V}_g - \beta_g A_g \bar{V}_g + \alpha_{g+1} A_{g+1} \bar{V}_{g+1}) \tag{54}$$

where Sc is the Schmidt number $Sc = \mu/\rho D$ based on monomer diffusivity and $Sc_g = \mu/\rho D_g$ is the Schmidt number based on drop diffusivity. Now define a set of dimensionless evaporation and condensation coefficients

$$\alpha_g^+ = A_g \alpha_g/\omega \qquad \beta_g^+ = A_g \beta_g/\omega \tag{55}$$

and a set of dimensionless concentration functions U and V_g:

$$\begin{aligned} U &= \frac{\rho_w f}{f_w \rho} = \frac{\rho_w}{f_w}\bar{U} = p_v/p_{vw} \\ V_g &= \frac{\rho_w c_g}{f_w \rho} = \frac{\rho_w}{f_w}\bar{V}_g \end{aligned} \tag{56}$$

Then a completely dimensionless form for the monomer and drop equations can be obtained:

$$\frac{d^2U}{dx^2} - Sc_f \hat{H}\frac{dU}{dx} = Sc_f \sum_{g_0}^{\infty} g(\beta_{g-1}^+ V_{g-1} - \alpha_g^+ V_g - \beta_g^+ V_g + \alpha_{g+1}^+ V_{g+1}), \tag{57}$$

$$\frac{d^2V_g}{dx^2} - Sc_{g_f}\,\hat{H}\,\frac{dV_g}{dx} = -Sc_{g_f}\left(\beta^+_{g-1}V_{g-1} - \alpha^+_g V_g - \beta^+_g V_g + \alpha^+_{g+1}V_{g+1}\right) \tag{58}$$

$$g = g_0,\ g_0+1,\ g_0+2,\ \ldots$$

The dimensionless boundary conditions are

$$U = 1,\quad V_g = \exp\left(-\frac{b}{kT_w}\,g^{2/3}\right) \text{ at } x = 0$$

$$U \to 0,\quad V_g \to 0 \qquad \text{as } x \to \infty \tag{59}$$

$$V_g = J^+(x)/\beta^+_g(x) \quad \text{at } g = g_0 \text{ in the nucleation zone}$$

$$V_g \to 0 \quad \text{as } g \to \infty$$

where
$$J^+(x) = \frac{\rho_w}{\rho f_w\,\omega}\,J(x) \tag{60}$$

The transcendental droplet energy Eq. (23) in dimensionless form is

$$(T_g/T_w)^4 + C_1\left(\frac{T_g}{T_w} - \frac{T}{T_w}\right) = 2 - C_2\left(\alpha^+_g - \beta^+_g\right)$$

$$C_1 = \frac{c_p A_{th}\,\beta^+_{gas}\,\omega}{\sigma\ \epsilon\ T_w^3\ A_g} \tag{61}$$

$$C_2 = \frac{\ell\omega}{\sigma\ \epsilon\ T_w^4\ A_g}$$

and the dimensionless evaporation and condensation coefficients α^+_g and β^+_g are:

$$\beta^+_g = A_g\,\beta_g/\omega$$

$$= \frac{A_g}{\omega}\,\frac{p_{vw}}{\sqrt{2\pi m k T_w}}\,\frac{U(x)}{\sqrt{T/T_w}}\,\frac{1}{\left(1+\frac{r_g}{D}\right)\sqrt{\frac{kT}{2\pi m}}} \tag{62}$$

$$\alpha_g^+ = A_g \alpha_g / \omega$$

$$= \frac{A_g}{\omega} \frac{p_{v,eq}(T_g)}{\sqrt{2\pi m k T_w}} \sqrt{\frac{T_w}{T_g}} \exp\left(\frac{2b}{3kT_g} g^{-1/3}\right) \frac{1}{\left(1 + \frac{r_g}{D}\sqrt{\frac{kT_g}{2\pi m}}\right)} \qquad (63)$$

The problem of condensation in the boundary layer around a hot rotating disk is then defined by the coupled set of ordinary differential Eqs. (57) and (58) with boundary conditions (59) and a transcendental energy balance Eq. (61). The coefficients in the source terms are given in Eqs. (62) and (63). The Eq. (58) is, in fact, an infinite coupled set of equations, one for each g greater than or equal to g_0. However, the equations need only be solved up to some large but finite g for the concentration of very large should be very small. The effect of these very large drops should be negligible because their growth and evaporation rates will be diffusion limited.

For completeness, a list of parameters which must be specified to solve Eqs. (57) to (63) is shown below. These parameters are sufficient to fix the dimensionless group associated with the problem. The parameters are:

1. temperature at the wall
2. temperature at infinity
3. angular velocity of the disk
4. Prandtl number
5. Schmidt number
6. diffusion coefficient
7. thermal conductivity of the gas
8. starting drop size g_0
9. number of groups
10. approximate boundary layer thickness

Properties of the vaporizing species

11. molecular weight
12. coefficient in the Clausius-Clapeyron equation
13. heat of vaporization
14. surface tension of the bulk liquid
15. density of the bulk liquid
16. specific heat of the bulk liquid.

7. Solution Method

The Eqs. (57)-(63) were solved numerically on a CDC 6600. However, even using a machine as fast as a CBC 6600, the amount of computer time required is excessive if Eq. (58) must be solved for a large number of drop sizes g. To circumvent this, a multigroup scheme was formulated. The drop size range was broken up into a number of smaller groups, each consisting of $n+1$ drop sizes. The initial interval was 10 and each following interval was 10 times the preceding one. Equation (58) was then averaged over these intervals and a single averaged equation obtained for the group. This was done for each group and the set of group equations then were solved for the group-averaged concentrations. The source term in the monomer equation was then written in terms of the group-averaged concentrations and hence the whole problem posed by Eqs. (57)-(63) could be solved in terms of group-averaged values. The amount of computing time required was considerably reduced.

The flow diagram of the iterative solution method employed is shown in Fig. 2. The process was continued until the monomer concentration showed no further change upon continued iteration. The specific equations obtained after averaging over the groups are shown in Appendix B. The computer program is shown in Appendix H.

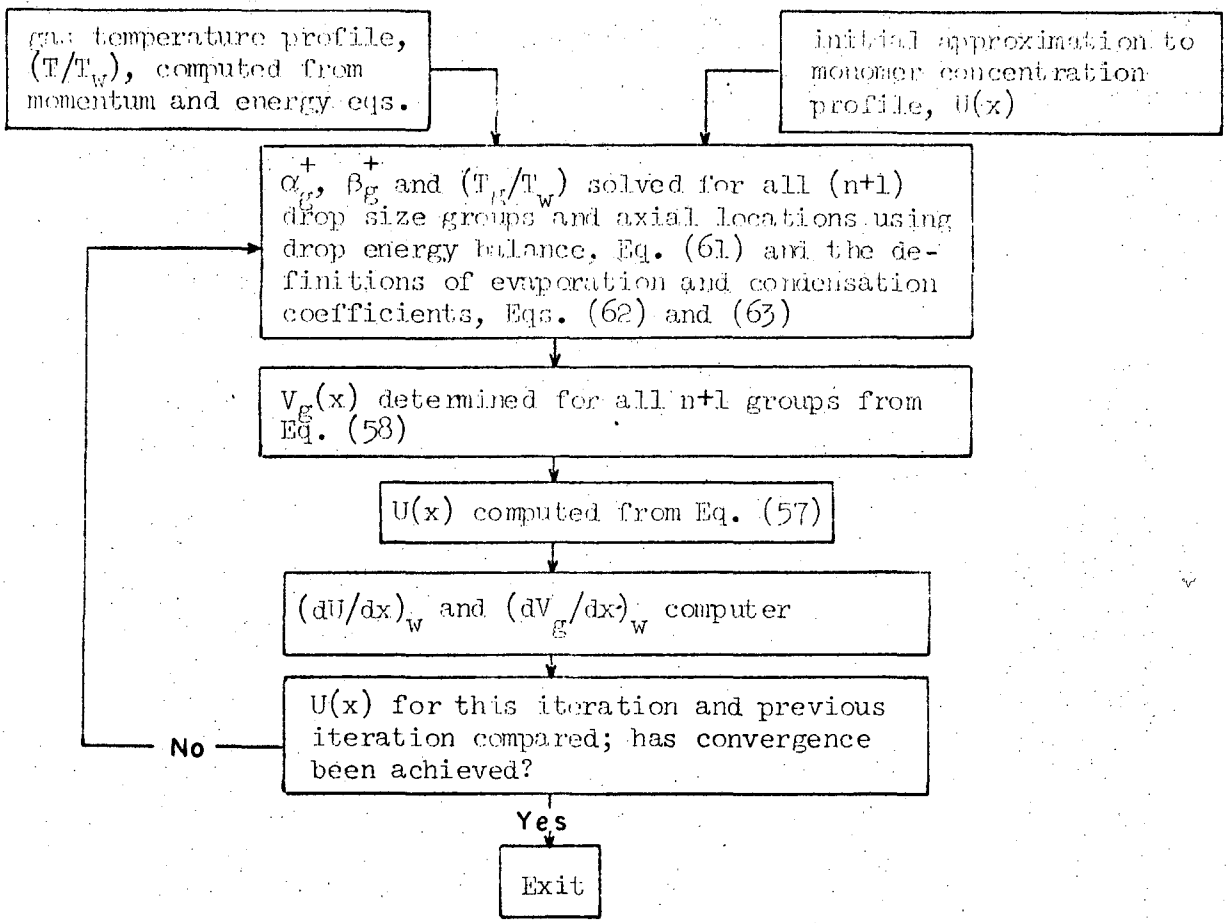

Fig. 2 Flow Diagram for the Computer Solution

C. ENHANCEMENT OF THE VAPORIZATION RATE

The change in the vaporization rate from that in an isothermal system is due to three factors:

1) Condensation

2) Property Variations

3) Thermal Diffusion (the Soret effect)

All three of these effects are due to the extremely large temperature difference (up to 1500°C) across the boundary layer which is only a fraction of a centimeter thick.

The mass flux at the wall is related to the concentration gradients by:

$$j_w = -m\,(\rho\,D)_w \left[\left(\frac{d}{dz} \quad (f/\rho) \right)_w + \sum_{g_0}^{\infty} g(D_g/D) \left(\frac{d}{dz} \quad (c_g/\rho) \right)_w \right] \tag{64}$$

or, in terms of the dimensionless parameters utilized in the solution method, by:

$$j_w = -(\rho\,D)_w \sqrt{\frac{\omega}{\nu_w}}\, c_w \left[\left(\frac{dU}{dx} \right)_w + \sum_{g_0}^{\infty} g(D_g/D) \left(\frac{dV_g}{dx} \right)_w \right] \tag{65}$$

$$\cdot \left[\left(\frac{\rho_w}{\rho_\infty} \right) \quad \frac{1}{\sqrt{\Lambda_f}} \sqrt{\frac{\nu_w}{\nu_\infty}} \right]$$

If non-isothermal effects and the source are neglected, the flux at the wall for the approximate solution of Eq. (57) based upon a linear axial velocity profile is (Eq. (48)):

$$j_w^* = (\rho D)_w \sqrt{\frac{\omega}{\nu_w}} \quad c_w \sqrt{\frac{Sc_w}{2\pi}} \tag{66}$$

where all properties are arbitrarily evaluated at the wall temperature.

Since the isothermal mass transfer rate in the rotating disk system is well known, the effects due to non-isothermal conditions are best presented by computing the ratio of the mass fluxes in the two cases:

$$j_w/j_w^* = \phi_{cond}\ \phi_{vp}\ \phi_{td} \tag{67}$$

where ϕ_{cond} is the factor by which the isothermal transfer rate is enhanced by condensation:

$$\phi_{cond} = -\sqrt{\frac{2\pi}{Sc_f}}\left[\left(\frac{dU}{dx}\right)_w + \sum_{g_0}^{\infty} g(D_g/D)\left(\frac{dV_g}{dx}\right)_w\right] \tag{68}$$

and ϕ_{vp} is the fractional increase due to temperature-induced property variations:

$$\phi_{vp} = \left(\frac{\rho_w}{\rho_\infty}\right)\frac{1}{\sqrt{\lambda_f}}\sqrt{\frac{\nu_w}{\nu_\infty}}\ \sqrt{\frac{Sc_f}{Sc_w}} \tag{69}$$

$$= \sqrt{(\rho^2 D)_w/(\rho^2 D)_f}$$

If $D \sim T^2$, then since $\rho \sim 1/T$, ϕ_V becomes unity. For the iron-argon system this is approximately true since $D \sim T^{1.95}$ (see Fig. G-1, Appendix G). For this reason property variations will be neglected.

The effect of thermal diffusion, ϕ_{td}, can be evaluated independently of the other two, and will not be considered here. Appendix C contains an analysis of the thermal diffusion effect and shows it to be small for the iron argon system.

Our interest is then only in the factor ϕ_{cond}, which can be calculated by three methods:

1. Bulk equilibrium condensation
2. Critical supersaturation by the Turkdogan-Rosner method
3. Present theory

In case 1, condensation is not kinetically limited and the equilibrium vapor pressure is assumed attained at each point in the boundary layer. The monomer concentration gradient at the wall is obtained directly from the gas temperature profile and drop diffusion and convection need not be considered. The partial pressure of the vapor in the boundary layer is given by the Clauius-Clapeyron equation:

$$\rho_v = C \exp\left(-\frac{\ell}{kT}\right) \tag{76}$$

If the energy conservation Eq. (45) is solved using the linear velocity approximation Eq. (47), the resulting temperature profile in the boundary layer is:

$$T(x) = T_w - (T_w - T_\infty)\ \mathrm{erf}\left(\sqrt{\frac{Pr_f}{8}}\, x\right) \tag{77}$$

Equation (56) shows that:

$$U = p_v / p_{vw} \tag{78}$$

the gradient at the wall using Eqs. (76) and (77) becomes:

$$\left(\frac{dU}{dx}\right)_w = \left(\frac{d}{dT}\ (p_v/p_{vw})_w\right)\ \left(\frac{dt}{dx}\right)_w \tag{79}$$

$$= -\sqrt{\frac{Pr_f}{2\pi}}\ \ \frac{\ell}{kT_w}\ \ (1 - T_\infty/T_w) \tag{80}$$

The gradient at the wall with no condensation is (from solving Eq. (57) with no source while using Eq. (47):

$$\left(\frac{dU}{dx}\right)^*_w = -\sqrt{\frac{Sc_f}{2\pi}} \tag{81}$$

The bulk equilibrium condensation factor is obtained by dividing Eq. (79) by Eq. (81)

$$\phi_{cond}\Big|_{\substack{\text{bulk}\\ \text{equilibriun}}} = \sqrt{\frac{Pr_f}{Sc_f}}\ \ \frac{\ell}{kT_w}\ (1 - T_\infty/T_w) \tag{82}$$

This derivation neglects the effect of the heat release due to condensation. Hills and Sackely[33,37] and Rosner and Epstein[47] have derived the same equation including heat release due to condensation for systems with a Lewis number (S_c/Pr) of unity. Their results show that the effect the condensation heat release is less than 4% for the cases considered here. For this reason, it has been neglected.

The results of the critical supersaturation model, case 2, can also be expressed as a condensation factor. The form of the Becker-Doring Zeldovich equation for the critical supersaturation which was recently verified experimentally by Katz and Ostermier[7] was used. The condensation factor, ϕ_{cond}, was obtained by graphical solution of Turkdogan's method. Rosner's analysis although more conveient, could not be used because at the temperatures in the iron-argon system which are practically attainable with a rotating disk apparatus, the logarithm of the supersaturation is not a linear function of reciprocal temperature. A nucleation current of $J = 10^{12}$, corresponding to the value which Epstein and Rosner[12] found to apply in their boundary layer study was used. The properties such as surface tension and density in the Becker-Doring-Zeldovich nucleation expression were evaluated at the film temperature of the boundary layer. The results for both the critical supersaturation and the equilibrium condensation cases are shown in Table I.

TABLE I

T_w (°K)	$\phi_{\text{critical supersaturation}}$	$\phi_{\text{equilibrium condensation}}$
1500	1.0	20.4
1800	1.9	17.4
1900	2.1	16.6
2000	2.2	16.0
2100	2.3	15.3

The results of the present theory, case 3, are presented in the next section.

D. RESULTS

The results obtained are presented in the following sections. The first section shows the effect of nucleation in the boundary layer upon the vaporization rate, the second shows the structure of the nucleation zone in the boundary layer, and the third indicates the sensitivity of the results to some parameter variations.

The effect of nucleation upon the vaporization rate was analyzed for two different cases. In the first case the diffusion coefficient of the drops was assumed to be equal to the diffusion coefficient of the monomer. In the second case the diffusion coefficient of the drops was assumed to vary as the monomer diffusion coefficient divided by the drop size to the two-thirds power. The approximation in the first case makes the drop conservation Eq. (58) much more tractable because the diffusion boundary layer thickness is the same for all drop sizes. This is important because the monomer and droplet equations are coupled and so they must be solved over the same axial distance. The boundary layer thickness for the drop conservation Eq. (58), varies inversely with the Schmidt number.[27] Consequently, as the drop size becomes larger the boundary layer thickness becomes smaller because the diffusion coefficient decreases with drop size and hence the Schmidt number increases. For drop sizes varying from one atom to 10^6 atoms, the boundary layer thickness varies approximately by a factor of one hundred. This means that the droplet equations must be solved over a distance of many boundary layers, which is very difficult to do numerically. This problem is avoided if the drop and monomer diffusion coefficients are assumed equal. This approach was tried first and is considerably easier to apply than the perturbation technique described below; the disadvantage of this approach is that mobility of the large drops is overestimated.

In the second case, the drop diffusion coefficient variation with drop size was assumed equal to $D/g^{2/3}$. To handle the variation in the drop boundary layer thickness with drop size, the method of singular perturbations[45] was used to develop expansions in the inner and outer regions of the droplet boundary layer. The expansions were then matched in a suitable fashion to give a continuous solution in the entire region. The method still required a numerical solution over the outer region but the solution over the inner region was given analytically. The advantage of this was that the inner region was the only one involving the variable boundary layer thickness; the outer region was always equal to the monomer boundary layer thickness. The technique and the resulting equations are shown in Appendix D.

The range of drops sizes used in solving the droplet conservation equation was from 10 to 10^{20} atoms. A range of this magnitude was required, even though drops of size greater than 10^{9} made no contribution to the monomer source terms and thus had no effect on the coupling between the monomer and drop equations, because the boundary condition for large g required setting the drop concentration equal to zero at some large drop size. Unless this point was considerably beyond 10^{9}, an effect upon the drop distribution was found; even though the large drops were not affecting the monomer concentration directly through the source term, they influenced drop concentrations at other drop sizes. For this reason 10^{20} was used for all cases.

The results were calculated for a temperature range of 1500°K to 1900°K for iron vaporizing into argon at 300°K.

The properties such as the surface tension and density of liquid iron in the nucleation kinetic parameters, coefficients, and expressions were evaluated at the film temperature of the boundary layer. This is consistent with the usual method of evaluating properties in a non-isothermal boundary layer. The properties used in the solution are shown in Appendix G.

1. Effect Upon the Vaporization Rate

The effect of nucleation in the boundary layer on the vaporization rate from a rotating disk is shown in Fig. 3. Here the condensation factor ϕ_{cond} is plotted as a function of wall temperature. The condensation factor is the ratio of the vaporization rate with condensation to that without condensation (Eq. (67)). The effect of drops diffusing back into the wall was neglected in calculating the condensation factor because it was less than 1% of the monomer mass flux at the wall in all cases. The results in Fig. 3. are for a rotational speed of 1500 rad/sec (the rotational speed enters the calculation via α_g^+ and β_g^+ in the monomer source term). For no condensation, ϕ_{cond} is independent of temperature and has a value of unity. The line labeled $D_g = D$ is obtained by assuming the drop diffusivity equal to the monomer diffusivity for all g. Figure 3 shows that below a wall temperature of 1600°K the effect of condensation is zero, and above it the effect increases with temperature. At a wall temperature of 1900°K the enhancement is a factor of two and one-half. The line labeled $D_g = D/g^{2/3}$ is obtained by solving the singular perturbation form of the droplet equation. The wall gradient in this case increases much faster with temperature than the gradient in the constant diffusivity case. At a wall temperature of 1900°K the enhancement is approximately a factor of six.

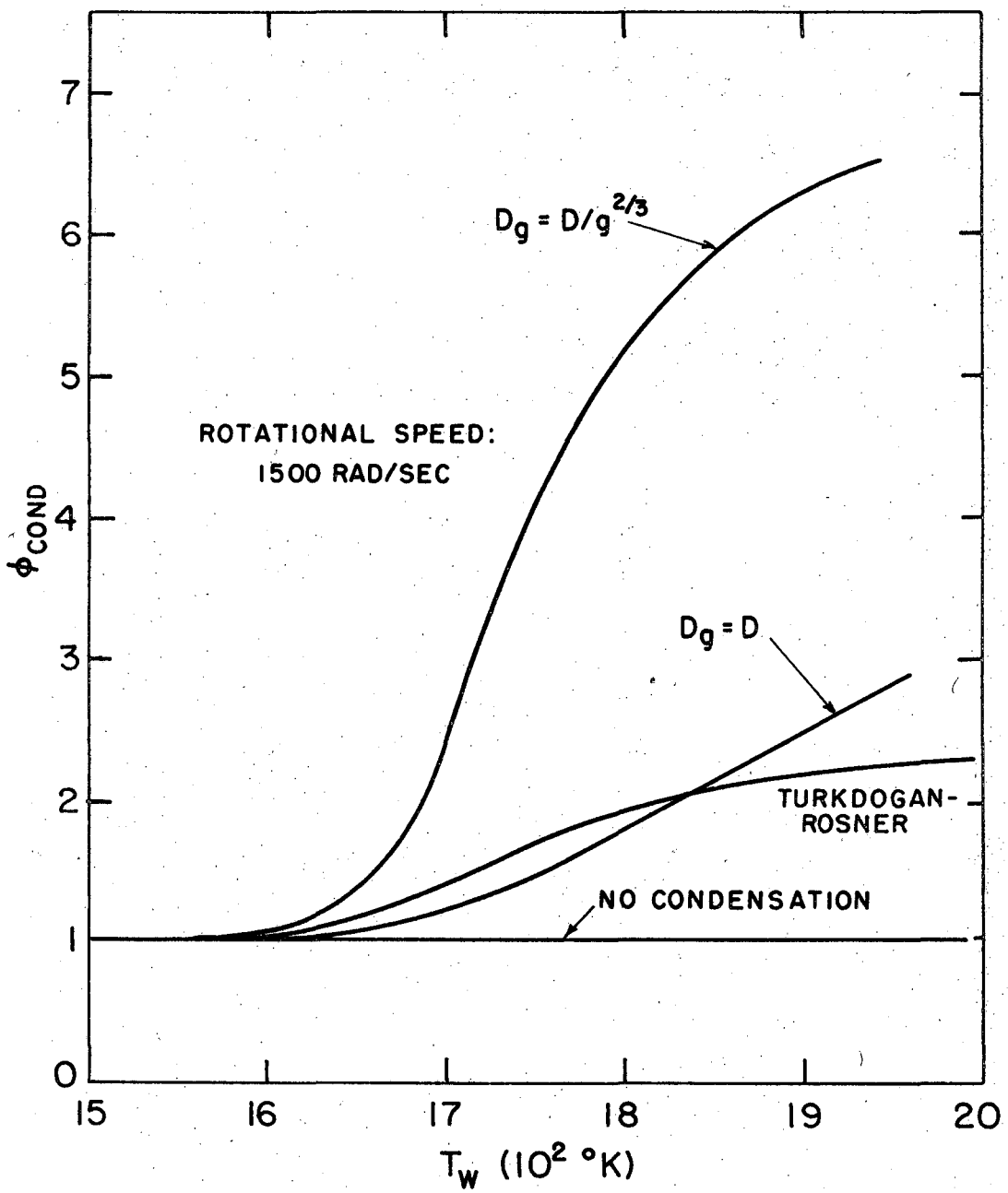
$D_g = D/g^{2/3}$
ROTATIONAL SPEED:
1500 RAD/SEC
$D_g = D$
TURKDOGAN-
ROSNER
NO CONDENSATION
ϕ_{COND}
T_w (10^2 °K)
0
1
2
3
4
5
6
7
15
16
17
18
19
20

Fig. 3

The reason for the greater enhancement in the variable diffusivity case is that the low diffusivity of the large drops gives them less mobility. They then have a greater tendency to move with the bulk velocity. This has two effects. First, the large drops find it more difficult to diffuse into the region close to the wall where the convection transport is weak. This is important because the region close to the wall is much hotter than the outer regions and a drop which tended to grow in the cooler outer region will tend to evaporate, or at least grow much less rapidly, near the wall. The drops tend to evaporate in this region because the evaporation coefficient α_g is a very sensitive function of temperature and increases rapidly as the temperature is raised. Thus the ability of the drops to evaporate is smaller in the variable diffusivity case and so the monomer sink is larger and hence the wall gradient is increased. The second effect arises from drops leaving the nucleation zone in the direction of the outer boundary layer edge. As the diffusion coefficient becomes smaller, the ability of the drops to move outward against the convective flow is lessened. Thus these drops have more of a tendency to stay in that part of the boundary layer where their effect on the monomer sink term is larger. In the outer regions of the boundary layer the drops may have a strong tendency to grow because of the low evaporation coefficient α_g^+ caused by the low temperature, but at the same time the monomer concentration in this region is very small and the effect of depressing it on the gradient at the distant wall is negligible. Thus any drop which diffuses into this region no longer contributes effectively to the monomer sink. Thus the smaller diffusion coefficient of the variable diffusivity case increases the monomer sink and so increases the net evaporation rate.

It can be seen in Fig. 3 that the effect of these two actions described above is to increase the condensation factor in the variable diffusivity case over that in the constant diffusivity case by a factor of two and one-half at 1900°K. However, the point at which nucleation becomes significant is practically the same in the two cases, i.e. 1600°K. This is consistent because a variation in the drop diffusion coefficient cannot affect the wall gradient until a large number of drops are formed by nucleation.

The Turkdogan-Rosner results from Table I are also shown in Fig. 3. The enhancement in this case is approximately equal to that in the constant diffusivity case.

Figure 4 shows the vaporization rate in milligrams per square centimeter per hour from an iron rotating disk as a function of wall temperature. The bulk equilibrium condensation results from Table I are also included in Fig. 4. Figure 4 shows that while the no-condensation vaporization rate increases rapidly with temperature, the rates for the nucleation cases increase more rapidly and the rate in the variable diffusivity case is beginning to approach the bulk equilibrium condensation rate. At 1900°K the rate in the variable diffusivity case is six times the no-condensation rate and only a factor of three below the bulk condensation rate. The constant diffusivity vaporization rate is smaller and is approximately a factor of ten below the bulk condensation rate.

Figure 5 shows the vaporization rate versus reciprocal temperature. The no-condensation and bulk condensation cases here are straight lines. The uniform diffusivity and perturbation cases are not straight lines indicating that the processes are not governed by a constant activation energy. However, they curve only a little and so a constant activation energy would be a good approximation.

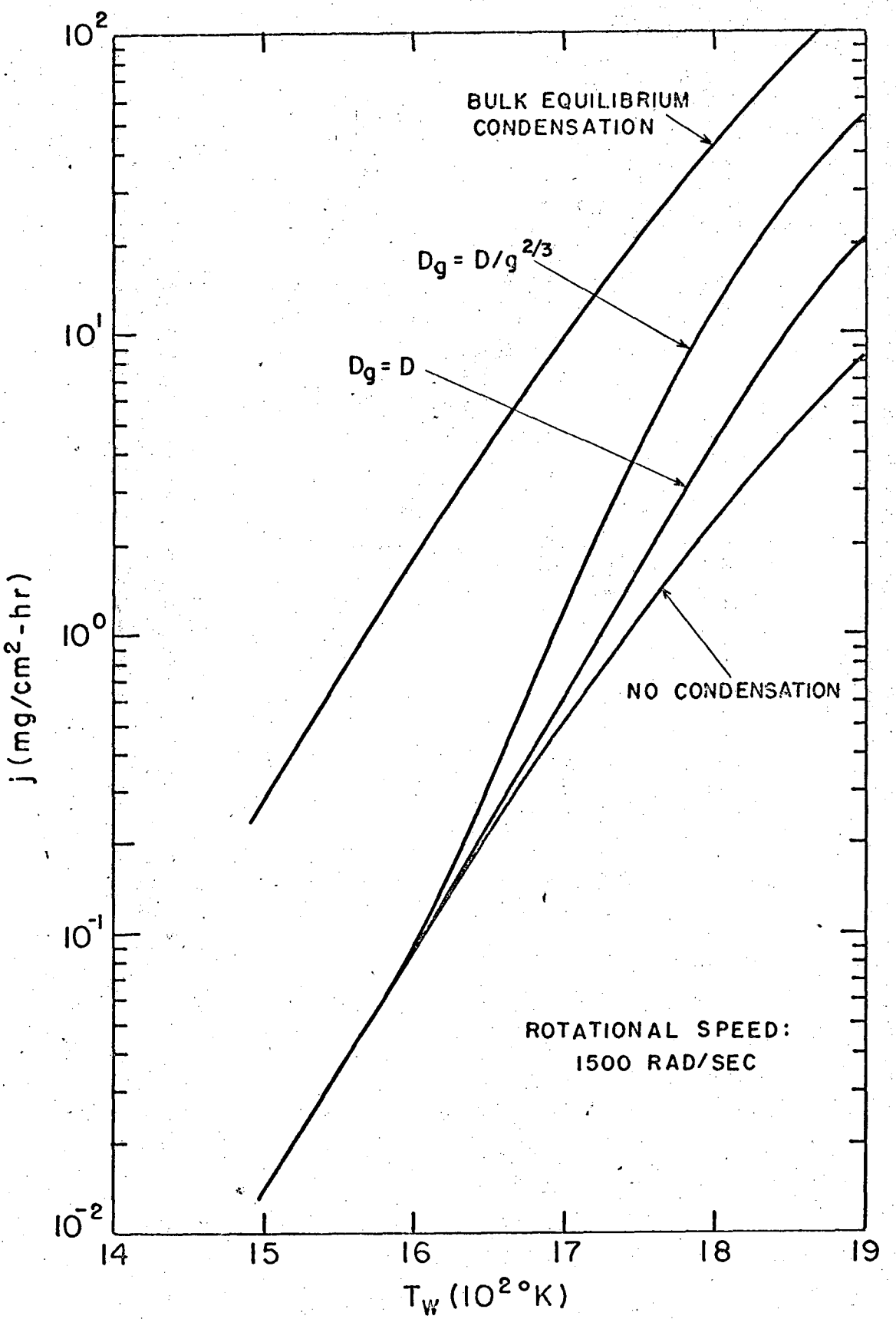
BULK EQUILIBRIUM CONDENSATION
$D_g = D/g^{2/3}$
$D_g = D$
NO CONDENSATION
ROTATIONAL SPEED: 1500 RAD/SEC
j (mg/cm²-hr)
T_w (10^2°K)
10^2
10^1
10^0
10^{-1}
10^{-2}
14
15
16
17
18
19

Fig. 4

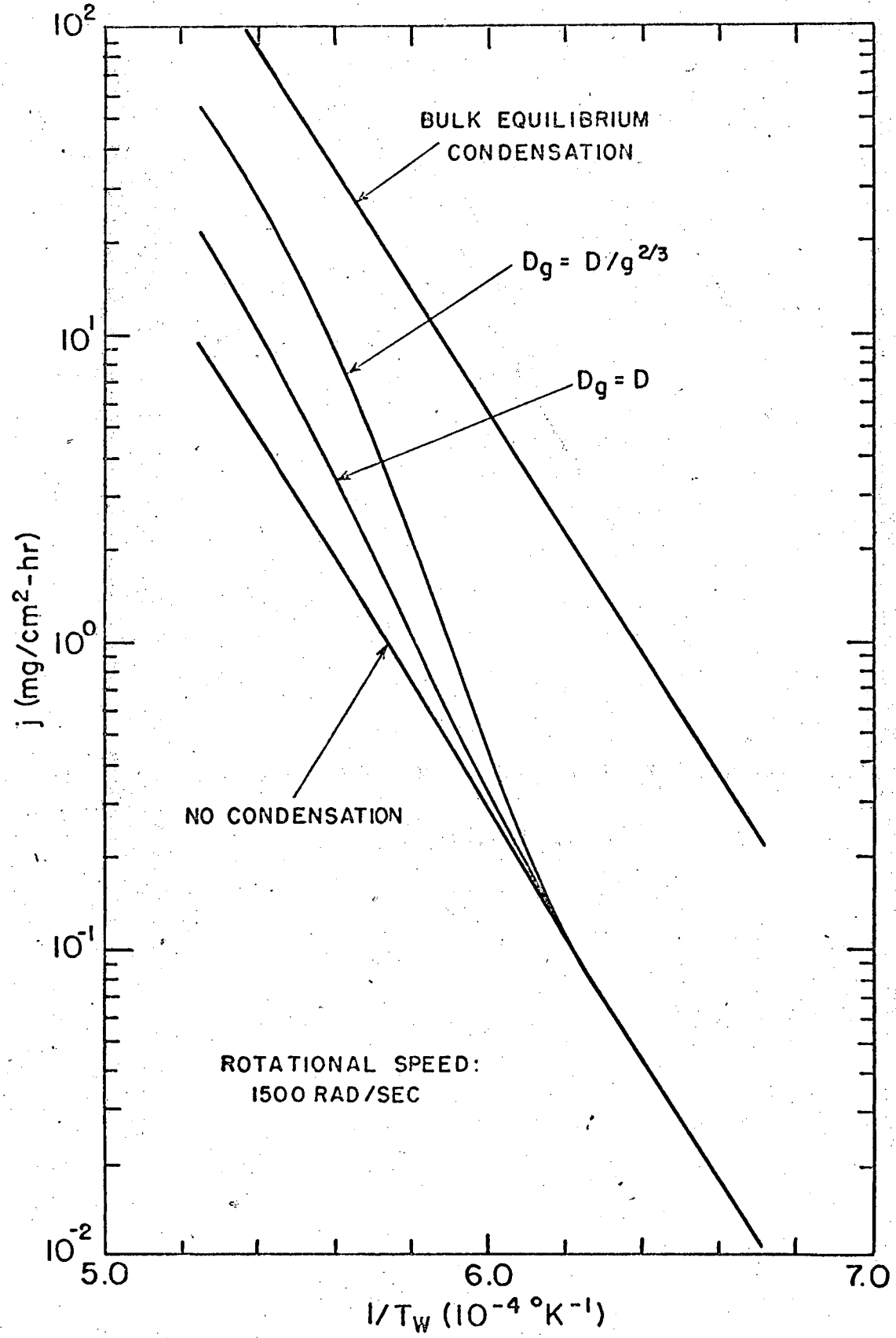
BULK EQUILIBRIUM CONDENSATION
$D_g = D/g^{2/3}$
$D_g = D$
NO CONDENSATION
ROTATIONAL SPEED: 1500 RAD/SEC
j (mg/cm²-hr)
10^2
10^1
10^0
10^{-1}
10^{-2}
5.0
6.0
7.0
$1/T_W$ (10^{-4} °K^{-1})

Fig. 5

The calculations could not be extended to very large enhancements where the vaporization rate approaches the bulk equilibrium condensation case. When this was attemped, the program became unstable and convergence could not be obtained. The reason for this is indicated in the next section.

2. Structure of the Nucleation Zone in the Boundary Layer

Figure 6 shows a typical nucleation rate J profile as a function of axial distance through the boundary layer.* Then nucleation rate was calculated from the classical Becker-Doring-Zeldovich expression, Eq. (26). The important characteristic of Fig. 6 is the existence of a "nucleation zone," i.e. a region where the nucleation rate is very high, and which is surrounded on either side by a region with a relatively low nucleation rate. Such a zone was also found by Ronser and Epstein.[12] It is in this nucleation zone that the drops are formed. The maximum nucleation rate in the zone occurs at x = 2.25, or a little more than half-way through the boundary layer. The rotating disk boundary layer is generally considered to end at x = 3.25. The zone is skewed toward the outer region of the boundary layer and occupies approximately 65% of it. The nucleation rate between x = 0 and x = 1, i.e. in the first 30% of the boundary layer is essentially zero compared to the nucleation rate further out in the boundary layer. The nucleation rate in the zone is approximately 10^{14} drops/cm^3-sec, which is comparable the maximum nucleation rate of 10^{14} drops/cm^3-sec, in Epstein and Rosner's study.[12] No special significance can be attached to this, however, for there is no obvious reason why they should be the same in different systems.

Figure 7 shows a typical droplet size distribution in the nucleation zone. The infinite-medium steady state solution is also plotted for comparison. The boundary layer solution approaches the infinite medium solution for small drop sizes as required by the boundary condition. For large drops, it falls increasingly below the infinite medium solution as drop size increases. This is expected behavior because in the

---

* The nucleation rate is the net rate at which drop of critical size are produced per cm^3 per sec; since the steady state infinite medium droplet distribution is assumed to exist for all drops smaller than g_0 the nucleation rate is also the rate at which drops of size g_0 are produced per cm^3 per sec.

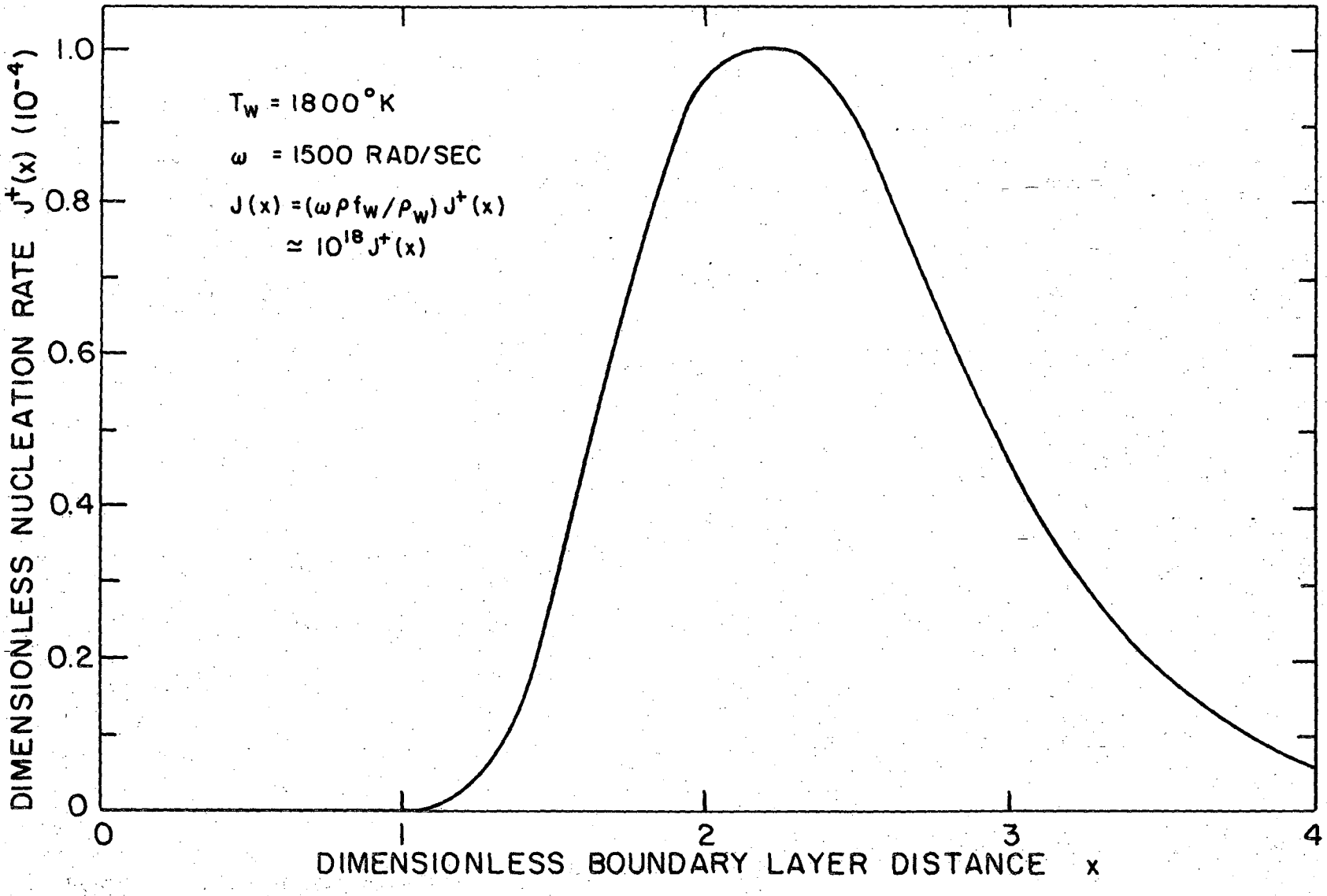
DIMENSIONLESS NUCLEATION RATE $J^+(x)$ (10^{-4})
1.0
0.8
0.6
0.4
0.2
0
T_w = 1800°K
ω = 1500 RAD/SEC
$J(x) = (\omega \rho f_w / \rho_w) J^+(x)$
$\simeq 10^{18} J^+(x)$
0
1
2
3
4
DIMENSIONLESS BOUNDARY LAYER DISTANCE x

Fig. 9

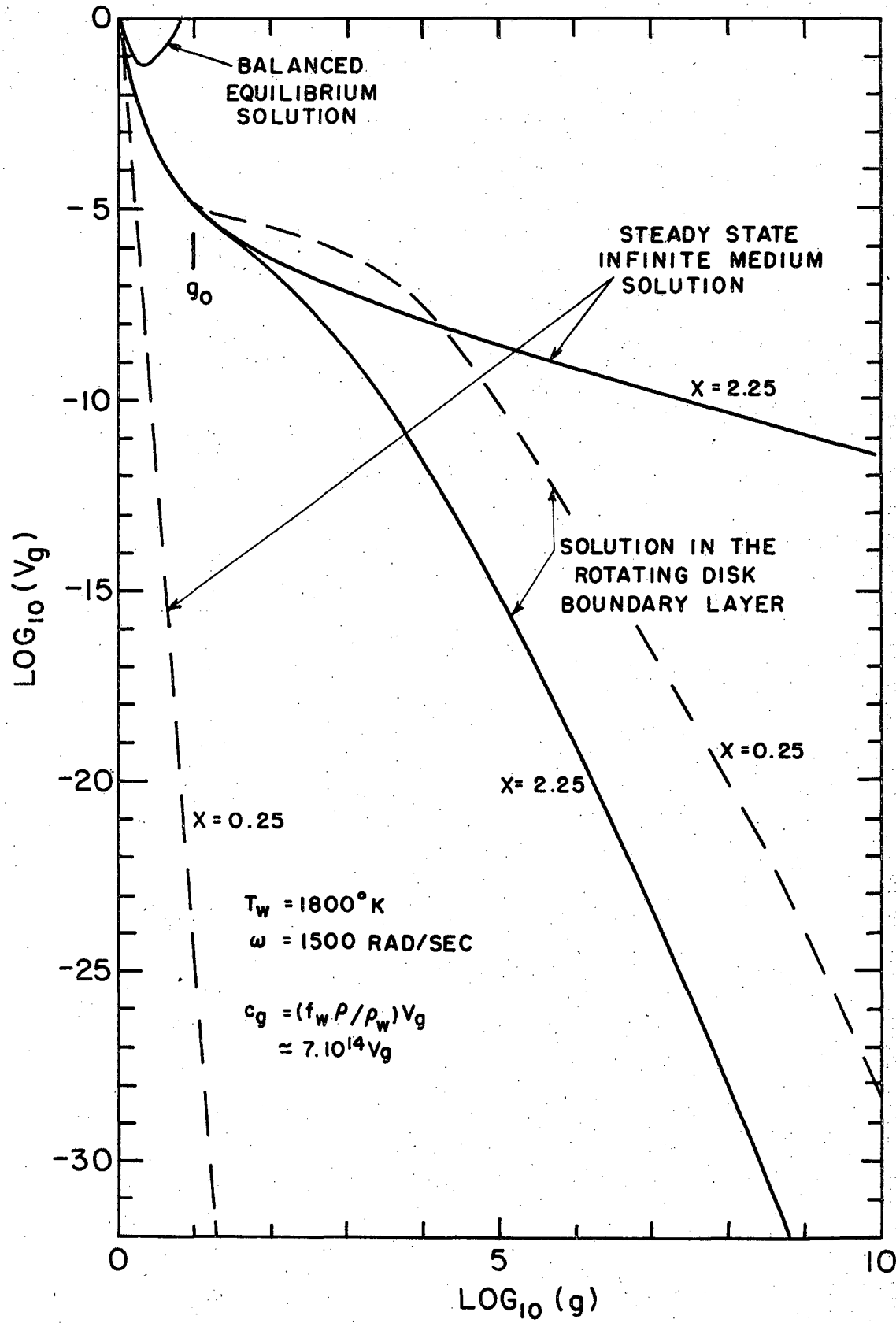
BALANCED
EQUILIBRIUM
SOLUTION
STEADY STATE
INFINITE MEDIUM
SOLUTION
g_o
X = 2.25
SOLUTION IN THE
ROTATING DISK
BOUNDARY LAYER
X = 0.25
X = 2.25
X = 0.25
T_w = 1800° K
ω = 1500 RAD/SEC
$c_g = (f_w \rho / \rho_w) V_g$
$\simeq 7.10^{14} V_g$
$LOG_{10}(V_g)$
$LOG_{10}(g)$
0
-5
-10
-15
-20
-25
-30
0
5
10

Fig. 7

infinite medium solution the drop current J is constant and hence the same number of drops pass through each size. In the boundary layer case, drops can also leave an incremental space-size volume by convection and diffusion. The infinite medium balanced equilibrium distrubtion is also shown in Fig. 7. The minimum of the curve is the critical drop size and the figure shows that it is approaching atomic size. The value of g_0, i.e. the match point between the infinite medium solution and the boundary layer solution, was ten of this case and is shown in the figure. Two dashed lines are also shown in Fig. 7. These are the infinite medium and boundary layer solutions at x = 0.25, i.e. far from the nucleation zone. They show that the boundary layer droplet concentration is much larger than the infinite medium concentration at this point; this is because drops have been transparted by diffusion and convection from the nucleation zone. Also note that the drop concentration for any particular size g is higher at x = 0.25 than at x = 2.25. This is because drops formed near x = 2.25 are transported away from the region and into the region near x = 0.25.

Figure 8 shows the variation of the evaporation and condensation coefficients with axial position in the boundary layer for a typical drop size. The evaporation coefficient α_g^+ is higher than the condensation coefficient β_g^+ near the wall where the temperature is high. This is because the vapor pressure is a rapidly increasingly function of temperature and evaporation coefficient is proportional to the vapor pressure at the drop temperature. As the temperature decreases through the boundary layer the evaporation coefficient falls rapidly and is considerably smaller than the condensation coefficient throughout most of the boundary layer. The linear scale is somewhat deceptive at large x, for at x = 4, the evaporation coefficient is orders of magnitude below the condensation coefficient. However, the

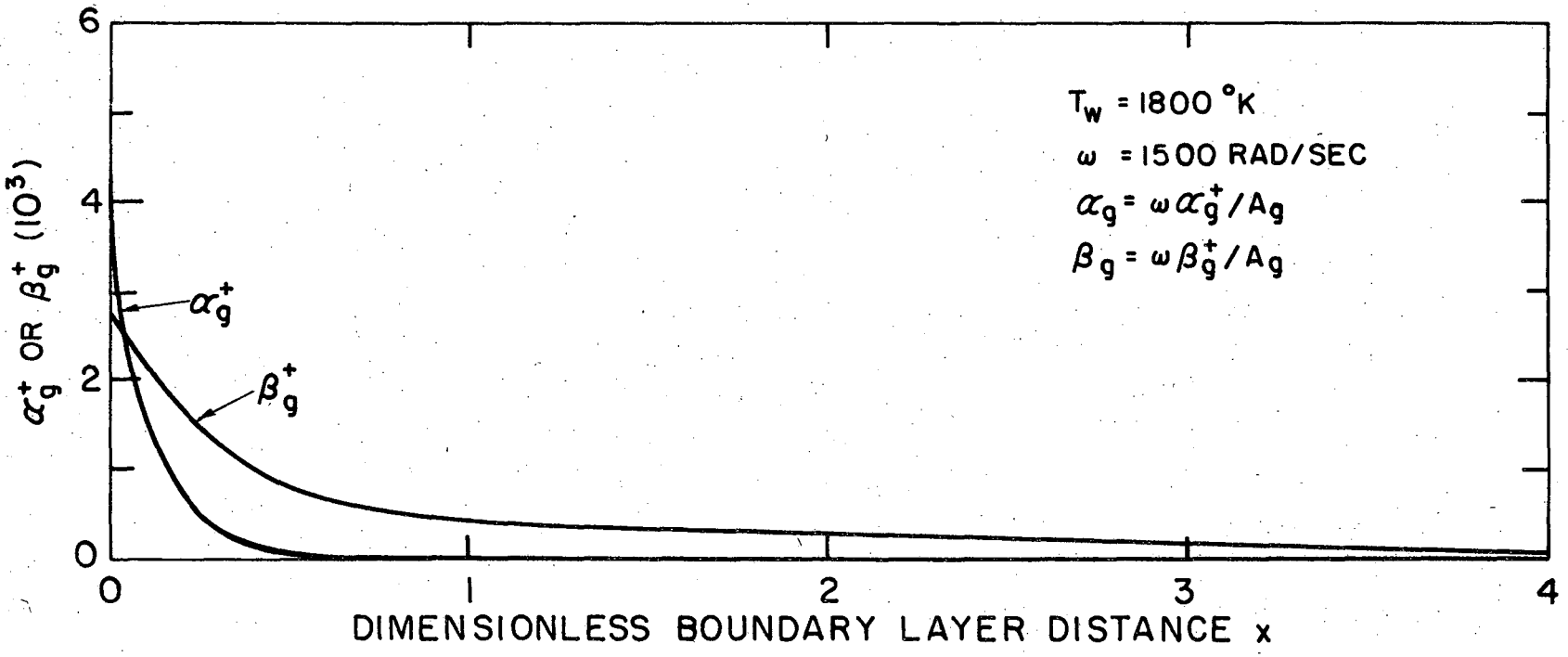
6
4
2
0
0
1
2
3
4
α_g^+ OR β_g^+ (10^3)
DIMENSIONLESS BOUNDARY LAYER DISTANCE x
T_w = 1800 °K
ω = 1500 RAD/SEC
$\alpha_g = \omega \alpha_g^+ / A_g$
$\beta_g = \omega \beta_g^+ / A_g$
α_g^+
β_g^+

Fig. 8

important point is that drops diffusing or convected towards the wall will tend to evaporate rather than grow.

Figure 9 shows the monomer source term versus axial distance through the boundary layer for a typical case. The source is positive close to the wall because of the high evaporation coefficient there. It, however, rapidly becomes very negative because the evaporation coefficient quickly decreases with axial distance while the condensation coefficient remains relatively high. Thus drops formed in the nucleation zone and transported to this region grow very rapidly and in doing so consume monomer, thus driving the monomer source term to large negative values. Note that Fig. 6 indicates that very few drops were born in the region where the large negative source occurs, and Fig. 9 indicating that little monomer is consumed in the nucleation zone. The small drops born in the nucleation zone comsume little monomer while being transported out of it; however at they grow to big drops nearer the wall the amount of monomer they consume increases tremendously. This is consistant with the results of steady-state infinite medium theory where it has been found that the larger drops consume the most monomer.[4] As x increases, the monomer source returns to zero because the monomer concentration and hence the condensation coefficient, has been depressed to the point where the drops grow much more slowly. Thus they do not deplete the monomer as rapidly and the monomer sink term is small.

The oscillatory nature of the monomer source caused many numerical problems in the machine program. It was the principle reason that the calculation could not be made for large enhancements in the vaporization rate, i.e. for vaporization rates approaching the bulk equilibrium condensation rate value. The reason for this is that the monomer source is, in effect, the small difference of two large numbers (note the large

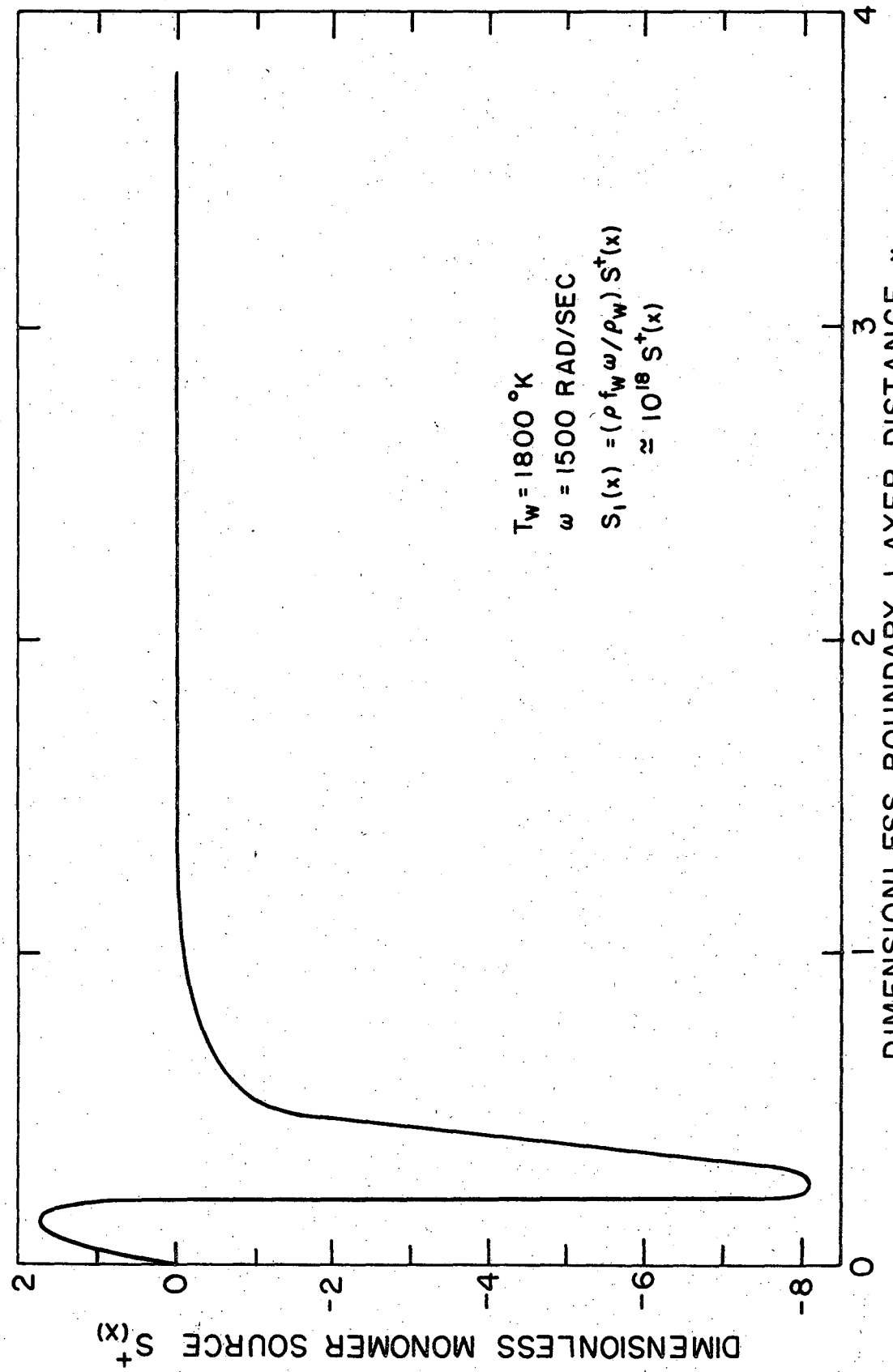
$T_w = 1800\ ^\circ K$
$\omega = 1500$ RAD/SEC
$S_1(x) = (\rho f_w \omega / \rho_w) S^+(x)$
$\simeq 10^{18} S^+(x)$
DIMENSIONLESS BOUNDARY LAYER DISTANCE x
DIMENSIONLESS MONOMER SOURCE $S^+_{(x)}$
0
1
2
3
4
2
0
-2
-4
-6
-8

Fig. 9

positive and negative variation in Fig. 9). Thus any error made in computing the source in the positive or negative regions has a large effect on the monomer concentration.

Figure 10 shows a schematic of the process of condensation and revaporization of the drops in the boundary layer. The case for an isothermal system is shown in the left. Here the gas is at the same temperature as the disk and the evaporating species simply diffuses out into the boundary layer. On the right, the non-isothermal system with condensation and revaporization of the drops is shown. Here the drops are formed out in the boundary layer and grow as they proceed toward the disk. As they come close to the hot disk, the tendency to evaporate becomes greater than the tendency to grow and so the drops began to revaporize.

Figure 11 shows the dimensionless contribution from the individual groups to the monomer source term for a typical case. The profile in g-space was taken at the position of the maximum negative monomer source, $x = 0.25$. Plotted on the ordinate is the product $g \cdot S_g^+(x)$ which is the negative of the contribution to the monomer source from a group with source $S_g^+(x)$. The total monomer source $S^+(x)$ is given by the sum of the contributions from the individual groups, i.e. $S^+(x) = - \sum_g g\, S_g^+(x)$, and so $S^+(x)$ is equal to the area under the curve in Fig. 11. The figure shows that drop sizes between 10^3 and 10^6 are the principle contributors to the monomer source. Drop sizes below 10^3 and above 10^6 have negligible contributions. For drop sizes below 10^3, the boundary layer droplet concentration in g-space (see Fig. 7) begins to approach the infinite medium solution for which $S_g^+(x) = 0$. Thus the contribution from groups of small drop size must approach zero. Figure 7 shows that the boundary layer droplet

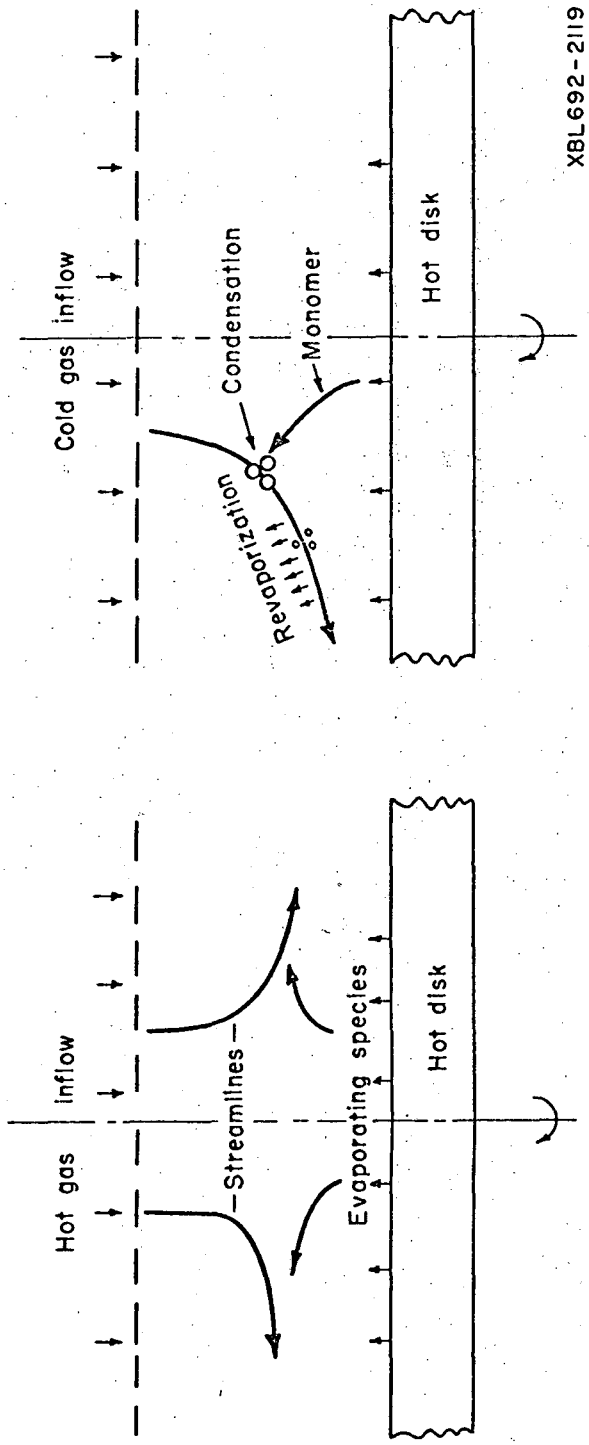
Cold gas
inflow
Condensation
Monomer
Hot disk
Revaporization
XBL692-2119
Hot gas
inflow
Streamlines
Evaporating species
Hot disk

Fig. 10

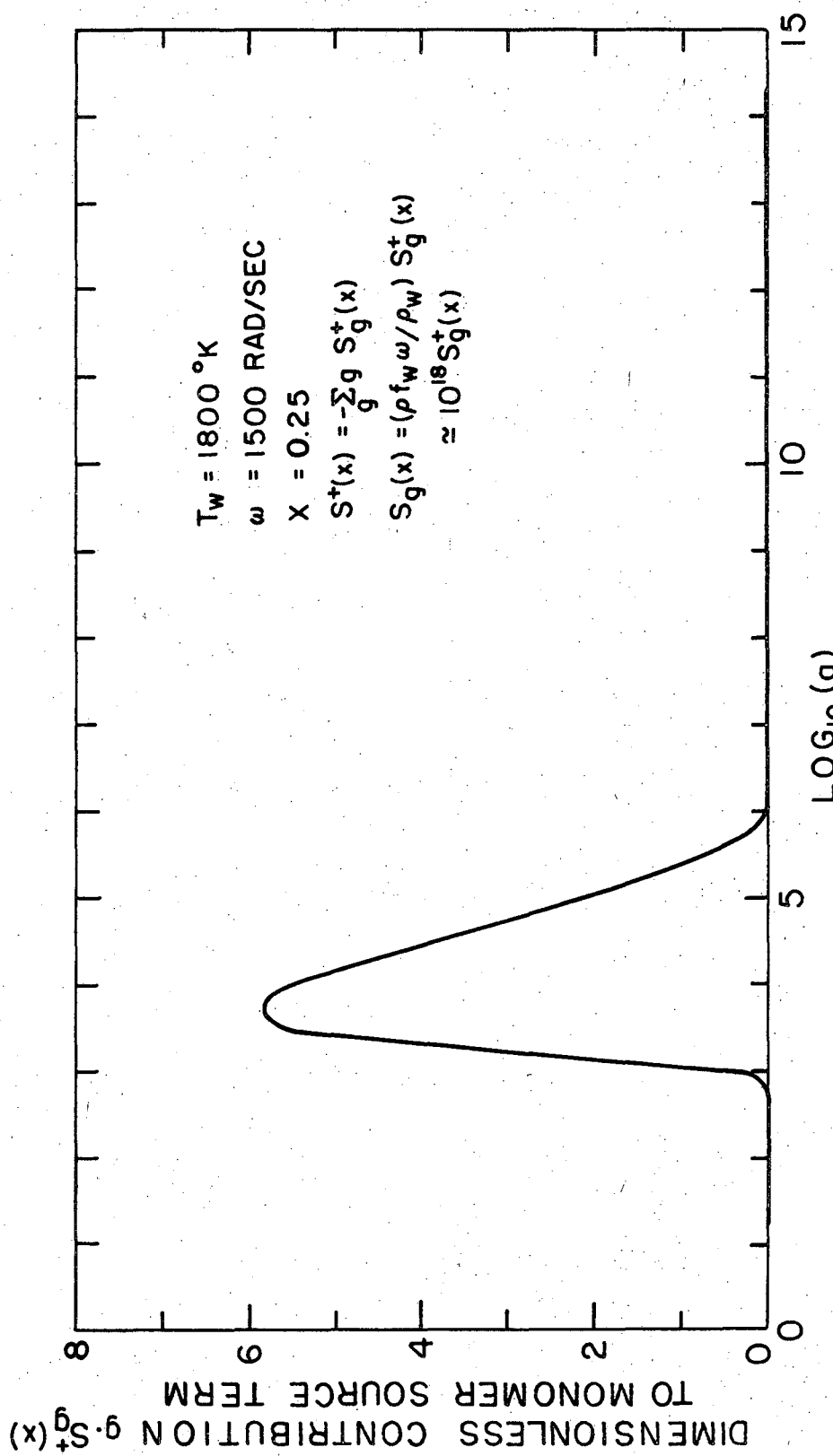
T_w = 1800 °K
ω = 1500 RAD/SEC
X = 0.25
$S^+(x) = -\sum_g g\, S_g^+(x)$
$S_g(x) = (\rho f_w \omega/\rho_w)\, S_g^+(x)$
$\simeq 10^{18} S_g^+(x)$
LOG$_{10}$(g)
0
5
10
15
0
2
4
6
8
DIMENSIONLESS CONTRIBUTION $g \cdot S_g^+(x)$
TO MONOMER SOURCE TERM

Fig. 11

concentration falls rapidly as the drop size increases. For drop sizes greater than 10^6, the contribution to the monomer source term again approaches zero because the droplet concentration becomes so small. Thus only intermediate drop sizes contribute to the source term.

Figure 12 shows the ratio of the drop temperature to wall temperature versus drop size for a location in the nucleation zone. For most drop sizes the drop temperature is equal to the temperature of the surrounding gas; only at the large drop sizes does the drop temperature differ from the gas temperature. As the drop increases beyond 10^{15} atoms in size, the drop temperature rises quite rapidly because of thermal radiation and approaches the wall temperature at a size of 10^{20}. The reason the drop temperature remained very close to the gas temperature over such a large range is that the rate at which heat was removed from the drop by gas atoms colliding with it was very large, i.e. coefficient of the fourth term in Eq. (29) was very large. The pressure of the surrounding gas in our calculations was one atmosphere. At this pressure the effect of radiation from the disk to the drops is important only for very large drops and these do not exist in appreciable quantites. For nucleation in rarified environments, however, the effect of radiation would become very important because the heat removed by gas atoms colliding with the drops would be much smaller and hence the drop temperature would depart from the gas temperature at much smaller drop sizes.

In summary, the structure of the nucleation in the boundary layer is such that drops are produced in significant quantites only near the middle of the boundary layer. Many of the drops formed there are than transported by diffusion and convection into the region close to the wall where they evaporate. This effect produces a cycle because the monomer

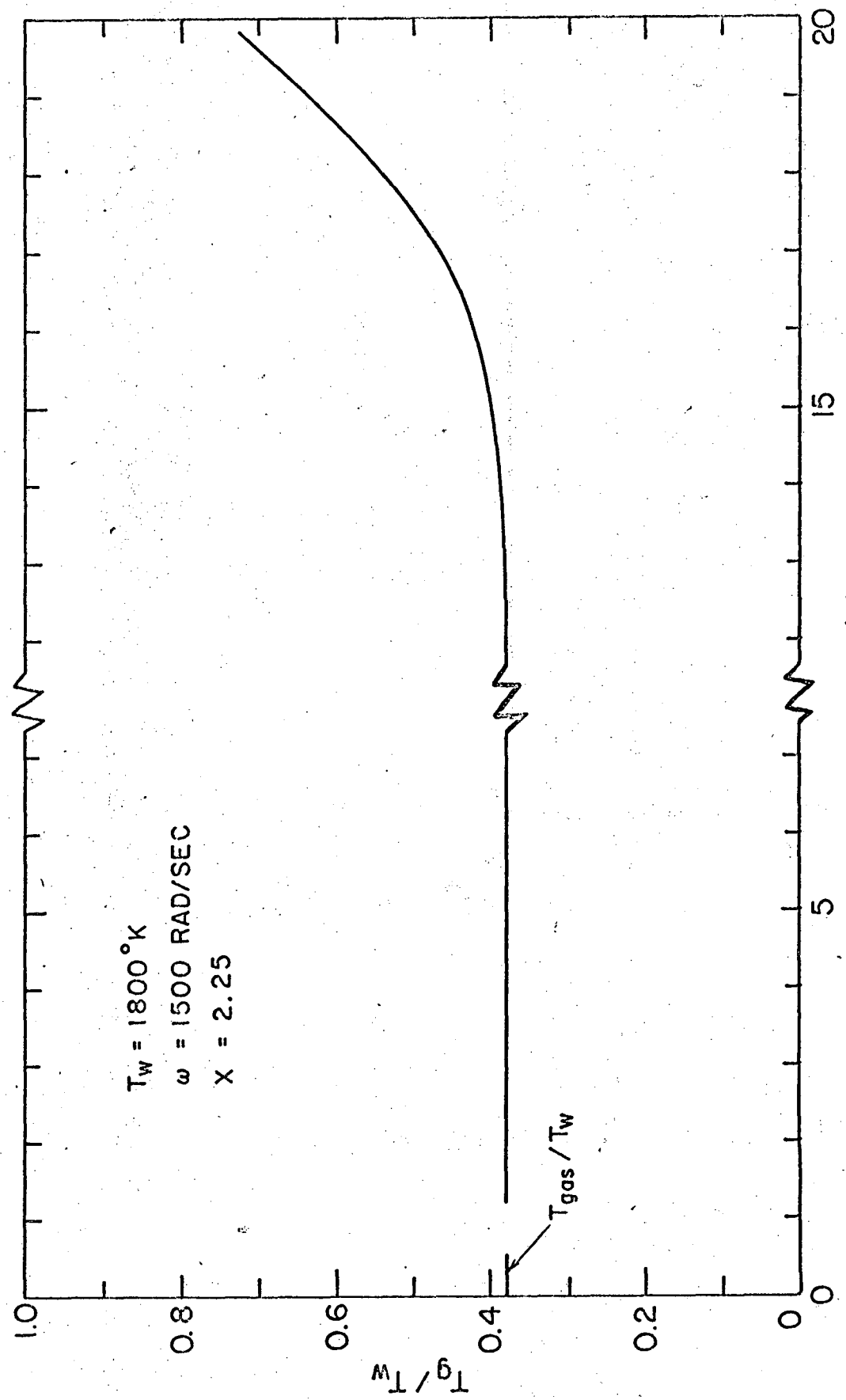
T_g / T_w
1.0
0.8
0.6
0.4
0.2
0
T_{gas} / T_w
T_w = 1800°K
ω = 1500 RAD/SEC
X = 2.25
0
5
15
20
$LOG_{10}(g)$

Fig. 12

produced by the drops evaporating is transported away from the wall and into the nucleation zone where some of it must again be formed into drops (see Fig. 10). The effect then repeats itself. Thus a recycle is superimposed upon the ordinary outward transport of the vaporizing species which normally occurs in the rotating disk boundary layer.

In addition, the drop concentration in g-space in the nucleation zone rapidly becomes much smaller than the concentration given by the infinite medium solution. Since the drop concentrations must be equal for small size, the behavior causes only the intermediate drop sizes to contribute to the monomer sink. Finally, the effect of thermal radiation from the hot disk to the drops is negligible if the surrounding gas is at atmospheric pressure.

3. Effect of Some Parameter Variations

The effects of variation of the angular velocity of the rotating disk, and the surface tension of the liquid metal upon the gradient at the wall were examined. Figure 13 shows the effect of angular velocity variation. Here the vaporization rate is plotted against the square root of the angular velocity. Experimentally the effect of natural convection would become quite strong below 300 rad/sec and so the calculations were terminated at this speed. As the angular velocity decreased from 2100 rad/sec to 300 rad/sec the gradient at the wall $(\frac{dU}{dx})$ increased monotonically. The gradual increase in the wall gradient is what would be expected because the angular velocity enters the source term through the dimensionless evaporation and condensation coefficients α_g^+ and β_g^+. As the angular velocity is decreased, droplet source terms become larger and so the monomer sink terms become larger. Thus the gradient at the wall increases. The vaporization rate j (which is proportional to $\sqrt{\omega}\ (\frac{du}{dx})_w$), however, increases with an increase in angular velocity as Fig. 13 shows. This is the expected behavior because both the no-condensation and bulk equilibrium condensation limits behave in this fashion.

Figure 14 shows the effect of a variation in surface tension on the gradient at the wall. The gradient increases as the surface tension decreases, because the evaporation coefficient α_g^+ decreases. Thus the rate at which drops evaporate near the rotating disk wall is lessened and so the gradient at the wall is increased.

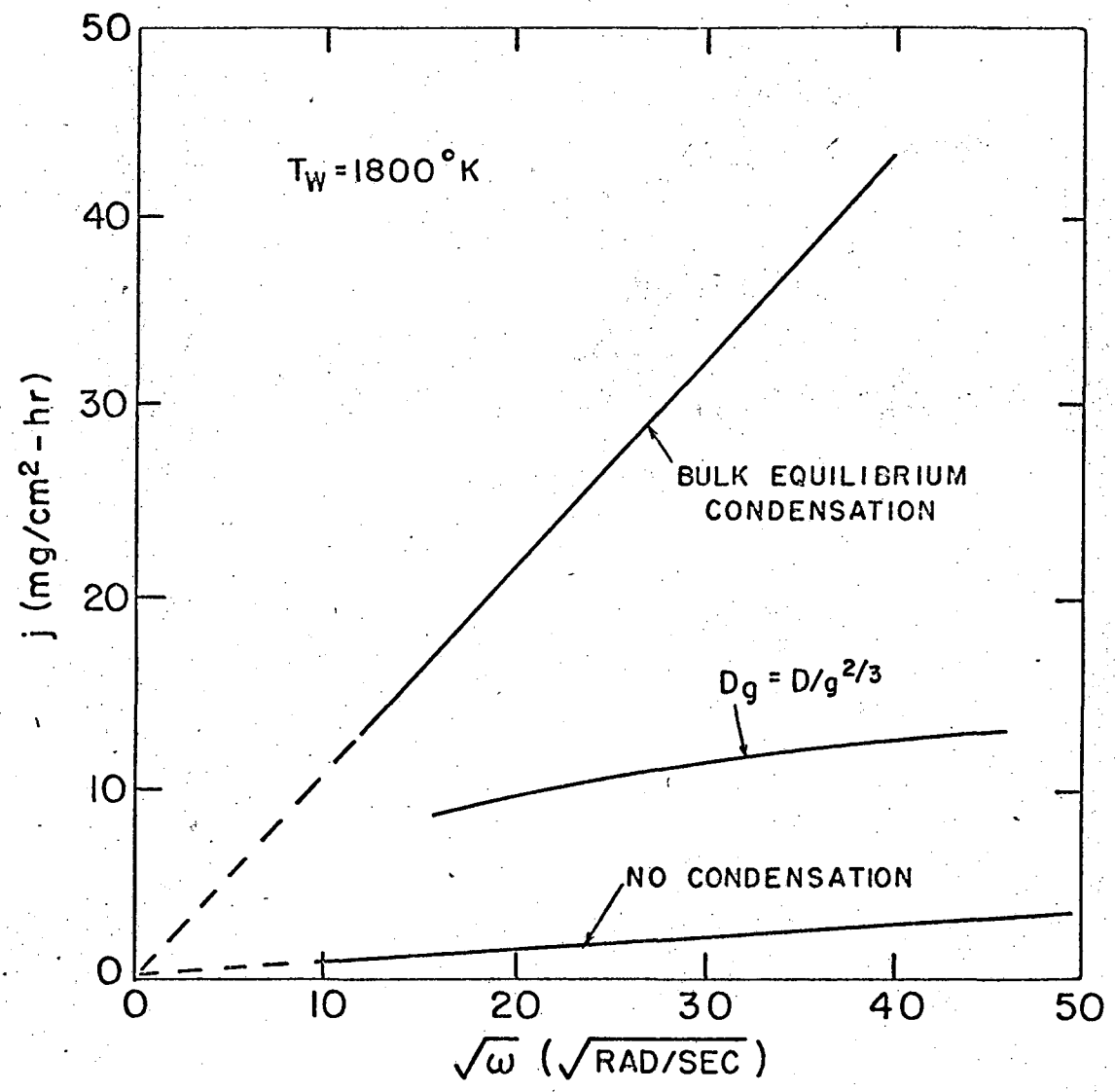
50
40
30
20
10
0
0
10
20
30
40
50
$T_W = 1800°K$
BULK EQUILIBRIUM CONDENSATION
$D_g = D/g^{2/3}$
NO CONDENSATION
j (mg/cm²-hr)
$\sqrt{\omega}$ ($\sqrt{\text{RAD/SEC}}$)

Fig. 13

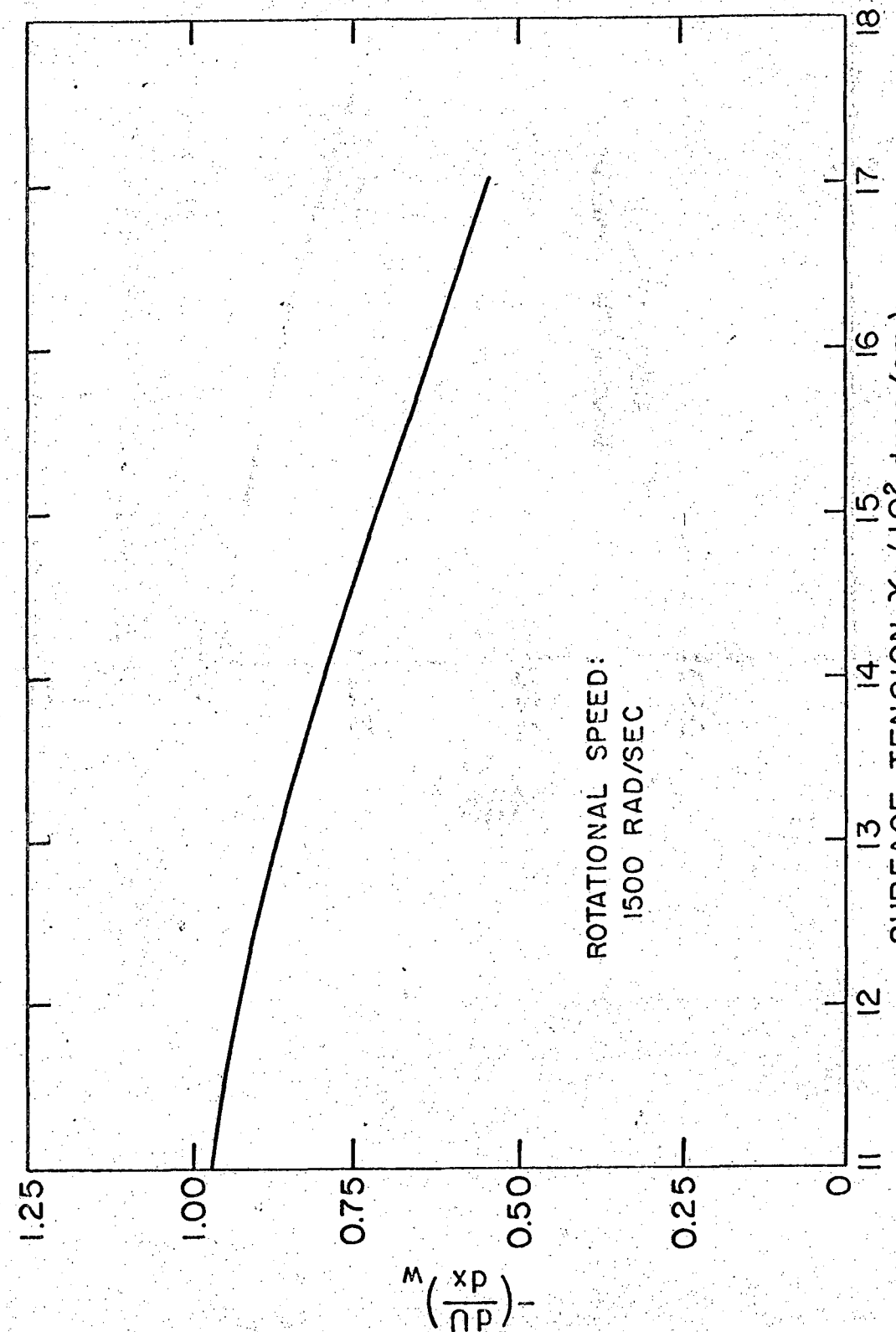
1.25
1.00
0.75
0.50
0.25
0
11
12
13
14
15
16
17
18
SURFACE TENSION γ (10² dyne/cm)
ROTATIONAL SPEED:
1500 RAD/SEC
$-\left(\frac{xp}{\Omega p}\right)_M$

Fig. 14

E. CONCLUSIONS

In conclusion, the calculations indicate the vaporization rate to be enhanced by nucleation in the boundary layer. The magnitude of the enhancement is affected by the diffusivity assigned to the drops, with a lower drop diffusivity resulting in a greater enhancement. If the drop diffusivity is assumed equal to the monomer diffusivity, the enhancement for iron is approximately a factor of two at 1800°K. If the drop diffusivity is given by the more accurate expression $D/g^{2/3}$, then the enhancement is approximately a factor of five at 1800°K. To use this more accurate expression which implies that the boundary layer thickness varies inversely with drop size, a singular perturbation type of analysis is required. This method of analysis shows that each drop size has an inner boundary layer region where diffusion and convection are the predominant modes of transport, and an outer region where convection and production predominate.

The structure of the nucleation in the boundary layer is such that drops are produced in significant quantities only near the middle of the boundary layer. Many of the drops formed there are then transported by diffusion and convection into the region close to the wall where they evaporate. This imposes a recycle effect upon the ordinary outward transport of the vaporizing species which normally occurs in the rotating disk boundary layer.

The drop concentration in g-space in the nucleation zone of the rotating disk is much smaller than the concentration given by the infinite medium solution for large drop sizes. This decrease causes only the intermediate drop sizes to contribute to the monomer sink. Finally, the effect of thermal radiation from the hot disk to the drops is negligible if the surrounding gas is at atmospheric pressure.

PART II EXPERIMENTAL

A. Introduction

The effect of condensation in the thermal boundary layer on the mass transfer rate from a hot metal surface was measured experimentally. This was done by measuring the vaporization rate of a hot rotating disk in a cold inert gas environment with the disk operating at temperatures and angular velocities calculated to produce nucleation in the boundary layer. It was shown theoretically in the previous section that the formation of nuclei should promote condensation and thus increase the vaporization rate. An experimental verification of the effect of condensation on the vaporization rate was sought.

Turkdogan and Mills[9] measured roughly the vaporization rate of molten iron spheres surrounded by helium and cooled by natural convection. The spheres were heated by an induction coil and were suspended by levitation within the coil. They measured a vaporization rate that was approximately three times the isothermal, diffusion-limited, condensation free value calculated from semi-empirical correlations. This factor of three increase in the vaporization rate agrees qualitatively with the predictions of a "critical supersaturation" model proposed by Turkdogan.[1] Their experiments, however, were not conducted with the express purpose of testing the theory of condensation enhancement of the vaporization rate. Therefore, no particular care was taken to insure that certain necessary boundary conditions were attained in the experiment. Thus their experimental results should be considered in the qualitative rather than the quantitative sense. Based on this factor of three increase in the vaporization rate, and on the qualitative agreement between the measured rate and their

"critical supersaturation" model, Turkdogan concluded that condensation in the boundary layer increases the vaporization rate.

Elenbaas[49] measured the vaporization rate of a resistance-heated tungsten filament wound in the shape of a coil and surrounded by krypton gas. The filament was cooled by natural convection. He found little enhnacement in the vaporization rate, and in fact found that the calculated concentration and thermal diffusion fluxes account for 77% of the measured fluxes. The fluxes were calculated using stagnant film theory. These results agree with a theory Elenbaas proposed.[11] This theory assumes that drops formed by nucleation move by diffusion only in a stagnant boundary layer and that they do not penetrate the outer edge of it. With these assumptions, Elenbaas shows that the enhancement should be zero. Elenbaas then concluded that condensation in the boundary layer has little effect on the vaporization rate.

We have attempted to determine the effect of condensation in the thermal boundary layer more precisely and so to resolve this contradiction between Turkdogan's and Elenbaas' conclusions by measuring the vaporization rate with condensation using a rotating disk system. The advantage of the rotating disk system is that the measured rate can be compared with an exactly calculated, condensation-free, theoretical rate. Both Turkdogan and Elenbaas calculated the enhancement by comparing the measured vaporization rate with a theoretical but inexact rate no-condensation rate. Turkdogan could not obtain an exact theoretical rate because semi-empirical correlations are required to calculate the temperature and concentration profiles for spheres cooled by natural convection. Likewise, Elenbaas required stagnant film theory to describe the concentration and temperature profiles around his coil. For the rotating disk system, however, the concentration and temperature profiles can be determined from first

principles and hence, the condensation free vaporization rate calculated exactly.[15,16,34] In addition, diffusion, convection, and growth of the drops formed by nucleation can be exactly described by a set of ordinary differential equations. The solution of these equations gives the condensation-enhanced vaporization rate. The measured rate can then be compared with a calculated rate assuming no nucleation and with a calculated rate considering nucleation where the calculated rates are exact solutions.

The rotating disk also has the advantage of being a precise experimental tool. For example, Olander[32] found very good agreement between theory and experiment while studying the diffusion-limited chemical reaction between iodine and germanium at moderate temperatures (approximately 300°C). Schofill[35] found very good agreement between theory and experiment while studying the diffusion-limited chemical reaction between oxygen and molybdenum at very high temperatures (up to 2000°K). Other studies[16,38] have also shown the exactness of this tool.

In this experiment, the material vaporized was chromium and the environment was cool helium. The disk was heated by induction. The vaporization rate was measured over a temperature range of approximately 100°K at approximately 1700°K.

B. Description of the Experiment

The rotating disk has what is called a "uniformly accessable surface." This is a term which is used to describe the experimental and theoretical fact that the mass flux leaving the disk, or the vaporization rate as we shall call it, is independent of position on the disk. Because of this position independence, the vaporization rate is obtained in an experiment simply by dividing the mass loss of the disk by its cross-sectional area and by the time over which the mass loss occurred. The problem experimentally then is to obtain a measurable mass loss reasonably free from error in a reasonable amount of time.

1. Selection of the Disk Material

The material used in this experiment was chromium. Chromium was chosen because it has a relatively high vapor pressure near its melting point (approximately 8 mm of mercury of 2120°K) while at the same time being relatively inert. The high vapor pressure was necessary to obtain a mass loss large enough to be measured. The material must be relatively inert in order to prevent reactions with other elements in the system from obscuring the mass loss caused by vaporization. For example, a chemical reaction between the disk and the crucible at the temperatures of this experiment could easily produce a large mass change in the disk. Also, simple diffusion of the crucible elements into the disk can be a large source of error. A reaction can also occur with impurities in the inert gas stream. Any one, or a combination of all of these, can easily introduce errors much larger than the value intended to be measured.

Iron was initially tried because the disks could be easily machined from it by conventional methods. However, the vapor pressure and melting

temperature of iron are lower than those of chromium, and to obtain a measurable mass loss, the disks had to be run very close to their melting point. This was difficult to do because iron has a phase transition near its melting point and at the transition the properties, especially the specific heat, change quite rapidly. This caused the temperature of the disk to change quite rapidly for small changes in input power from the induction heater with the consequence that the disks invariably melted. Thus chromium was chosen. It, however, was considerably more difficult to fabricate since it cannot be machined but must be spark-cut. This had the effect of limiting the number of data points which could be taken because of the considerable effort required to make a disk.

2. Equipment Description

The experiment is sketched in Fig. A. The chromium disk to be vaporized was rotated by a synchronous electric motor while heated by an induction heater. The disk was contained in a boron nitride crucible which was attached to a tantalum shaft. A thin tungsten liner was placed between the chromium and the boron nitride in order to prevent a chemical reaction between them; The reaction between tungsten and boron nitride is much smaller than that between chromium and boron nitride. The synchronous motor drove the tantalum shaft through a water-cooled bearing block. The water cooling was required to prevent overheating of the bearings and the electric motor. The shaft was made long and thin to reduce the amount of heat transferred from the hot disk down the shaft to the bearings and motor. The shaft was 0.25 inches in diameter and six inches long with approximately three inches of it extending above the water-cooled bearing block. The boron nitride holder was approximately one centimeter high by slightly more than one centimeter in diameter at its top. The motor was driven at constant

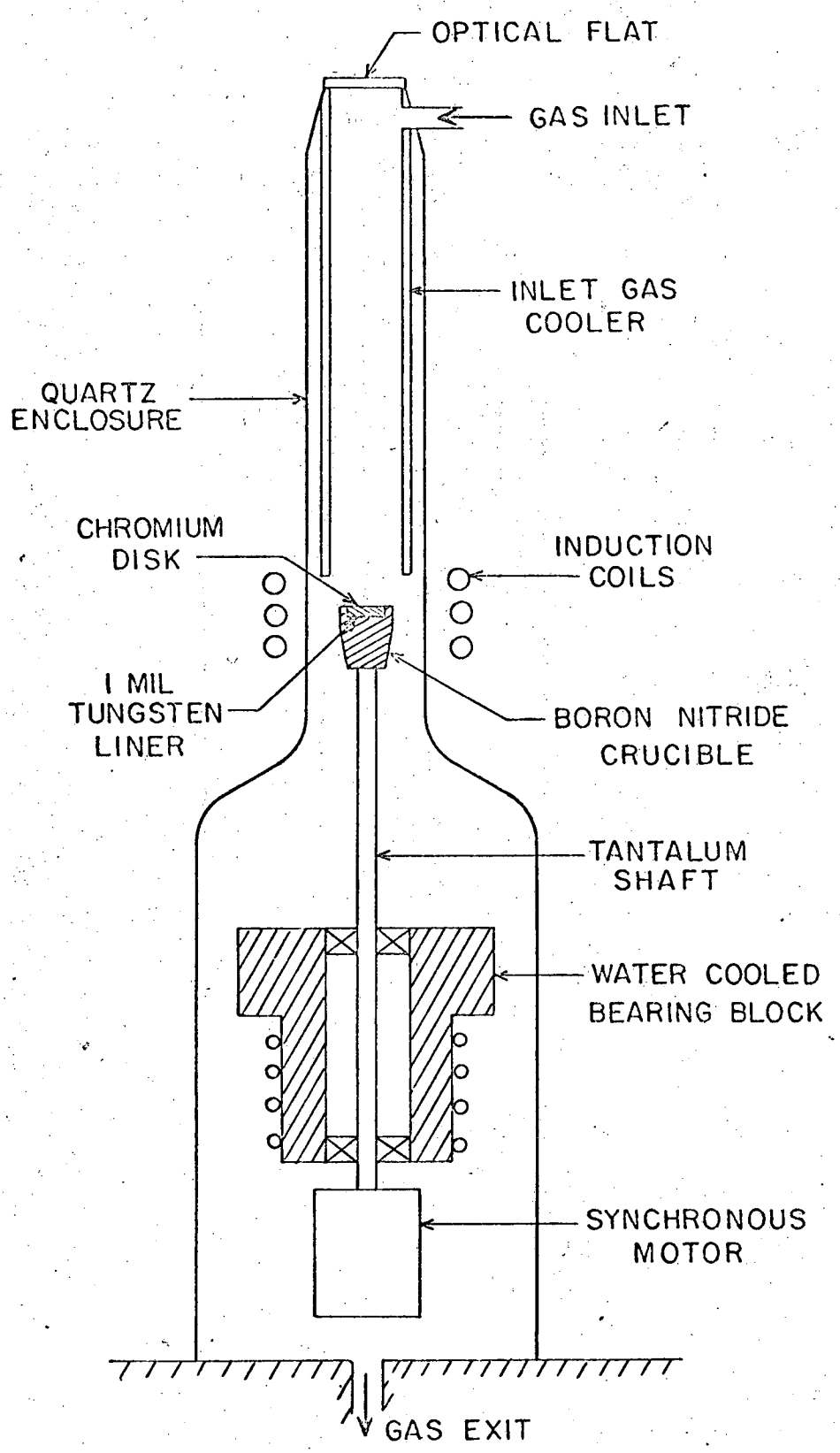
OPTICAL FLAT
GAS INLET
INLET GAS COOLER
QUARTZ ENCLOSURE
CHROMIUM DISK
INDUCTION COILS
1 MIL TUNGSTEN LINER
BORON NITRIDE CRUCIBLE
TANTALUM SHAFT
WATER COOLED BEARING BLOCK
SYNCHRONOUS MOTOR
GAS EXIT

Fig. A

speed by an audio-oscillator connected to a power amplifier. The oscillator provided a variable frequency source to control the motor speed and the amplifier provided the power necessary to drive the motor. The system was designed to run at speeds betwen 3000 and 15,000 rpm. The chromium disk along with the boron nitride holder, tantalum shaft, and synchonous motor were enclosed in a large quartz tube. The induction coils outside the quartz enclosure encircled the chromium disk. The interior of the tube during a run was filled with a 96% He-4% hydrogen mixture. The 4% hydrogen was added to inhibit the formation of chromium oxide on the disk surface.

The helium-hydrogen mixture was treated prior to entering the apparatus by a gas purification system. This consisted of filtering the gas through a packed filter of pyrex filtering fiber and then passing it through two Drierite dissicators and finally through another packed pyrex filter to remove dust particles. The gas purification system was constructed entirely of stainless steel which had been chemically polished to remove surface impurities. All lines leading from the bottled gas supply to the quartz enclosure were also chemically polished stainless steel. The only exception was a very short piece of copper line where the metal-to-quartz joint was made. The gas purification system and these lines leading from the gas supply to the quartz enclosure were kept in an argon atmosphere whenever the system was not operating. These precautions were taken to prevent impurities from entering the system and later depositing on the hot chromium surface.

The apparatus was assembled for operating by placing the weighed tungsten liner and then the chromium disk into the boron nitride crucible and then threading the crucible onto the tantalum shaft. The quart tube was placed around the disk assembly and the helium-hydrogen supply connected. The gas flow rate was adjusted to a value equal to that pumped by the disk plus a

small additional amount to insure that no back mixing occurred. The additional amount was calculated, using the results in Ref. 16 to be small enough not to affect the velocity profiles around the disk significantly. Upon entering the quartz tube, the gas mixture was cooled with a water-cooled heat exchanger. The heat exchanger prevented the gas from being heated by the quartz enclosure as it traveled toward the disk. The temperature of the quartz enclosure was higher than ambient because the hot disk radiated to it. By cooling the gas, a precisely known boundary condition at the outer edge of the boundary layer was maintained.

The temperature of the disk was measured with an optical pyrometer which viewed the disk through a right-angle prism and an optical flat located on top of the quartz enclosure. The temperature correction for the optical flat had been previously determined by calibrating it with a tungsten lamp. The pyrometer was sighted on the disk and also on a small hole located in the center of the disk. The hole had a length-to-diameter ratio of approximately unity, and though it was not a perfect block body, it did have an emissivity considerably higher than the chromium surface. This hole was used to calculate the emissivity of the disk surface.

The emissivity of the disk was measured by a set of temperature measurements taken while the disk was being heated to and cooled from its operating temperature for the run. The measurements consisted of recording the temperature of the hole drilled in the disk and then the temperature of the surface immediately adjacent to the hole for a sequence of different disk temperatures. If an axial temperature gradient does not exist, the true temperature of the hole should be equal to the true temperature of the surface. By equating these temperatures and making some approximations, as shown in Appendix F, the ratio of the emissivity of the hole to the emissivity of the surface can be calculated. Then using the results

of Sparrow and Albers,[36] the emissivity of the surface of the disk can be obtained since the ratio of the emissivities is a known function of the surface emissivity and the length-to-diameter ratio of the hole. The details of the method, including the effect of an axial temperature gradient, are shown in Appendix F.

Photographs of the equipment are shown in Fig. B to F. Figure B shows the entire experimental setup. Figure C shows a closeup of the rotating disk system including the quartz enclosure. Figure D shows the rotating disk drive system including the boron nitride crucible inside the quartz enclosure. Figure E shows a view of the gas purifying system. Figure F is a photograph of the rotating disk in operation at approximately 1500°C and 12,000 rpm. Notice the intense heat generated by the disk. This gives an indication of the difficulties encountered in trying to operate at these high temperatures and speed.

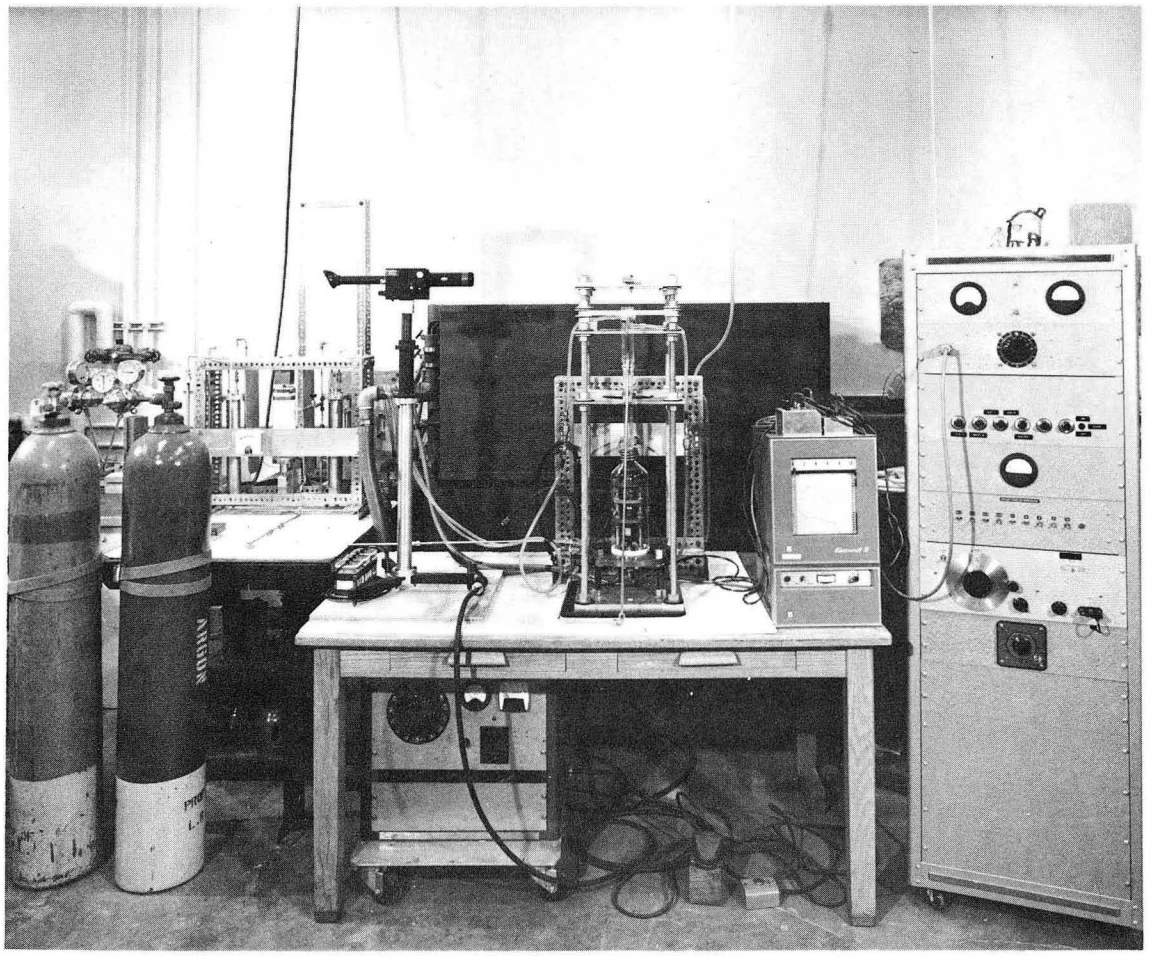

XBB 698-5364

Fig. B

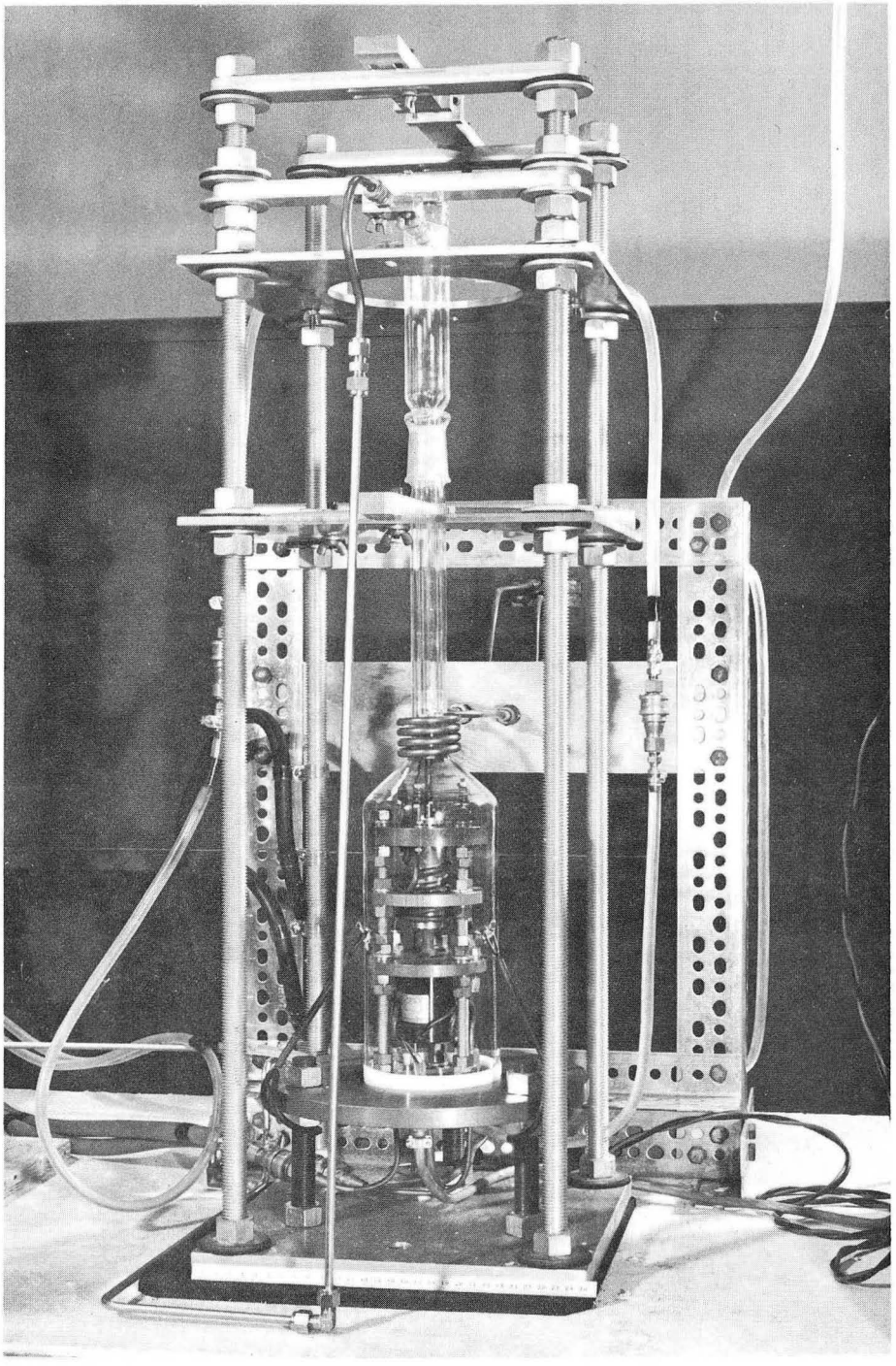

XBB 698-5362

Fig. C

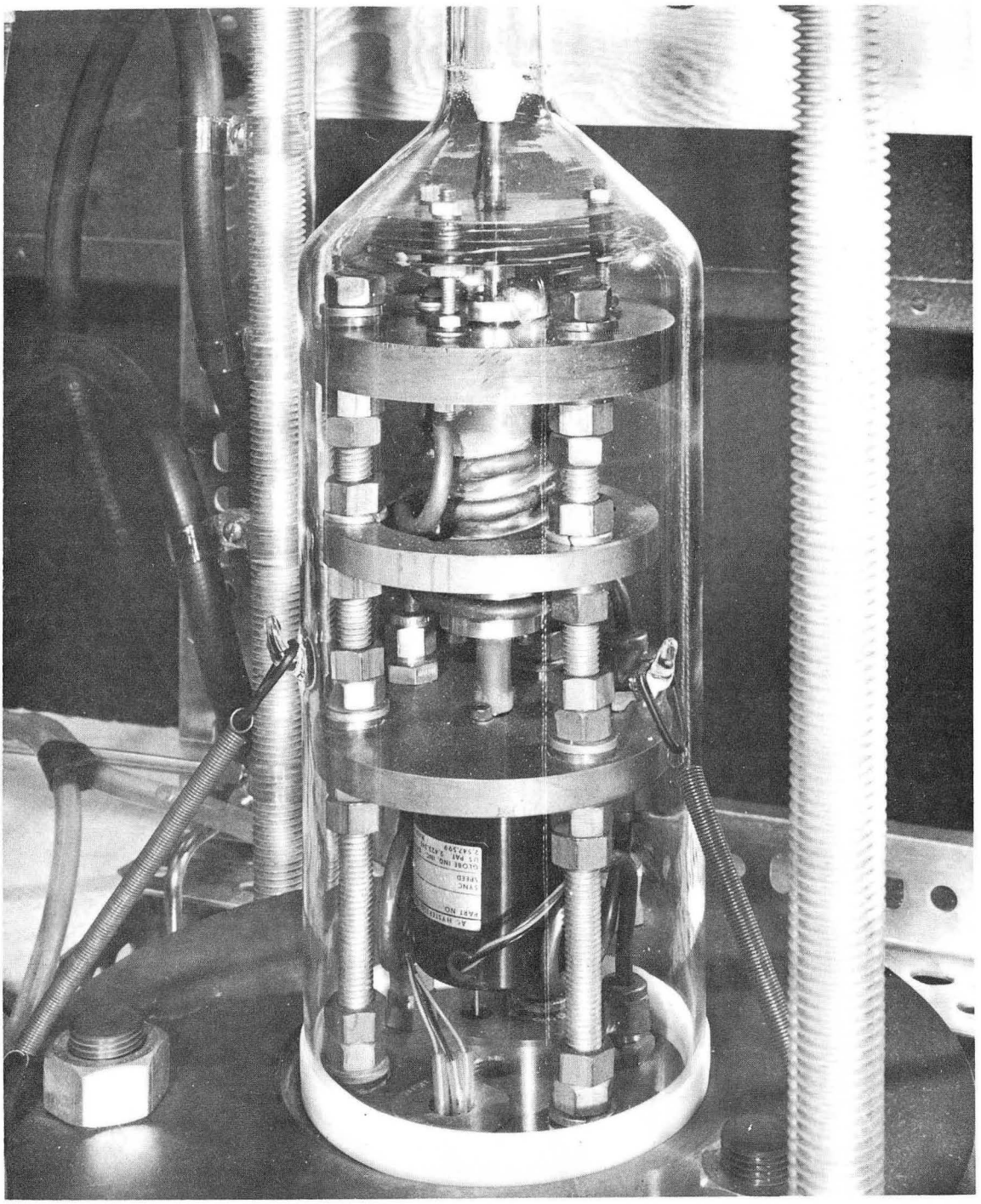

XBB 698-5363

Fig. D

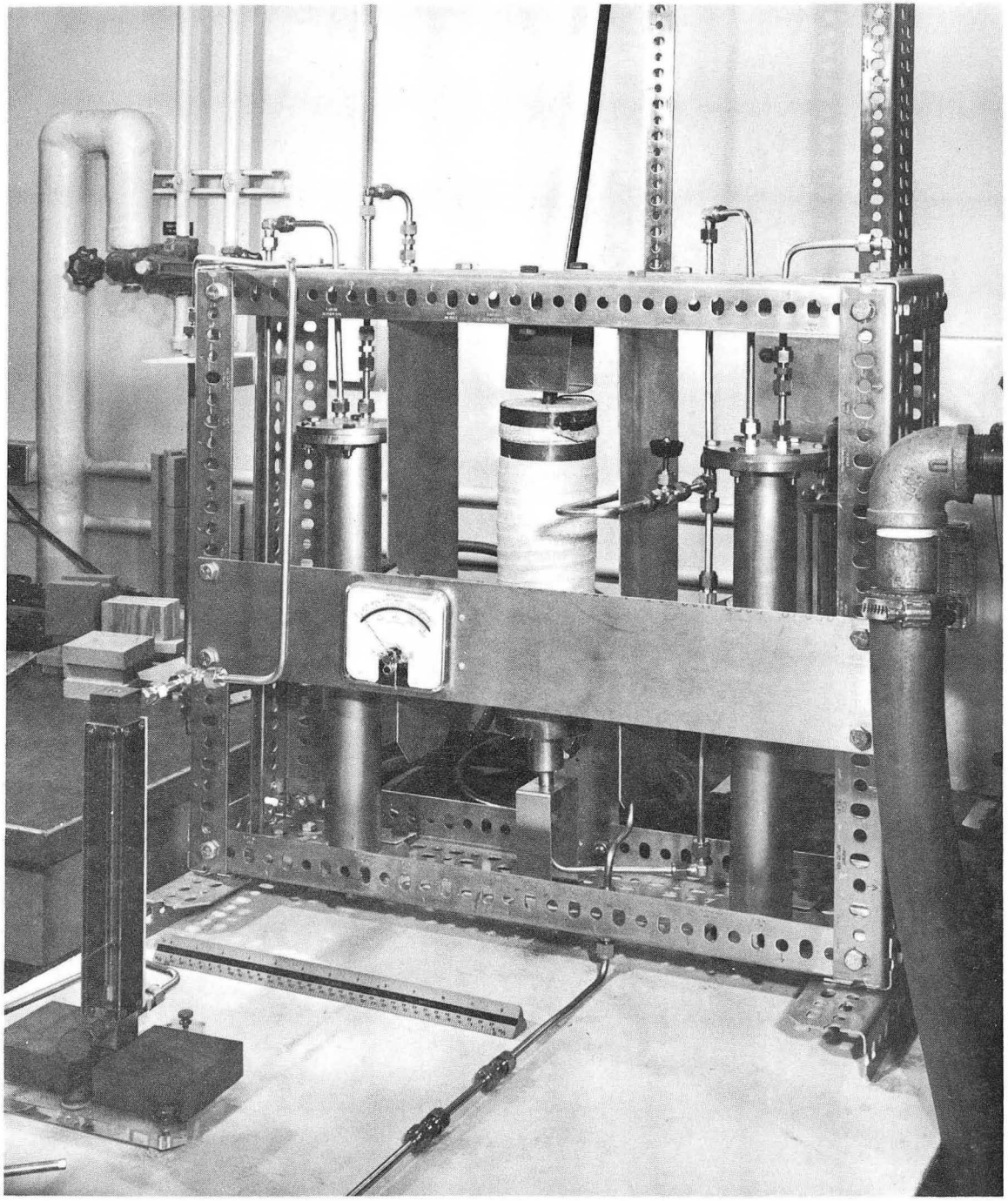

XBB 698-5365

Fig. E

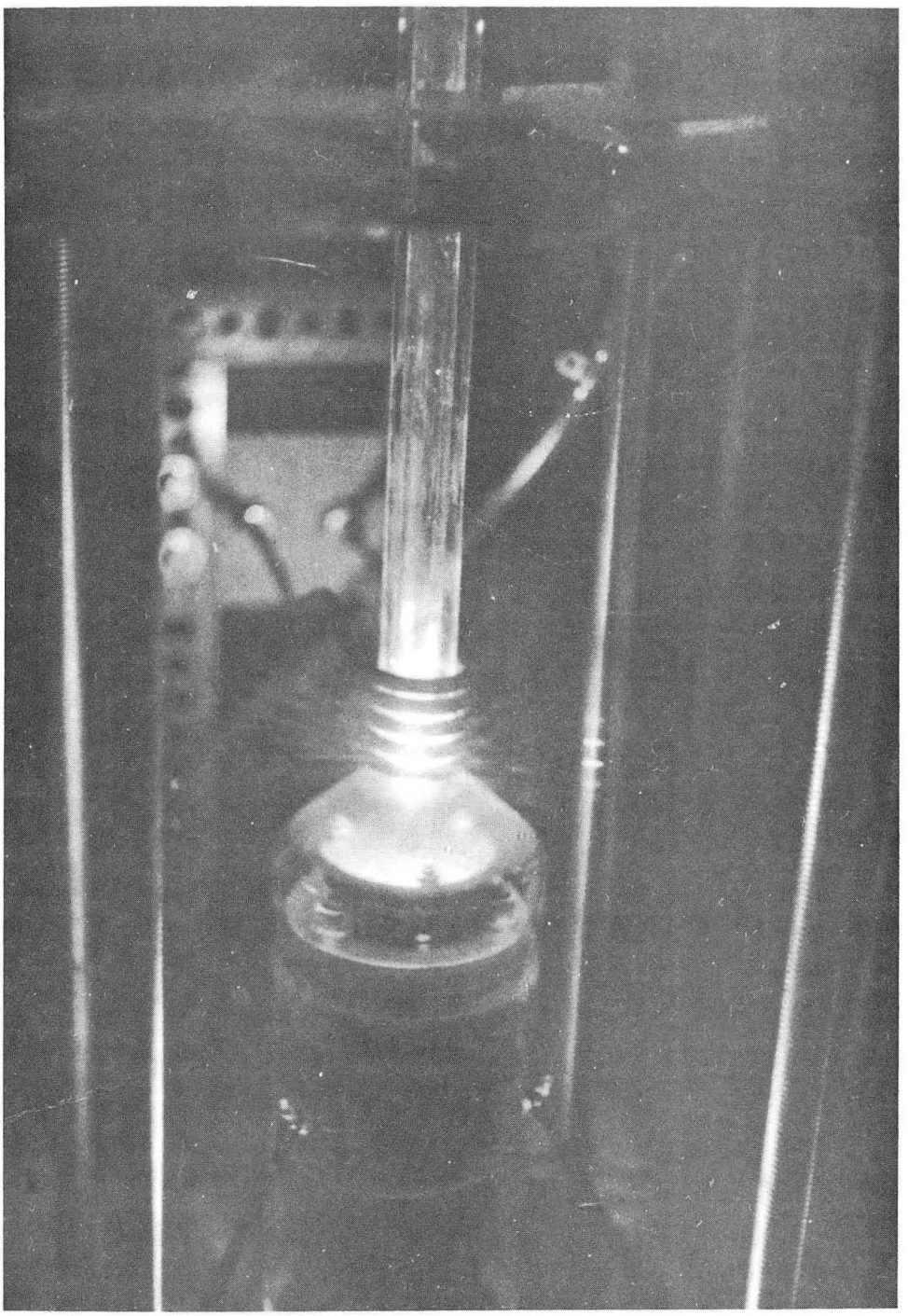

CBB 698-5328

Fig. F

3. Disk Fabrication

The chromium disks were spark-cut from electrolytically formed chromium flakes of 4N5 metallic purity and 3N5 desolved gaseous purity. The disks were approximately one centimeter in diameter by one millimeter thick. After cutting, the entire disk surface was chemically cleaned with hydrochloric acid at 35°C for several minutes. The surface to be vaporized was then polished on a rotary wheel with silicon carbide paper beginning with 380 grit and proceeding to 600 grit. An attachment held the disk on the wheel with a uniform pressure and automatically rotated it at the same time. The disk was finished with six micron diamond powder. The tungsten liners were cleaned by hand with 400 grit silicon carbide paper. The disk, liners, and crucible were finally cleaned with acetone and methonal in an ultrasonic cleaner. They were then stored in a dissicator under forepump vacuum until they were used.

C. Experimental Procedure

To begin the experimental run, the synchronous motor and induction heater were turned on and the disk speed and the temperature were adjusted to the values intended for the run. The runs lasted from twenty minutes to one hour, and were calculated so that the total mass loss from the disk would be between one and ten milligrams. Above ten milligrams the amount of material vaporized was so large that the upper surface of the disk receded below the upper surface of the crucible which disturbed the boundary layer to such an extent that chromium condensed in large quantities on the disk edge between the chromium and the boron nitride crucible. At mass losses below one milligram the accuracy of the measurement began to be affected by the small reaction which took place between the tungsten liner and the boron nitride, and by the small amount of chromium which always condensed on the disk edge between chromium and the boron nitride crucible. The amount of metal vaporized was determined by the difference between the initial and final weights of the chromium disk and tungsten liner. The tare weight of the tungsten liner was considered because after the run it could not be seperated from the chromium disk because a diffusion bond always formed between them.

The disk temperature during the run was recorded, and adjusted if necessary, approximately once every minute. The temperature variation for any point on the disk during the run was generally held to less than ± 5 °C by manually adjusting the power applied to the induction coil. Readings were taken at three different radical positions: the center ($r/r_o \approx 0$), halfway between the center and the edge ($r/r_o \approx 1/2$), and at the edge ($r/r \approx 1$). The variation from the center of the disk to the edge was usually on the order of 15°C. The average temperature at the three

radial positions for the run was taken as the simple average of all the temperatures recorded at that position during the run. The mean temperature of the disk was then calculated from these three time-averaged temperatures. This was done by first passing a parabola through the three temperatures T(0), T(1/2) and T(1), to obtain $T(r/r_0)$. The average vapor pressure $\bar{p}_v$ over the disk surface was then calculated, i.e. $\bar{p}_v = (\int p_v(T)dA)/(\int dA)$, and the mean temperature taken as the temperature corresponding to this vapor pressure. This method was used because the mass loss rate is proportional to the vapor pressure and to the incremental area over which its exists. The details of this calculation are shown in Appendix E.

Three different sets of runs were made. In the first set, the rotational speed of the disk was held constant at 12,000 rpm and the temperature varied from 1620°K to 1745°K. This determined the effect of temperature upon the vaporization rate at constant rotational speed.

In the second set, the temperature was held constant at 1715°K ± 5°K and the speed varied from 4200 rpm to 12,000 rpm. This set showed the effect of rotational speed on the vaporization rate at constant temperature.

The third set consisted of three runs at 12,000 rpm with a resistance heater replacing the inlet gas heat enchanger. The incoming gas was heated to approximately 500°K by the heater. This increased the temperature in the boundary layer and thus increased the equilibrium vapor pressure. The supersaturation was then reduced and the amount of material condensing should then also be reduced if nucleation is in fact occurring.

For all the experimental runs, the Grashoff number divided by the Reynolds number squared for the disk was held to less than 0.05. In most cases it was on the order of 0.002. This insured that the effect of natural convection was small.

Photographs of a typical chromium rotating disk and boron nitride crucible after operation are shown in Figs. G and H. Figure G shows the disk inside the crucible as it was during operation and Fig. H shows the disk separation from the crucible. Notice the reflection of the pennies in the disk. This is the most important point in both photographs because it shows that the disk surface is both shiny and clear. This is very important because impurities on the disk surface can affect the vaporization rate tremendously. This clean disk surface was typical of the disk surfaces after the experimental run.

Figures I and J are typical micrographs of the disk surface before and after the experimental run. Their magnification is 100 times. Figure I was taken before the run and shows a surface distinguished only by light polishing scratches. Figure J was taken after the run and shows the large grains which grow in the disk at these high temperatures.

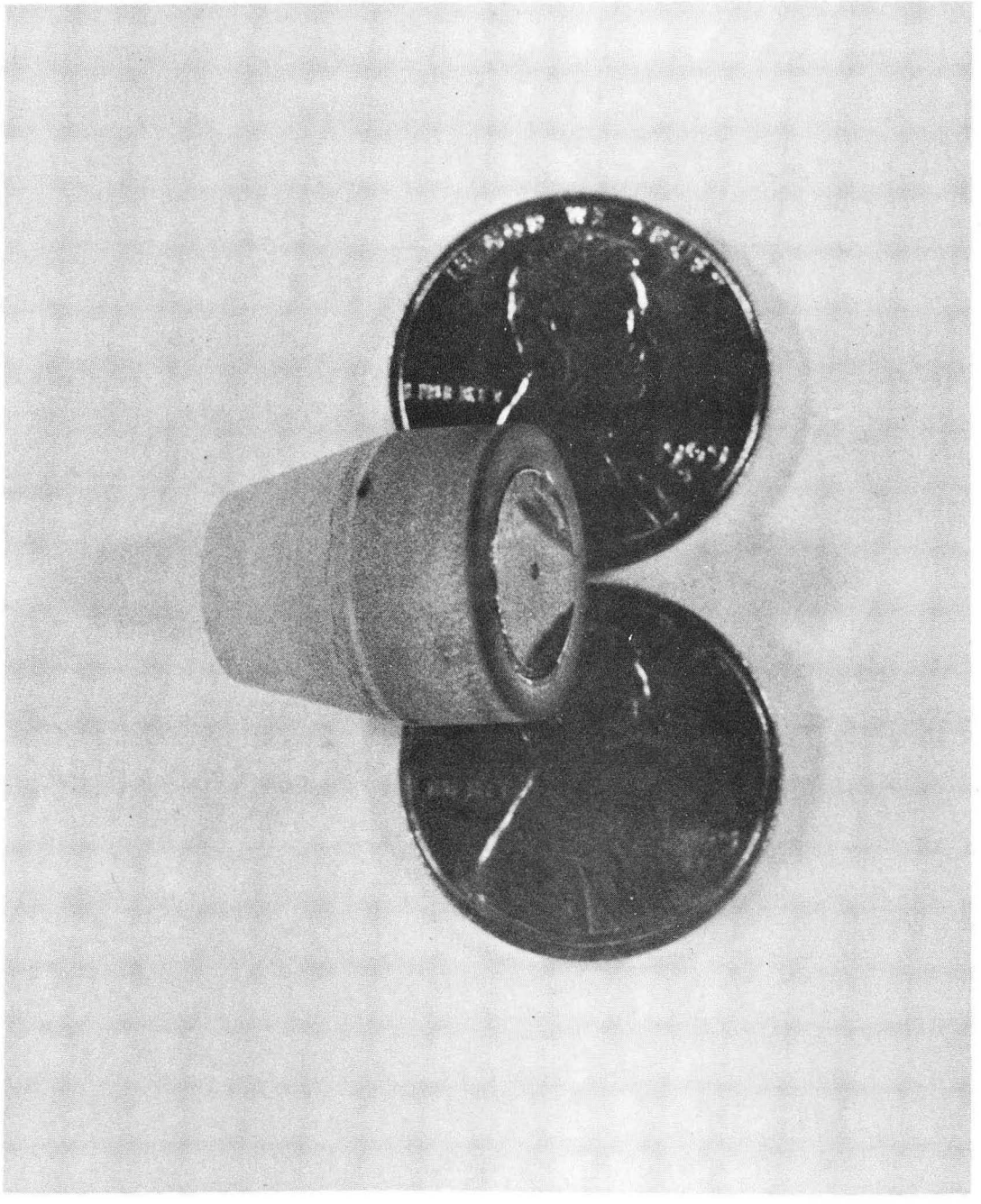

XBB 698-5327

Fig. G

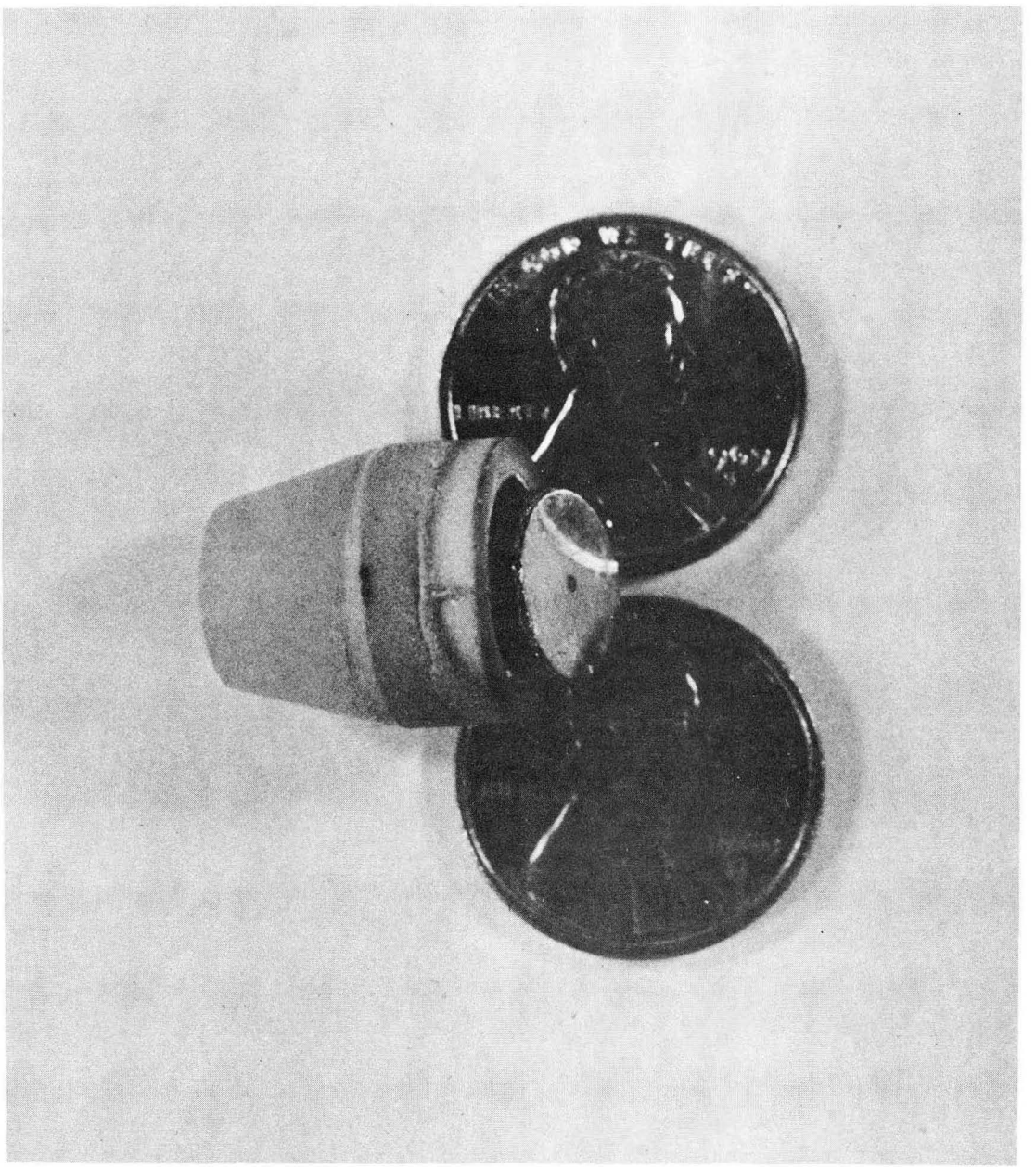

XBB 698-5326

Fig. H

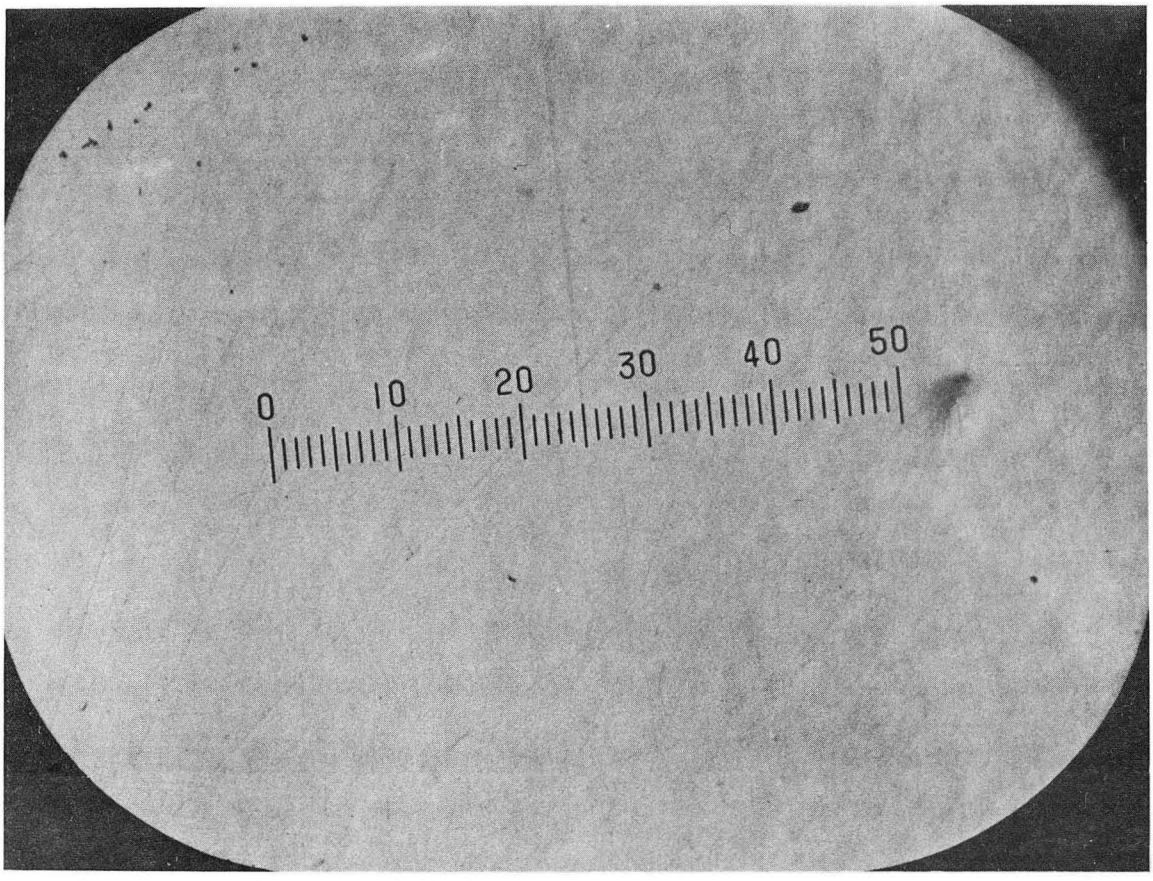

XBB 698-5325

Fig. I

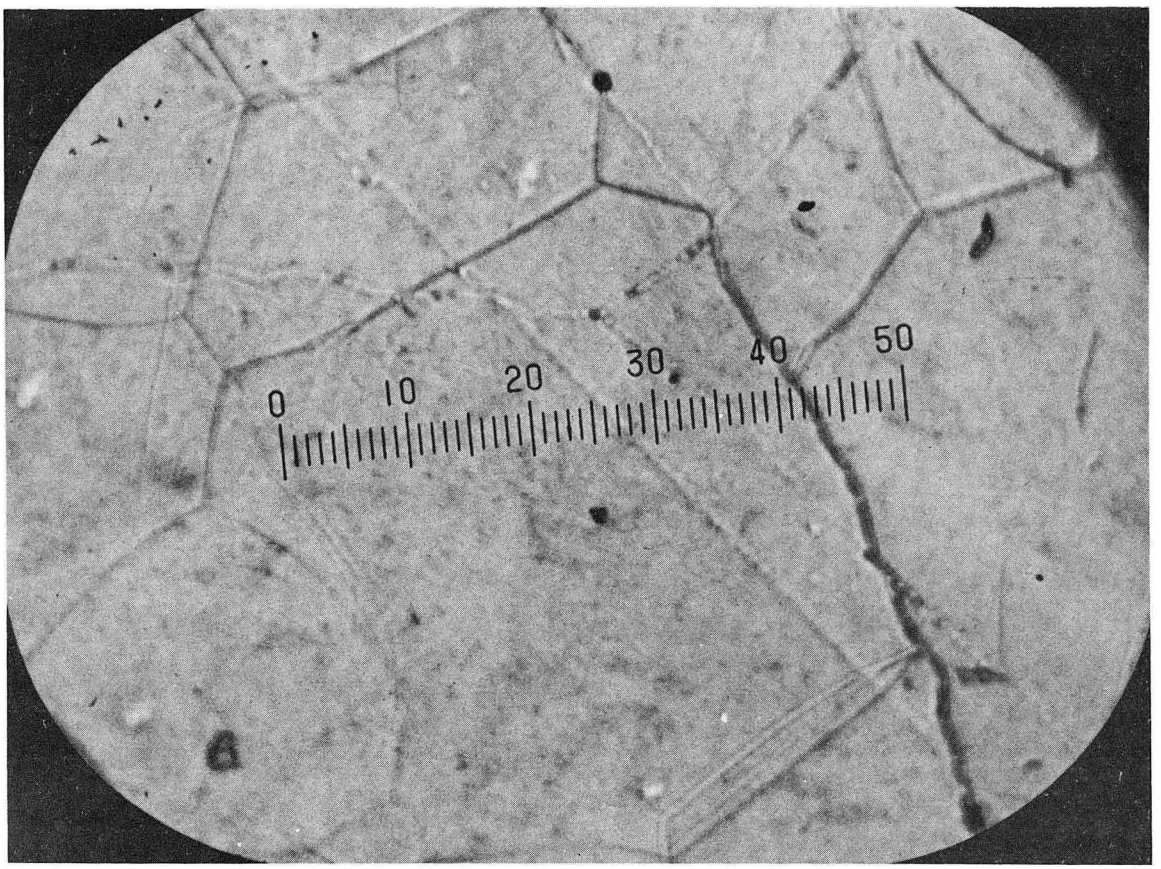

XBB 698-5324

Fig. J

D. Results

A tabulation of the results is shown in Table II. The experimentally measured vaporization rate of chromium as a function of disk temperature is shown in Fig. 15. The function and points on the graph denoted by circles are for an inlet gas temperature of 290°K. The wall temperature for these points ranges from 1620°K to 1745°K. A total of seven points were taken in this range. The figure shows that the vaporization rate increases rapidly in the vicinity of 1620°K to 1635°K and increases much more slowly from 1635°K to 1745°K. The points show very little scatter. The two points denoted by upward triangles were taken with the inlet gas at approximately 500°K. These points lie below the points taken with the cooler inlet gas temperature of 290°K indicating that nucleation was in fact occurring in the boundary layer. The point denoted by a downward triangle was taken with the heater installed but at zero power. This was done to see if the measurement of the disk temperature was affected simply by the physical presence of the heater. The proximity of this point to the line drawn through the other cold inlet gas points shows the effect to be small.

The chief characteristic of the data shown in Fig. 15 is the rapid increase in the vaporization rate over a small temperature range followed by a gradual increase in the vaporization rate over a much larger temperature range. The theoretical no-condensation and bulk equilibrium condensation vaporization rates are also shown in the figure. It can be seen that as the wall temperature is increased, the experimental rate proceeds from the vicinity of the no-condensation line to the vicinity of the bulk equilibrium condensation line. The vaporization rate could not be measured below 1620°K. for two reasons. First, the errors in the experiment began to

TABLE II

Data Summary

Run No.	Weight Loss (mg)	Time (min)	Speed (rpm)	T_{app} (°K)	T_t (°K)	j (mg/cm^2-hr)
1	6.61	10	12,000	1667	1745	48.9
2	0.93	50	12,000	1552	1620	1.38
3	10.28	50	12,000	1615	1688	15.2
4	5.54	60	12,000	1584	1655	6.83
5	8.04	20	12,000	1642	1718	29.8
6	4.24	60	12,000	1567	1636	5.23
7	2.26	60	12,000	1556	1624	2.79
8	4.45	20	9,000	1644	1720	16.5
9	12.7	45	6,000	1638	1714	20.9
10	15.4	60	4,200	1635	1710	19.0
11	10.2	30	8,400	1638	1714	25.2
12	7.21	15	12,000	1666	1744	35.6
13	8.46	45	12,000	1616	1690	14.0
14	6.52	20	12,000	1638	1714	24.1

Nos. 12 and 13 were run with heater installed and on; No. 14 with heater installed but no power.

T_{app} is the apparent temperature of the disk, i.e. the observed temperature uncorrected for emissivity.

T_t has been corrected for a surface emissivity of 0.55.

Area of the disk is 0.81 cm^2.

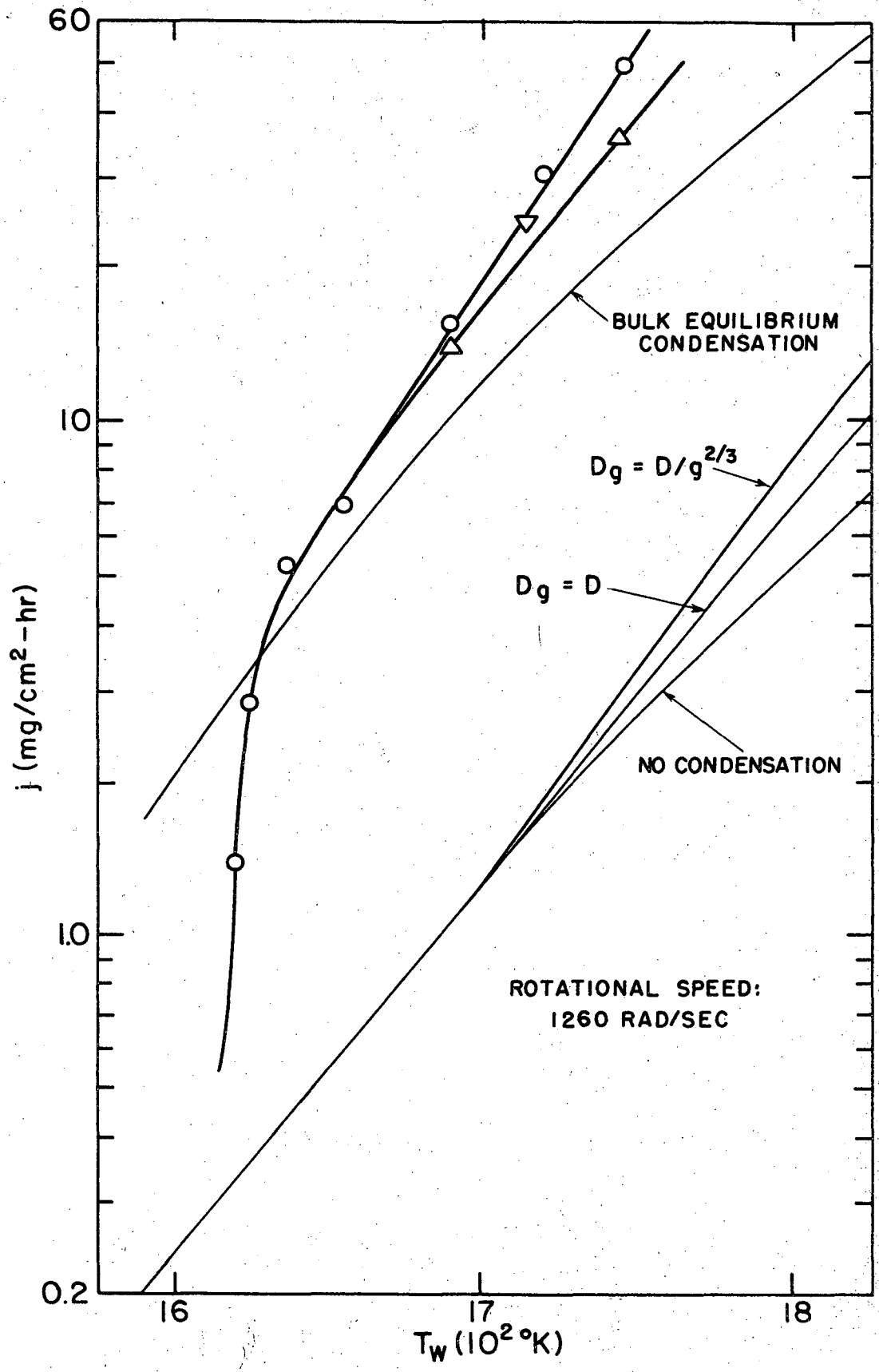
60
10
1.0
0.2
j (mg/cm²-hr)
16
17
18
T_W (10^2 °K)
BULK EQUILIBRIUM CONDENSATION
$D_g = D/g^{2/3}$
$D_g = D$
NO CONDENSATION
ROTATIONAL SPEED:
1260 RAD/SEC

Fig. 15

become a significant fraction of the mass loss due to vaporization at these temperatures. Secondly, the vaporization rate is changing quite rapidly with temperature in this region and so small errors in temperature measurement become quite important. At the high temperature end, the data approaches the bulk equilibrium condensation line. The agreement is only within a factor of two; however, this is not bad considering the measured vaporization rates range over a factor of forty.

Excellent agreement between theory and experiment was not anticipated in this work. There are several reasons for this. First, the experimental vapor pressure data given in the literature scatters widely. Nesmeyanov[42] surveys most of the vapor pressure data available for the elements. Chromium has one of the better known vapor pressures and yet the data Nesmeyanov presents scatter by ± 50%. In addition, all the reliable data that Nesmeyanov presents for chromium are at 1550°K and below. Thus there is no vapor pressure data in the range in which we were working; we were on the average of 150°K above the nearest data, and so were required to use an extrapolation given by Nesmeyanov. Hultgren, et. al[48] also lists recommended vapor pressures for the elements. For chromium at 1800°K, his recommended vapor pressure is about two-thirds of Nesmeyanov's recommended value. This, however, falls within the scatter of the data shown in Nesmeyanov and so Hultgren's data falls within the error bands shown in Fig. 16.

The second source of error in this experiment is in the measurement of the surface emissivity. As discussed in Appendix F, this is a difficult measurement to make. Our measured value was 0.55. The data presented in Ref. 43 scatter widely but the most reliable value is indicated to be 0.43. If the surface emissivity were in fact 0.43 instead of 0.55, all the data points in Fig. 15 would be shifted to a temperature approximately 25°K higher.

The effect of the possible emissivity error and the effect of the vapor pressure errors are shown in Fig. 16. The shaded areas around the no-condensation and bulk equilibrium condensation lines indicate the uncertainty in them due to scatter in the literature vapor pressures. The line labeled $\epsilon_s = 0.43$ is the line which would be drawn through the data points if the surface emissivity were 0.43 rather than 0.55. The lower emissivity improves agreement between equilibrium condensation theory and the data. The shaded area between the two lines indicates the error in the data due to a possible error in the emissivity.

Returning to the previous Fig. 15, the constant diffusivity ($D_g = D$) and variable diffusivity ($D_g = D/g^{2/3}$) solutions are plotted here also. These definitely fall below the bulk equilibrium condensation line and the measured data. This indicates that the monomer sink, and likewise the drop concentrations, calculated in the program were less than those physically existing in the boundary layer. The droplet concentrations in the program are directly related to the expression used for the nucleation rate, for this expression determines the droplet concentrations at small drop sizes and these concentrations are used as the boundary condition. The Becker-Doring-Zeldovich expression for the nucleation rate was used in our calculations. This was because of the agreement between theory and experiment which Katz and Ostermier obtained while using it in their diffusion chamber experiments.[7] Despite this agreement, however, this expression is currently in dispute.[21-24] Lothe and Pound have developed an expression for the nucleation rate which includes quantum-mechanical corrections to the classical expression.[24] These corrections change the nucleation rate by a factor of 10^{17}. This is a considerable change and would definitely increase the magnitude of the droplet concentration and of the

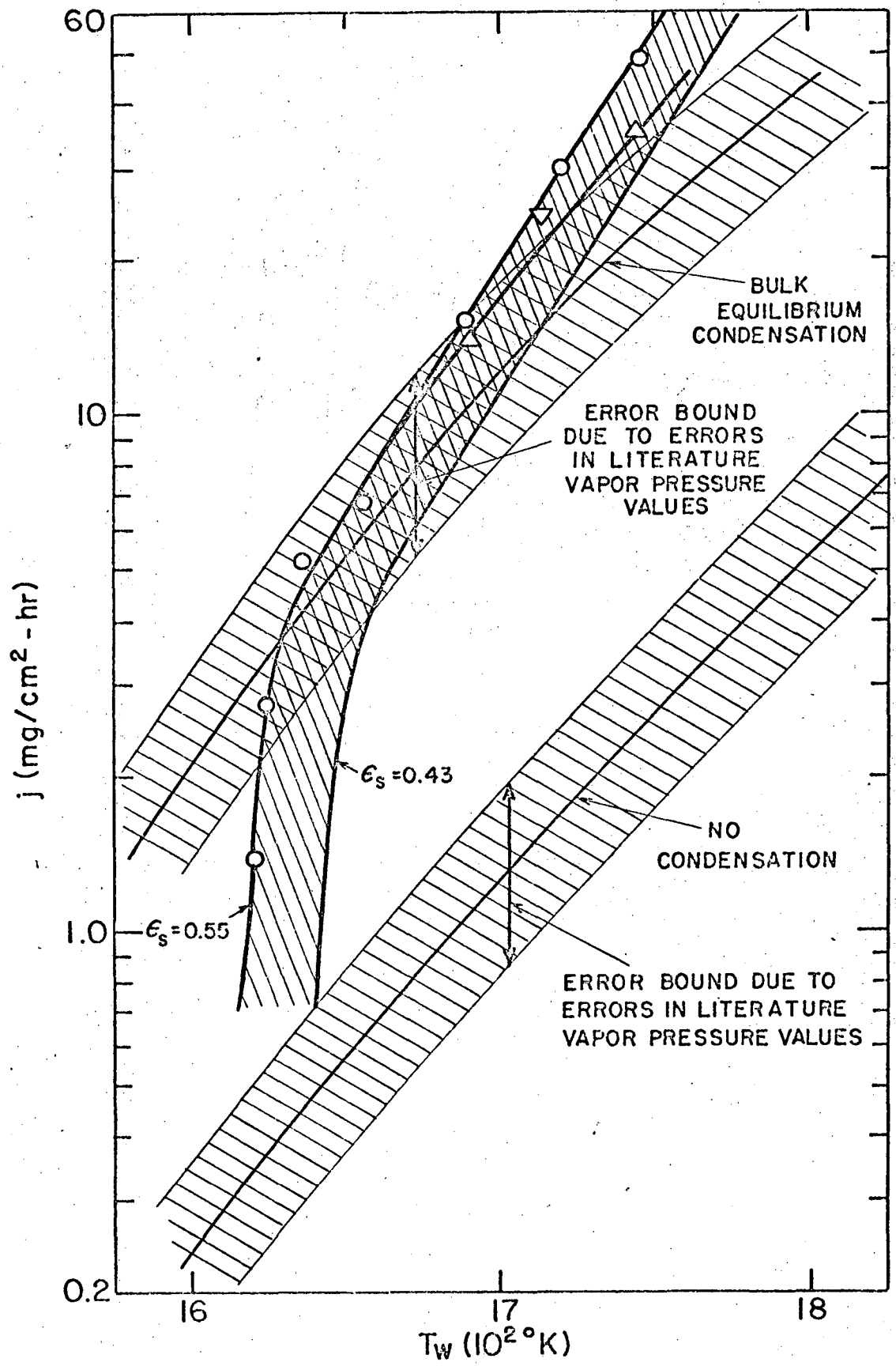
60
10
1.0
0.2
16
17
18
j (mg/cm² - hr)
T_W (10^2 °K)
BULK EQUILIBRIUM CONDENSATION
ERROR BOUND DUE TO ERRORS IN LITERATURE VAPOR PRESSURE VALUES
ϵ_s = 0.43
ϵ_s = 0.55
NO CONDENSATION
ERROR BOUND DUE TO ERRORS IN LITERATURE VAPOR PRESSURE VALUES

Fig. 16

monomer sink term in the program, and hence increase the calculated vaporization rate at the wall. Several runs of the program were tried using the Lothe-Pound expression. However, the nucleation rate calculated from the Lothe -Pound expression was an extremely sensitive function of the monomer concentration and numerical problems arose because the monomer concentration could not be interpolated between points accurately enough. However, if the calculations could be made, the Lothe-Pound expression should increase the calculated vaporization rate. This change is in the correct direction because an increase in the calculated nucleation rate will increase the agreement between theory and experiment.

Figure 17 shows the same experimental data plotted against inverse temperature.

Figure 18 shows a set of five points taken at an approximately constant temperature of 1715°K with different angular velocities. The speeds corresponding to the angular velocities range from 4200 rpm to 12,000 rpm. The vaporization rate is plotted against the square root of the angular velocity. The figure shows the measured vaporization rate to be a linear function of the square root of the angular velocity and to have a zero intercept. This type of behavior would be expected if vaporization were occurring at the bulk equilibrium condensation rate or at the no-condensation rate because then the theoretical equations show the vaporization rate to be directly proportional to the square root of the angular velocity. Figure 13 shows a case where the vaporization rate is not at either limiting value. When this occurs the rate cannot be proportional to the square root of the angular velocity because the angular velocity occurs in the source term. Thus Fig. 18 shows two things; first, Fig. 18 shows that vaporization is occuring at the bulk equilibrium condensation rate at 1715°K. Second, Fig. 18 indicates that true rotating disk behavior was being obtained in

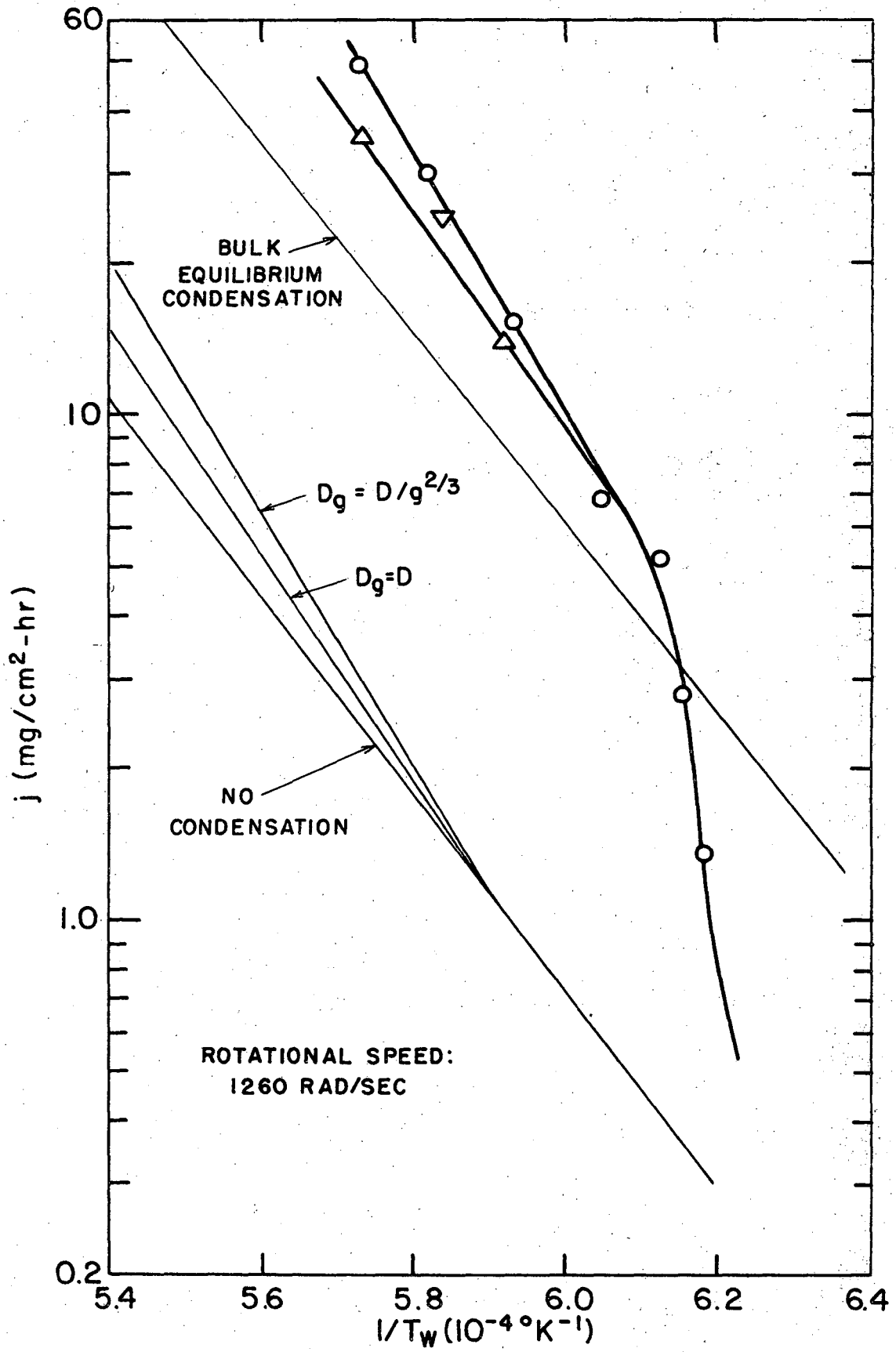
60
10
1.0
0.2
j (mg/cm²-hr)
BULK
EQUILIBRIUM
CONDENSATION
$D_g = D/g^{2/3}$
$D_g = D$
NO
CONDENSATION
ROTATIONAL SPEED:
1260 RAD/SEC
5.4
5.6
5.8
6.0
6.2
6.4
$1/T_w (10^{-4} °K^{-1})$

Fig. 17

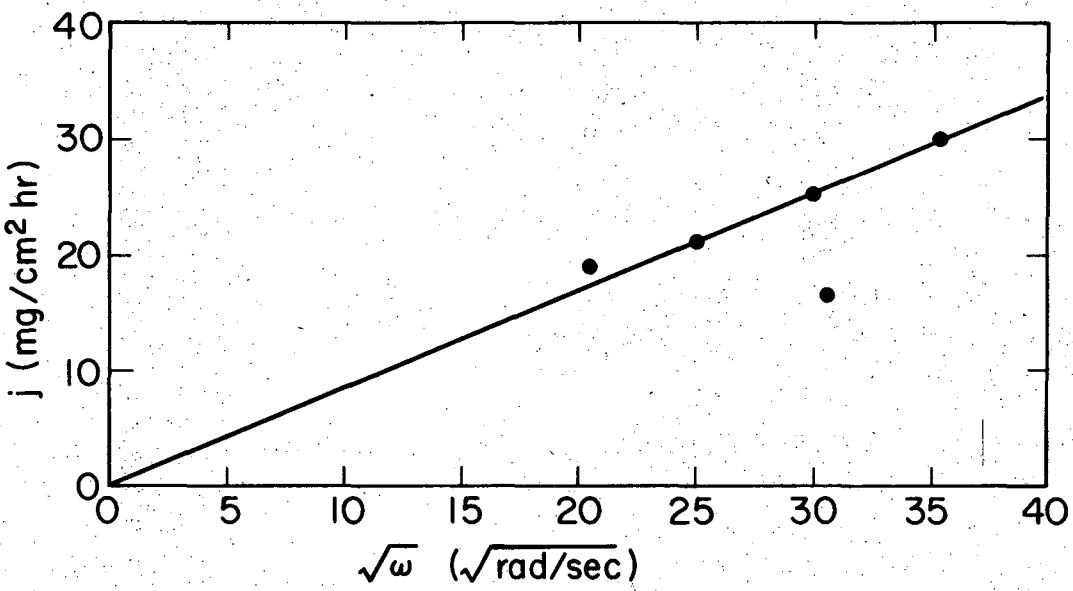

XBL699-3798

Fig. 18

the boundary layer. One point in Fig. 17 falls far below the others; something was definitely wrong in this measurement but what it was is not known.

The theoretical lines in the Figs. 14-16 were calculated neglecting property variations and thermal diffusion. Property variations were neglected because the diffusion coefficient of chromium through helium is approximately proportional to temperature squared (see Fig. G-1, Appendix G) and so the effect should be small. Thermal diffusion was neglected because the Lennard-Jones parameters for chromium-helium and iron-argon are very similar. For example, note the small change in the diffusion coefficients in Fig. G-2, Appendix G. Thus, the effect of thermal diffusion for chromium should be the same order of magnitude as that of iron (see Appendix C). In addition, even at the considerably higher temperature of 3200°K, Elenbaas[49] found the affect of thermal diffusion for tungsten through kyrpton to be only 18% of the ordinary diffusion current. Thus the affect of thermal diffusion should be small compared to the variations involved in Figs. 14-16.

Figure 19 shows the present data and Turkdogan's data[1] on the same graph. The results are not strictly comparable because the present data are for chromium and Turkdogan's are for iron. However they do indicate two basic trends. First, at low temperatures, the vaporization rate rises from the no-condensation value to the equilibrium value as the temperature increases. Second, at higher temperatures, the vaporization rate again approaches the no-condensation rate as the temperature is increased because the heat generated by the large volume of condensing vapor lowers the bulk equilibrium line. The lowering the of the bulk equilibrium line because of the latent heat release and the fact that Turkdogan's data in general follow this line was pointed out in Refs. 37 and 47.

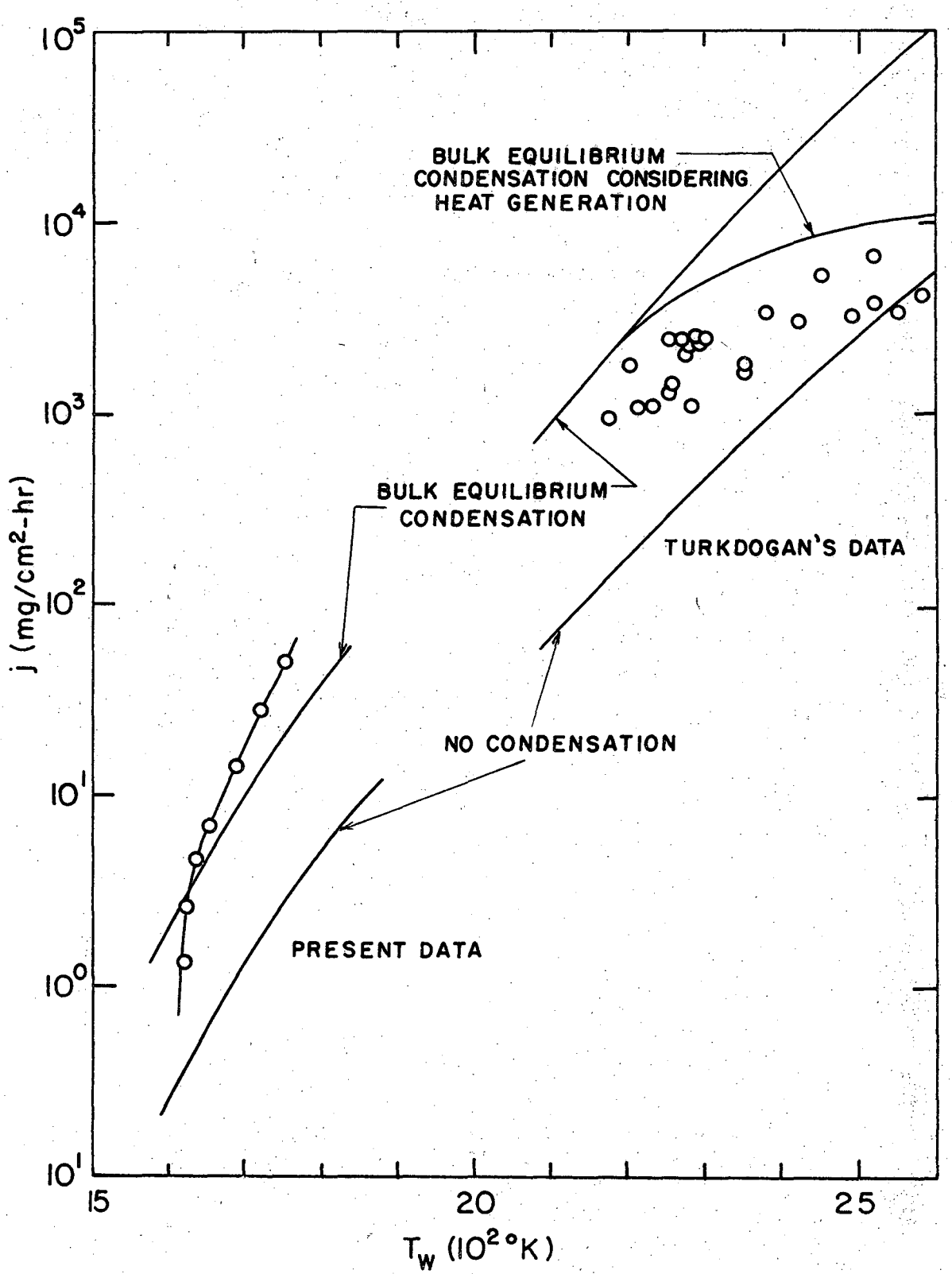
BULK EQUILIBRIUM CONDENSATION CONSIDERING HEAT GENERATION
BULK EQUILIBRIUM CONDENSATION
TURKDOGAN'S DATA
NO CONDENSATION
PRESENT DATA
j (mg/cm²-hr)
T_W (10² °K)
10⁵
10⁴
10³
10²
10¹
10⁰
10¹
15
20
25

Fig. 19

E. Conclusions

In conclusion, condensation enhancement was measured in rotating disk boundary layer with the vaporization rate proceeding from near the condensation-free value to the bulk equilibrium condensation value over a small temperature range.

Comparing the present data and Turkdogan's data (Fig. 19) shows the following. At low temperatures no condensation enhancement is obtained. This is reasonable because here the system begins to approach the isothermal state. As the wall temperature is increased, condensation enhancement occurs and the vaporization rate proceeds to that value determined by the equilibrium vapor pressure. As the wall temperature is increased further, the vaporization rate again approaches the condensation-free rate; this is because the heat released by the larger amount of vapor condensing in the boundary layer tends to make the system more isothermal.

Comparison of the experimental vaporization rate with the theoretically calculated rate showed that good agreement could not be obtained using the classical Becker-Doring-Zeldovich nucleation expression. Though calculations could not be carried out using the Lothe-Pound expression, it is felt that the change in the vaporization rate which would occur would provide better agreement between experiment and theory.

APPENDIX A

FORCES ON A SMALL DROP NEAR A ROTATING DISK

It was assumed in the formulation of the droplet conservation problem for the rotating disk that the droplets move with the velocity of bulk gas. This implies that the gravitational and centrifugal forces on the droplet are negligible compared to the viscous drag force. In this Appendix these forces are evaluated for the droplet sizes which exist in concentrations large enough to be important to the solution. The analysis first divides the boundary layer into three sections: the top, the middle, and the bottom. The calculation in each section was then based on the force and velocity component characteristic of the section while all other effects were neglected. The effect of property variations was neglected. The buoyancy force was also neglected since the density of a metal is much greater than that of air.

Near the Top of the Boundary Layer

Consider a drop near the top of the boundary layer moving at equilibrium velocity. Since the radial and centrifugal velocities at this position are small compared to the axial velocity, the drop will be moving vertically. The gravitational force is given by

$$F_g = \frac{4}{3} \pi R^3 \rho g \qquad \text{(A-1)}$$

where R is the radius and ρ is the density of the drop, and g is the acceleration of gravity. The viscous drag force is given by Stokes law[17]

$$F_v = 6\pi \mu R(V-w) \qquad \text{(A-2)}$$

where μ is the viscosity and w the velocity of the gas, and V is the velocity of the drop. The gas velocity is given by

$$w = \sqrt{\omega\nu}\, H(x)$$

and $H \approx 1$ near the top of the boundary layer.[15]

Since the drop is in equilibrium

$$F_g - F_v = 0 \tag{A-3}$$

Putting Eqs. (A-1) and (A-2) in Eq. (A-3) and rearranging gives

$$\frac{V-w}{w} \approx \frac{1}{5} \frac{\rho R^2 g}{\mu\sqrt{\nu\omega}} \tag{A-4}$$

This equation show the departure of the drop velocity from the bulk velocity as a function of drop radius.

Near the Middle of the Boundary Layer

Near the middle of the boundary layer the radial velocity is at its maximum. Here the two important effects are the radial velocity and the gravitational force. The axial and tangential velocities will be neglected.

Assume the drop falls by gravity while moving outward with the velocity of the fluid. Then from Stokes law the viscous force on the drop is

$$F_v = 6\pi\,\mu\,R\,V \tag{A-5}$$

where V is vertical velocity at which the drop is falling. Since

$$F_g - F_v = 0 \tag{A-6}$$

we have after using Eq. (A-1)

$$V = \frac{2}{9} \frac{\rho R^2 g}{\mu} \tag{A-7}$$

This is the velocity at which the drop falls while moving radially with the bulk fluid. The effect of this velocity will be found by computing the ratio of the distance traveled radially to the distance traveled vertically.

BLANK PAGE

Let t be the time required to move radially from r_i to r_o with bulk velocity u. Since

$$u = r\omega F(x) \tag{A-8}$$

and $F(x) \approx 1/5$ in the center of the boundary layer, we find t is given by

$$u \Delta t = \Delta r \tag{A-9}$$

or

$$t = \frac{5}{\omega} \int_{r_i}^{r_o} \frac{dr}{r} \tag{A-10}$$

$$= \frac{5}{\omega} \ln\left(\frac{r_o}{r_i}\right) \tag{A-11}$$

Let Δz be the loss in height while traversing the radial distance r_i to r_o. Then

$$\Delta z = V t$$

$$= \frac{\rho R^2 g}{\mu \omega} \ln\left(\frac{r_o}{r_i}\right) \tag{A-13}$$

If δ is the boundary layer thickness,

$$\delta \approx 3\sqrt{\frac{\nu}{\omega}} \tag{A-14}$$

then the important parameter to consider is the ratio of the height fallen to the boundary layer thickness. This is, with $r_o/r_i = 10$,

$$\frac{\Delta z}{\delta} = \frac{2}{3} \frac{\rho R^2 g}{\mu \sqrt{\nu\omega}} \tag{A-15}$$

Note that the variables are the same as in case (1), only the coefficient has changed.

Near the Bottom of the Boundary Layer

Near the bottom of the boundary layer the axial and radial velocities approach zero and the tangential velocity approaches its maximum. So near the bottom of the boundary layer only the tangential velocity com-

ponent will be considered. This component induces a centrifugal force F_c on the drop with F_c given by

$$F_c = \frac{4}{3} \pi R^3 \rho \frac{V_t^2}{2} \tag{A-16}$$

where V_t is the tangential velocity component. This assumes that the drop moves tangentially with the bulk velocity; assuming this is conservative because it gives the maximum force F_c. The centrifugal force moves the drop radially outward and this movement produces a viscous drag force given by

$$F_v = 6 \pi \mu R(V-u) \tag{A-17}$$

where V is the velocity of the drop and u is the radial velocity component of the bulk gas. If the drop is moving in equilibrium

$$F_c - F_v = 0 \tag{A-18}$$

The radial and tangential velocity components are given by

$$u = r \omega F(x) \tag{A-19}$$

$$V_t = r \omega G(x)$$

and $F(x) \approx 1/5$, $G(x) \approx 1$ near the bottom of the boundary layer. Putting Eqs. (A-16), (A-17) and (A-19) into Eq. (A-18) gives, after rearranging

$$\frac{V-u}{u} = \frac{\rho R^2 g}{\mu \sqrt{\nu\omega}} \left(\frac{\omega \sqrt{\nu\omega}}{g} \right) \tag{A-20}$$

Again the same combination of variables $\rho R^2 g/(\mu \sqrt{\nu\omega})$ occurs. In this case, however, the coefficient is not a constant but a variable.

Evaluation of the Effect of the Forces

The effect of gravitational forces will be small if the parameter $\rho R^2 g/(\mu \sqrt{\nu\omega})$ is small, for if this is true the "velocity defect" given

by Eq. (A-4) and the "distance defect" given by Eq. (A-15) are small. The effect of centrifugal forces will be small if in addition the parameter $\omega\sqrt{\nu\omega}/g$ is not large for then the "velocity defect" given by Eq. (A-20) will be small. If these "defects" are small, then the drops move with the bulk velocity of the fluid. For a drop of 10^6 atoms composed of iron we have

$$n = 10^6$$

$$\rho \approx 7 \text{ gm/cm}^3$$

$$R \approx 10^{-6} \text{ cm}$$

$$g = 980 \text{ cm/sec}^2$$

$$\nu \approx 1 \text{ cm}^2/\text{sec}$$

$$\mu \approx 10^{-3} \text{ gm/cm-sec}$$

$$\omega \approx 1500 \text{ rad/sec}$$

These give

$$\frac{\rho R^2 g}{\mu\sqrt{\nu\omega}} \approx 10^{-6}$$

and

$$\frac{\omega\sqrt{\nu\omega}}{g} \approx 60$$

Thus all drops less than 10^6 atoms definitely move with the bulk velocity of the fluid, because the velocity and distance defects at the top, middle, and bottom of the boundary layer are 10^{-6}, 10^{-6} and $60 \cdot 10^{-6}$ respectively.

APPENDIX B

THE GROUP EQUATIONS

The method used for converting the individual drop conservation equation, Eq. (58), to a group conservation equation is as follows. First sum Eq. (58) over the n + 1 drop sizes in the group from g_i to g_{i+n}, this gives

$$\frac{d^2}{dx^2}\left(V_{g_i} + V_{g_{i+1}} + \ldots + V_{g_{i+n}}\right) -$$

$$-Sc_{\bar{g}_i}\,\hat{H}(x)\,\frac{d}{dx}\left(V_{g_i} + V_{g_{i+1}} + \ldots + V_{g_{i+n}}\right) =$$

$$= -Sc_{\bar{g}_i}\left[\left(\beta^+_{g_{i-1}} V_{g_{i-1}} - \alpha^+_{g_i} V_{g_i} - \beta^+_{g_i} V_{g_i} + \alpha^+_{g_{i+1}} V_{g_{i+1}}\right) +\right.$$

$$+\left(\beta^+_{g_i} V_{g_i} - \alpha^+_{g_{i+1}} V_{g_{i+1}} - \beta^+_{g_{i+1}} V_{g_{i+1}} + \alpha^+_{g_{i+2}} V_{g_{i+2}}\right) +$$

$$+ \ldots + \qquad\qquad (B\text{-}1)$$

$$\left.+\left(\beta^+_{g_{i+n-1}} V_{g_{i+n-1}} - \alpha^+_{g_{i+n}} V_{g_{i+n}} - \beta^+_{g_{i+n}} V_{g_{i+n}} +\right.\right.$$

$$\left.\left.+\,\alpha^+_{g_{i+n+1}} V_{g_{i+n+1}}\right)\right]$$

Where the Schmidt number ν/D_g has been evaluated at the mean drop size $\bar{g}_i$ for the group. The mean drop size is given by:

$$\bar{g}_i = g_i + \frac{n}{2} \qquad (B\text{-}2)$$

Noting that most of the terms on the right-hand size of the equation cancel the equation becomes

$$\frac{d^2}{dx^2}\left(V_{g_i} + V_{g_{i+2}} + \ldots + V_{g_{i+n}}\right) - Sc_{g_i}\,\hat{H}(x)\cdot \frac{d}{dx}\left(V_{g_i} + V_{g_{i+1}} + \ldots + V_{g_{i+n}}\right) = Sc_{g_i}\cdot \left(\beta^{+}_{g_{i-1}} V_{g_{i-1}} - \alpha^{+}_{g_i} V_{g_i} - \beta^{+}_{g_{i+n}} V_{g_{i+n}} + \alpha^{+}_{g_{i+n+1}} V_{g_{i+n+1}}\right) \tag{B-3}$$

Now the mean droplet concentration for the group $V^{-}_{g_i}$ is by definition

$$V^{-}_{g_i} = \frac{1}{n+1}\left(V_{g_i} + V_{g_{i+1}} + \ldots + V_{g_{i+n}}\right) \tag{B-4}$$

and hence Eq. (B-3) becomes:

$$\frac{d^2}{dx^2} V^{-}_{g_i} - Sc^{-}_{g_i}\,\hat{H}(x)\,\frac{dV^{-}_{g_i}}{dx} = -\frac{1}{n+1} Sc^{-}_{g_i}\cdot \left(\beta^{+}_{g_{i-1}} V_{g_{i-1}} - \alpha^{+}_{g_i} V_{g_i} - \beta^{+}_{g_{i+n}} V_{g_{i+n}} + \alpha^{+}_{g_{i+n+1}} V_{g_{i+n+1}}\right) \tag{B-5}$$

Suppose the group under consideration is called the i^{th} group. Then physically $\beta^{+}_{g_{i-1}} V_{g_{i-1}}$ in the source term belongs to the i-1 group and is the rate of transfer of drops from the i-1 group into the i^{th} group by atoms condensing on drops and $\alpha^{+}_{g_i} V_{g_i}$ is the rate of transfer of drops from the i^{th} group into the i-1 group by evaporation of atoms from drops. Likewise, $\beta^{+}_{g_{i+n}} V_{g_{i+n}}$ is the rate of transfer of drops from the i^{th} group to the i+1 group and $\alpha^{+}_{g_{i+n+1}} V_{g_{i+n+1}}$ which belongs to the i+1 group, is the rate of transfer of drops from the i+1 group to the i^{th} group. Thus, $\beta^{+}_{g_{i-1}} V_{g_{i-1}} - \alpha^{+}_{g_i} V_{g_i}$ is the rate of transfer of drops across the group interface at the low g end and $\beta^{+}_{g_{i+n}} V_{g_{i+n}} - \alpha^{+}_{g_{i+n+1}} V_{g_{i+n+1}}$ is the rate of transfer of drops across the group interface at the high g end.

The terms on the right-hand side of Eq. (B-5) are obtained by interpolation, since during the solution only the values at the mean for the groups, i.e. at $\bar{g}_i$, are known.

The source term for the monomer equation in this multigroup formulation may be derived in exactly the same manner as was Eq. (22), i.e. by multiplying Eq. (B-5) by $\bar{g}_i$, and summing all such equations along with the monomer equation to obtain a general continuity equation for both drops and monomer. By inspection of the process leading to Eq. (22) it can be seen that the monomer source term S_1 in the multigroup formulation will be:

$$S_1 = \sum_{i=1}^{\infty} \bar{g}_i \, (n+1) \, S^{+}_{\bar{g}_i} \qquad \text{(B-6)}$$

$$S^{+}_{\bar{g}_i} = \frac{1}{n+1}\left(\beta^{+}_{g_{i-1}} V_{g_{i-1}} - \alpha^{+}_{g_i} V_{g_i} - \beta_{g_{i+n}} V_{g_{i+n}} + \alpha^{+}_{g_{i+n+1}} V_{g_{i+n+1}}\right) \qquad \text{(B-7)}$$

The monomer then becomes:

$$\frac{d^2U}{dx^2} - Sc_f \, \hat{H}(x) \, \frac{dU}{dx} = Sc_f \sum_{i=1}^{\infty} \bar{g}_i \, (n+1) \, S^{+}_{\bar{g}_i} \qquad \text{(B-8)}$$

The group mean drop size $\bar{g}_i$ is given in terms of i and g_0 by the equation

$$\bar{g}_i = g_0 + i\,(n+1) - (1+n/2) \qquad \text{(B-9)}$$

For completeness, the entire set of equations which define the problem are listed in the multigroup formulation. The boundary conditions are:

$$U = 1, \quad V_{\bar{g}_i} = \exp\left(-\frac{b}{kT_w}\,\bar{g}_i^{\,2/3}\right) \quad \text{at } x = 0$$

$$U \to 0, \; V_{\bar{g}_i} \to 0 \quad \text{as } x \to \infty \tag{B-10}$$

$$V_{\bar{g}_i} = J^{+}(x)/\beta^{+}_{\bar{g}_i}(x) \text{ at } i = 0 \text{ in the nucleation zone}$$

$$V_{\bar{g}_i} \leftrightarrow 0 \quad \text{as } \bar{g}_i \to \infty$$

The transcendental droplet equation is

$$\left(T_{\bar{g}_i} / T_w\right)^4 + C_1\left(T_{\bar{g}_i}/T_w - T/T_w\right) = 2 - C_2\left(\alpha^{+}_{\bar{g}_i} - \beta^{+}_{\bar{g}_i}\right) \tag{B-11}$$

$$C_1 = \frac{c_p A_{th} \beta^{+}_{gas} \omega}{\sigma \epsilon T_w^{\,3} A_{\bar{g}_i}}$$

$$C_2 = \frac{\ell\omega}{\sigma\epsilon T_w^{\,4} A_{\bar{g}_i}}$$

where the area $A_{\bar{g}_i}$ is

$$A_{\bar{g}_i} = 4\pi\left(\frac{3}{4\pi\bar{N}}\right)^{2/3} \bar{g}_i^{\,2/3} \tag{B-12}$$

and the evaporation and condensation coefficients are:

$$\beta^{+}_{\bar{g}_i} = \frac{A_{\bar{g}_i}}{\omega} \frac{p_{vw}}{\sqrt{2\pi m k T_w}} \frac{U(x)}{\sqrt{T/T_w}} \frac{1}{\left(1 + \frac{r_{\bar{g}_i}}{D}\sqrt{\frac{kT}{2\pi m}}\right)} \tag{B-13}$$

$$\alpha^{+}_{\bar{g}_i} = \frac{A_{\bar{g}_i}}{\omega} \frac{p_{v,eq}\left(T_{\bar{g}_i}\right)}{\sqrt{2\pi m k T_w}} \sqrt{\frac{T_w}{T_{\bar{g}_i}}} \exp\left(\frac{2b}{3kT_{\bar{g}_i}}\,\bar{g}_i^{\,-1/3}\right) \cdot$$

$$\cdot \frac{1}{\left(1 + \frac{r_{\bar{g}_i}}{D}\sqrt{\frac{kT}{2\pi m}}\right)} \tag{B-14}$$

The Eqs. (B-5) - (B-14) define the problem in the multigroup formulation.

APPENDIX C

THE EFFECT OF THERMAL DIFFUSION

The effect of thermal diffusion in the boundary layer upon the vaporization rate is shown below. If condensation is neglected, the monomer equation including thermal diffusion is from Eq. (6)

$$w \frac{d}{dz} (\rho_v/\rho) = \frac{d}{dz} \left(\rho D \frac{d}{dz} (\rho_v/\rho) + D_T \frac{1}{T} \frac{dT}{dz} \right) \tag{C-1}$$

where the radial terms have been dropped. D_T is the thermal diffusion coefficient. In the dimensionless variables of this problem the equation becomes

$$\frac{d^2U}{dx^2} - Sc \, \hat{H}(x) \frac{dU}{dx} = - \left(\frac{n_{gas}}{n_v} \right)_w \frac{d}{dx} \left(\frac{k_T}{T} \frac{dT}{dx} \right) \tag{C-2}$$

where n_{gas} and n_v are the molar concentrations of inert gas and vapor, respectively, and k_T is the thermal diffusion ratio

$$k_T = \frac{1}{M_v \, M_{gas} \, n^2} \frac{\rho D_T}{D} \tag{C-3}$$

with M_{gas} and M_v the molecular weights of the gas and vapor, respectively, and n the molar concentration in moles/cm^3 of the mixture.

The thermal diffusion factor α_T is defined

$$\alpha_T = \frac{k_T}{X_v \, X_{gas}} \tag{C-4}$$

and is generally considered to be a weak function of temperature.[17]

Since the system is dilute in the vapor, $X_{gas} \approx 1$. Equation (C-2) then becomes

$$\frac{d^2U}{dx^2} - Sc\ \hat{H}(x)\ \frac{dU}{dx} = -\left(\frac{1}{X_v}\right)_w\ \frac{d}{dx}\ \left(X_v\ \frac{\alpha_T}{T}\ \frac{dT}{dx}\right) \qquad (C\text{-}5)$$

and this equation was solved assuming α_T constant. Since Eq. (C-5) must be integrated over the entire boundary layer, the thermal diffusion factor α_T was evaluated at the recommended mean temperature for thermal diffusion $\bar{T}$.[17]

$$\bar{T} = \frac{T_w - T_\infty}{T_w\ T_\infty}\ \ln\ (T_w/T_\infty) \qquad (C\text{-}6)$$

With the straight line approximation to the velocity profile

$$\hat{H} = -\ 1/4\ x \qquad (C\text{-}7)$$

an integrating factor can be found for Eq. (C-5) and the equation solved for the gradient at the wall giving

$$\left(\frac{dU}{dx}\right)_w = -\sqrt{\frac{Sc}{2\pi}}\left(1 - \alpha_{\bar{T}} \int_0^\infty \exp\ \left(-\frac{1}{8} Sc\ \eta^2\right) \int_0^\eta \exp\ \left(\frac{1}{8} Sc\ \xi^2\right) \cdot \right.$$

$$\left. \cdot\ \frac{d}{d\xi}\ \left(\left(\frac{X_v}{X_{vw}}\right)\ \frac{1}{T}\ \frac{dT}{dx}\right) d\xi\ \ d\eta\right) \qquad (C\text{-}8)$$

$$= -\sqrt{\frac{Sc}{2\pi}}\ \ (1 - \alpha_{\bar{T}}\ \frac{Pr}{2\pi}\ R) \qquad (C\text{-}9)$$

where R has simply been defined as the value of the integral in Eq. (C-8) over $Pr/2\pi$. A Prandtl number dependence in R is incurred through T and dT/dx inside the integral and defining R in this way makes the dependence weaker. R was numerically calculated as a function of temperature using

the concentration unperturbed by thermal diffusion for X_v. This should not be a bad assumption if the effect of thermal diffusion is small.

The thermal diffusion current is defined

$$\vec{j}_T = D_T \frac{1}{T} \nabla T \tag{C-10}$$

Thus the mass flux at the wall including thermal diffusion is

$$j = - (\rho D) \frac{d}{dz} (\rho_v/\rho) + D_T \frac{1}{T} \frac{dT}{dz} \quad \text{at } z = 0 \tag{C-11}$$

and in the dimensionless variables of this problem is:

$$j = - (\rho D)_w \sqrt{\frac{\omega}{\nu_w}} c_w \left[\left(\frac{dU}{dx}\right)_w + \alpha_{T_w} \left(\frac{1}{T} \frac{dT}{dx}\right)_w \right] \tag{C-12}$$

where α_T must be evaluated at the wall temperature T_w. Now the solution of the energy Eq. (5) using Eq. (C-7) can be shown to be

$$T = T_w - (T_w - T_\infty) \operatorname{erf} \left(\sqrt{\frac{Pr}{8}} x\right) \tag{C-13}$$

and hence

$$\left(\frac{1}{T} \frac{dT}{dx}\right)_w = - \sqrt{\frac{Pr}{2\pi}} \left(1 - \frac{T_\infty}{T_w}\right) \tag{C-14}$$

Thus the mass flux j becomes

$$j = - (\rho D)_w \sqrt{\frac{\omega}{\nu_w}} c_w \left[\left(\frac{dU}{dx}\right)_w - \alpha_{T_w} \sqrt{\frac{Pr}{2\pi}} \left(1 - \frac{T_\infty}{T_w}\right) \right] \tag{C-15}$$

Using the value of $\left(\frac{dU}{dx}\right)_w$ from Eq. (C-9) the vaporization rate can now be written as

$$j = (\rho D)_w \sqrt{\frac{\omega}{\nu_w}} c_w \sqrt{\frac{Sc}{2\pi}} \left[1 - \alpha_{\bar{T}} \frac{Pr}{2\pi} R + \alpha_{T_w} \sqrt{\frac{Pr}{Sc}} \left(1 - \frac{T_\infty}{T_w}\right) \right] \tag{C-16}$$

The thermal diffusion factors in Eq. (C-16) were calculated from Chapman-Enskog theory using the Lennard-Jones (6-12) potential.[17,44] The Lennard-Jones parameters for iron were calculated from the properties of iron at the melting point.

If we define

$$\phi_{td} = 1 - \alpha_T \frac{Pr}{2\pi} R + \alpha_{T_w} \sqrt{\frac{Pr}{Sc}} \left(1 - \frac{T_\infty}{T_w}\right) \qquad (C\text{-}17)$$

then

$$j = j^* \phi_{td} \qquad (C\text{-}18)$$

where ϕ_{td} gives the effect of thermal diffusion upon the isothermal mass flux j^*. The results are shown in Table III. It is seen that the effect of thermal diffusion is small, on the order of 3% to 4%. For this reason we have neglected it in the calculations

Table III. Effect of thermal diffusion

T_w (°K)	$\bar{T}$ (°K)	α_{T_w}	$\alpha_{\bar{T}}$	R	ϕ_{td}
1500	590	0.052	-0.0026	3.05	1.033
1600	605	0.055	-0.0011	3.10	1.036
1700	620	0.057	0.0003	3.13	1.039
1800	635	0.059	0.0017	3.16	1.042

APPENDIX D

THE SINGULAR PERTURBATION FORM OF THE DROPLET EQUATION

The method of singular perturbation was applied to the droplet conservation equation so that the effect of diffusion of the drops could be considered in a more exact manner. As noted in the discussion section of this manuscript, each drop size has its own Schmidt number and hence its own boundary layer thickness. The boundary layer thickness varies inversely with the one-third power size of the drop. Since we are interested in the effect of the drops on the monomer concentration, all the equations must be solved over the boundary layer region of the monomer. This means that the droplet problem for large drops must be solved over a region of many boundary layers. However, it is in general very diffcult to solve an equation numerically over a distance of many boundary layers. It was fortunate, in this case, that the droplet equation could be handled by the method of singular perturbation.[45] This method allows one to perturb the solution in such a manner that the drop concentration within the droplet boundary layer was given in terms of the solution outside the droplet boundary layer. Outside of the droplet boundary layer the concentration had to be calculated numerically, but this was relatively easy to do compared to numerically trying to handle the problem in both regions.

The technique is as follows. The drop concentration equation is

$$\frac{d^2V_g}{dx^2} - \hat{H}(x)\ Sc\ g^{2/3}\frac{dV_g}{dx} = -g^{2/3}\ Sc\ S_g^{+}(x) \qquad (D\text{-}1)$$

with boundary conditions

$$V_g = V_{g,eq} \quad \text{at } x = 0 \qquad (D\text{-}2)$$

$$V_g \to 0 \quad \text{as} \quad x \to \infty$$

$V_{g,\,eq}$ implies the balanced equilibrium concentration at zero supersaturation and is given by Eq. (59) in the main section of this report. The following relationship has also been used:

$$Sc_g = \frac{\nu}{D_g} \quad \frac{\nu}{(D/g^{2/3})} = Sc\, g^{2/3}$$

If we define

$$\mu_g = 1/g^{2/3} \tag{D-3}$$

where μ_g is a small parameter because g is in general quite large, then Eq. (D-1) becomes

$$\mu_g \frac{d^2V_g}{dx^2} - \hat{H}(x) \quad Sc \frac{dV_g}{dx} = - Sc\, S_g^+(x) \tag{D-4}$$

Note that a regular perturbation expansion about the small parameter μ_g cannot be made because the zero order perturbation requires setting $\mu_g = 0$ and this eliminates the second derivative thus giving a lower order differential equation than the original Eq. (D-4). Hence a singular perturbation must be used. This is done by constructing an inner expansion valid for small distances x and an outer expansion valid for large distances x and then matching them in some manner.

For the outer expansion, a regular perturbation problem is formulated in the usual fashion.[45] Let V_g be explained in terms of power of μ_g

$$V_g = V_{0g} + \mu_g V_{1g} + \mu_g^2 V_{2g} + \ldots \tag{D-5}$$

Putting this expansion into Eq. (D-5), collecting the coefficients of like powers of μ_g, and then requiring these coefficients to be equal to zero because μ_g is an arbitrary parameter, gives the following set of differential equations

$$
\begin{aligned}
-\hat{H}(x)\ Sc\ \frac{dV_{0g}}{dx} &= -\ Sc\ S_g^+(x) \\
-\hat{H}(x)\ Sc\ \frac{dV_{1g}}{dx} &= -\ \frac{d^2V_{0g}}{dx^2} \\
-\hat{H}(x)\ Sc\ \frac{dV_{2g}}{dx} &= -\ \frac{d^2V_{1g}}{dx^2} \\
&\cdots\cdots\cdots \\
&\cdots
\end{aligned}
\qquad \text{(D-6)}
$$

In this problem we will be satisfied with only the zero order perturbation, i.e. we keep only the first equation. Thus the solution in the outer region is given by

$$\hat{H}(x)\ \frac{dV_g^{OE}}{dx} = S_g^+(x) \qquad \text{(D-7)}$$

where the superscript OE implies outer expansion.

For the inner expansion a new distance τ is defined

$$\tau = x/\mu_g$$

where, since μ_g is small, τ is enlarged interior distance. Then Eq. (D-4) becomes

$$\frac{d^2V_g}{d\tau^2} - \hat{H}(x)\ Sc\ \frac{dV_g}{d\tau} = -\mu_g\ Sc\ S_g^+(\tau) \qquad \text{(D-8)}$$

and note that it is now in a form amenable to regular perturbation about the parameter μ_g. Applying regular perturbation in the usual fashion gives[45]

$$V_g = V_{0g} + \mu_g V_{1g} + \mu_g^2 V_{2g} + \cdots \qquad \text{(D-9)}$$

and the following set of perturbed equations

$$\frac{d^2V_{0g}}{d\tau^2} - \hat{H}(\tau)\ Sc\ \frac{dV_{0g}}{d\tau} = 0$$

$$\frac{d^2V_{1g}}{d\tau^2} - \hat{H}(\tau)\ Sc\ \frac{dV_{1g}}{d\tau} = -Sc\ S_g^+(\tau) \qquad \text{(D-10)}$$

$$\frac{d^2V_{2g}}{d\tau^2} - \hat{H}(\tau)\ Sc\ \frac{dV_{2g}}{d\tau^2} = 0$$

. . . . . .

. . .

Again we will keep only the zero order equation

$$\frac{d^2V_g^{IE}}{d\tau^2} - \hat{H}(\tau)\ Sc\ \frac{dV_g^{IE}}{d\tau} = 0 \qquad \text{(D-11)}$$

where the superscript IE denotes inner expansion.

Equation (D-7) describes the droplet concentration outside the droplet boundary layer and Eq. (D-11) describes the droplet concentration inside the droplet boundary layer. Note that Eq. (D-7) says phsycially that the concentration in the outer region is determined by a balance between the source and the convective term and that diffusion is of second order. Equation (D-11) says physically that the concentration in the inner region is determined by a balance between the diffusive and convective terms and that the source is of second order. Both of these are precisely what would be expected.

The solution of the inner and outer Equations (D-7) and (D-11) will be greatly simplified if an approximate velocity profile can be used. For the outer equation, i.e. Eq. (D-7) the normal approximation

$$\begin{aligned} \hat{H}(x) &= 1/4x \qquad 0 < x < x_o \\ \hat{H}(x) &= -\hat{H}_\infty \qquad x_o < x < \infty \\ \hat{H}_\infty &= 0.866 \qquad x_o = 3.54 \end{aligned} \qquad \text{(D-12)}$$

is certainly satisfactory. However, for the inner equation this profile will not be valid because all distances x are very small. Sparrow and Gregg[30] have shown that a solution based on the approximation $\hat{H}(x) = -x^2/2$ for small x can be found, but the solution is in terms of the incomplete gamma function and this function is difficult to generate inside a machine. A profile similar in form to Eq. (D-12) would be desirable because an analytic solution in terms of error functions is immediately available. In view of this, the following technique was used. If Eq. (D-11) is written in terms of the distance x, it can be shown, using the results of Sparrow and Gregg's paper, that the gradient at the wall is given by

$$\left(\frac{dV_g}{dx}\right)_w \approx \frac{1}{\Gamma(4/3)} \sqrt[3]{\frac{g^{2/3}\, Sc}{6}} \qquad \text{(D-13)}$$

Since the film thickness δ is approximately equal to $\left(\frac{dV_g}{dx}\right)_w^{-1}$, we have

$$\delta \approx \Gamma(4/3) \sqrt[3]{\frac{6}{g^{2/3}\, Sc}} \qquad \text{(D-14)}$$

In general δ is not the boundary layer thickness but about three-fourths of it. If at the distance δ an approximate velocity profile $\hat{H}(x) = \epsilon x$, ϵ an arbitrary parameter, is matched to the better approximation $\hat{H}(x) = -x^2/2$, and approximate linear velocity profile will be the result. This turns out to be, in terms of τ

$$\hat{H}(\tau) = -2\, a_g\, \tau$$

$$a_g = 1/4\, \mu_g\, \Gamma(4/3) \sqrt[3]{\frac{6\mu_g}{Sc}} \qquad \text{(D-15)}$$

The inner Eq. (D-7) can now be solved to give

$$V_g^{IE}(x) = C_1 \sqrt{\frac{\pi}{4a_g}}\, \text{erf}\,(\sqrt{a_g}\,\tau) + V_{g,eq} \qquad \text{(D-16)}$$

The solution of the outer Eq. (D-11) is

$$V_g^{OE}(x) = C_2 + \int_0^x \frac{1}{\hat{H}(\eta)} S_g^+(\eta)\, d\eta \qquad \text{(D-17)}$$

The constant C_2 can be found from the boundary condition $V_g \to 0$ as $x \to \infty$. This gives

$$C_2 = - \int_0^\infty \frac{1}{\hat{H}(\eta)} S_g^+(\eta)\, d\eta \qquad \text{(D-18)}$$

The constant C_1 can be found only by matching the inner and outer solutions in some fashion. One method which gives a continuous solution is to determine the "common part", i.e. to require that

$$\lim_{x\to 0} V_g^{OE} = \lim_{\tau\to\infty} V_g^{IE} = \text{common part} \qquad \text{(D-19)}$$

The complete solution V_g is then given by

$$V_g = V_g^{IE} + V_g^{OE} - \text{common part} \qquad \text{(D-20)}$$

Applying this to Eqs. (D-16) and (D-17) gives

$$\text{common part} = C_2 \qquad \text{(D-21)}$$

and

$$C_1 = \sqrt{\frac{4a_g}{\pi}} (C_2 - V_{g,eq}) \qquad \text{(D-22)}$$

Thus the complete singular perturbation solution becomes

$$V_g = V_{g,eq} (1 - \text{erf} (\sqrt{a_g}\, g^{2/3} x)) + C_2 \text{ erf} (\sqrt{a_g}\, g^{2/3} x) + \int_0^x \frac{1}{\hat{H}(\eta)} S_g^+(\eta)\, d\eta \qquad \text{(D-23)}$$

where

$$C_2 = - \int_0^\infty \frac{1}{\hat{H}(\eta)} S_g^+(\eta)\, d\eta \qquad \text{(D-24)}$$

and $\hat{H}(x)$ is given by Eq. (D-12).

These two equations were used to determine the droplet concentration V_g. The parts involving the source term $S_g^+(x)$ were determined in the program from a previous iteration.

APPENDIX E

CALCULATION OF THE EFFECTIVE DISK TEMPERATURE

While the disk was operating at high temperature, a small radial temperature variation of the approximately 15°C usually existed across it. Because of this radial temperature variation, three temperature measurements were taken; the location of these measurements was at $r/r_0 \approx 0$, $r/r_0 \approx 1/2$, and $r/r_0 \approx 1$, where r_0 is the radius of the chromium disk. The effective temperature of the disk was then determined from these three measurements in the following fashion.

If the three temperatures are denoted T_0, $T_{1/2}$ and T_1, then $T(r)$ can be approximated by passing a parabola through these three points to give:

$$T(r) = T_0 + 2(T_{1/2} - T_0)\ \frac{r}{r_0} + 2(T_1 - 2T_{1/2} + T_0)\ \frac{r}{r_0}\ \left(\frac{r}{r_0} - \frac{1}{2}\right) \tag{E-1}$$

This function $T(r)$ was used to calculate the vapor pressure at any point on the disk. The effective temperature cannot be calculated from $T(r)$ directly because its effect upon the vaporization rate is through the vapor pressure. For a disk with a constant vapor pressure across its surface, the mass loss m is proportional to the vapor pressure and the area, i.e.

$$m \sim p(T)\ A \tag{E-2}$$

For a disk with a small radial variation in vapor pressure, the mass loss should be approximately proportional to the integral of the vapor pressure over the area

$$m \sim \int_A p(T)\ dA = \bar{p} \int_A dA \tag{E-3}$$

where the last equality is simply the definition of the average pressure $\bar{p}$ over the disk. The effective temperature of the disk was then taken

to be the temperature corresponding to this average pressure. From the Clausius-Clapeyron equation

$$p = C \exp\left(-\frac{\lambda}{kT}\right) \qquad \text{(E-4)}$$

and so

$$\bar{T} = \frac{\lambda}{k \ln (C/\bar{p})} \qquad \text{(E-5)}$$

Putting Eq. (E-4) into Eq. (E-3) and using the definition Eq. (E-5) gives

$$e^{-\lambda/k\bar{T}} = \frac{2}{r_0^2} \int_0^{r_0} e^{-\lambda/kT(r)}\, r dr \qquad \text{(D-6)}$$

Multiplying both sides by e^{λ/kT_0} and approximating the exponential by

$$\exp\left(\frac{\lambda}{kT_0\bar{T}}\,(\bar{T} - T_0)\right) \approx 1 + \frac{\lambda}{kT_0\bar{T}}\,(\bar{T} - T_0) \qquad \text{(E-7)}$$

gives

$$\bar{T} = \frac{2}{r_0^2} \int_0^{r_0} T(r)\, r\, dr \qquad \text{(E-8)}$$

where it has been assumed that $1/T \approx 1/\bar{T}$. Note that Eq. (E-8) is simply the definition of the average temperature over the disk and that the effect of the vapor pressure has cancelled out.

Using Eq. (E-1) gives

$$\bar{T} = T_{1/2} + 1/3(T_1 - T_{1/2}) \qquad \text{(E-9)}$$

This equation was used to calculate the effective temperature of the disk from the three readings at different radii.

APPENDIX F

DETERMINATION OF THE SURFACE EMISSIVITY

The most general method of determining the emissivity of a surface is to measure the true temperature of the surface with a thermocouple while at the same time measuring the brightness temperature with an optical pyrometer. Knowing the true temperature and the brightness temperature, the emissivity of the surface can be calculated from Plank's radiation law.[46] However, for a small rotating disk system designed to run at high temperatures and high speeds such as was used in this experiment, it is very difficult to place a thermocouple in direct contact with the disk. Any modification which is made in the disk system to install the thermocouple compromises the integrity of the system while operating and the integrity is marginal at best.

An alternative method of measuring the emissivity is to drill a blackbody of the correct length-to-diameter ratio in the disk and to read the temperature of this hole directly. Generally a length-to-diameter ratio of four is required. This is difficult to do, however, because a rotating disk operating at 1500°C is a highly non-isothermal system, and the bottom of the hole will probably be at a different true temperature than the surface. The calculated emissivity will thus be in error.

A third method is to drill a hole of ℓ/d considerably less than four and to try to calculate the emissivity of the surface from the observed temperature of the hole and of the surface. This requires correcting for the axial temperature gradient and for the non-unity emissivity of the hole. This was the procedure followed in this experiment. The method is outlined below.

Consider a disk with a hole drilled in it of $\ell/d < 4$. If the disk is

in an axial temperature gradient, the observed temperature at the bottom of the hole will differ from the true temperature of the surface by an effect due first to the apparent emissivity of the hole and second to the axial temperature gradient. The observed temperature of the surface will differ from the true temperature of the surface by an effect due to the emissivity of the surface.

From Plank's radiation law, the true temperature T_t is related to the apparent temperature T_o for a surface with emissivity ϵ at wavelength λ by

$$T_t = \frac{C_2/\lambda}{\ln [\epsilon (\exp(C_2/\lambda T_o - 1) + 1]} \qquad \text{(F-1)}$$

where $C_2 = 1.438 \cdot 10^4 \ \mu \cdot {}^\circ K$ and $\lambda = 0.655 \ \mu$ for an optical pyrometer. If T_o is small enough, i.e.

$$T_o << C_2/\lambda \approx 10^4 \ {}^\circ K$$

then Plank's law can be approximated by[39]

$$\frac{1}{T_t} = \frac{1}{T_o} + \frac{\lambda}{C_2} \ln \epsilon \qquad \text{(F-2)}$$

Uniform Temperature

First consider the case where the hole is not in an axial temperature gradient. Then the true temperature of the hole and surface are the same and from Eq. (F-2)

$$\frac{1}{T_{s_o}} + \frac{\lambda}{C_2} \ln \epsilon_s = \frac{1}{T_{h_o}} + \frac{\lambda}{C_2} \ln \epsilon_h \qquad \text{(F-3)}$$

or

$$T_{h_o} - T_{s_o} \approx T_{s_o}^2 \frac{\lambda}{C_2} \ln \frac{\epsilon_h}{\epsilon_s} \qquad \text{(F-4)}$$

where the approximation $T_{h_o} T_{s_o} \approx T_{s_o}^2$ has been used.

From Eq. (F-4) we can calculate the ratio of the emissivities directly from the observed hole and surface temperatures. Using the results from a paper by Sparrow and Albers[36] the emissivity of the surface can now be calculated directly. Sparrow and Albers calculated the apparent emissivity of a cylindrical hole by solving the associated integral equation numerically. In Fig. F-1 their results have been plotted to give the emissivity ratio ϵ_h/ϵ_s as a function of emissivity of the surface ϵ_s and length to diameter ratio ℓ/d. From this figure it can be seen that knowing the emissivity ratio and the length-to-diameter ratio, the emissivity of the surface can be found.

In actual practice, a series of hole and surface temperatures can be measured for different values of the surface temperature and the differences of hole and surface temperature divided by the surface temperature squared can be plotted as a function of surface temperature squared. Equation (F-4) says that these results should plot as a straight line of zero slope; if they do then the effect of temperature gradients is small and ratio of the emissivities can be determined from the average value of $(T_{h_o} - T_{s_o})/T_{s_o}^2$. If, however, temperature gardients are not negligible, then the points $(T_{h_o} - T_{s_o})/T_{s_o}^2$ versus $T_{s_o}^2$ should fall on a straight line of non-zero slope. This will be shown below.

Axial Temperature Gradient

Consider a hole in an axial temfperature gradient. The relation between the true temperature of the bottom of the hole and the true temperature of the surface is given by the solution to the heat conduction equation

$$k \nabla^2 T + Q = 0 \qquad \text{(F-5)}$$

Assume that the problem is one-dimensional, i.e. the disk is much wider than it is deep. Also assume, for simplicity, that the source due to the

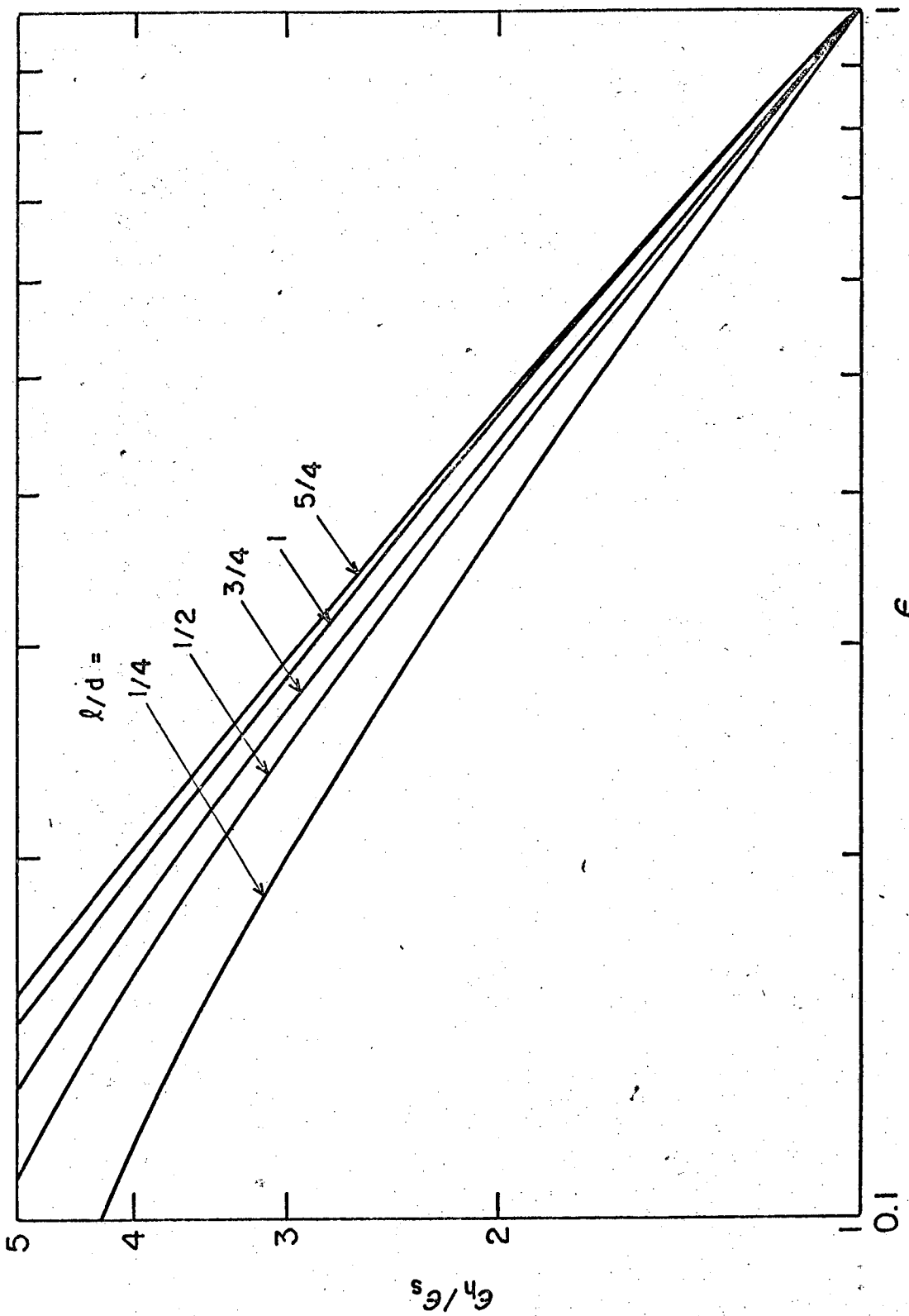

Fig. F-1

induction heating is constant. Then

$$\frac{d^2T}{dz^2} = -\frac{Q}{k} \tag{F-6}$$

and

$$T = (1/2k)\, Qz^2 + C_1 z + C_2 \tag{F-7}$$

If we call the temperature at the lower edge of the disk ($z = 0$) T_0 and the temperature at the upper edge ($z = \ell$) T_ℓ, then

$$T = -\frac{1}{2k}\, Qz^2 + (T_\ell - T_0)\, \frac{x}{\ell} + \frac{x\ell}{2k}\, Q + T_0 \tag{F-8}$$

where T_0 and T_ℓ are unknown at this point and are merely an artifice to determine the interior temperature in terms of the surface temperature. At the upper edge the heat transfer is by radiation and so

$$-k\left(\frac{dT}{dz}\right)_\ell = \sigma \epsilon_s T_\ell^4 \tag{F-9}$$

and applying this boundary condition to Eq. (F-8) gives

$$T_\ell - T_0 = \frac{\ell}{k}\left(\frac{\ell Q}{2} - \sigma \epsilon_s T_\ell^4\right) \tag{F-10}$$

Now the heat transfer from the lower side for the rotating disk was by conduction through several different materials in series. To determine the lower boundary condition would be a very difficult problem. Suppose we assume for simplicity that the lower edge is adiabatic and that the heat generated in the disk always leaves through the upper surface by radiation. Then

$$\sigma \epsilon_s T_\ell^4 = Q\ell \tag{F-11}$$

and so Eq. (F-10) becomes

$$T_0 - T_\ell = \frac{\ell}{k}\, \sigma \epsilon_s T_\ell^4 \tag{F-12}$$

If Eq. (F-8) is evaluated at the hole depth h and Eqs. (F-11) and (F-12) substituted into it, it will be found that the temperature of the hole

T_h minus the surface temperature T_ℓ, is proportional to $T_0 - T_\ell$ (T_ℓ is identical to T_s). The proportionality constant will not be calculated, however, but simply called a. Thus from Eqs. (F-8), (F-11) and (F-12)

$$T_h - T_\ell = a(T_0 - T_\ell) \tag{F-13}$$

and from Eq. (F-12)

$$T_h - T_\ell = \frac{a\ell\sigma\epsilon_s}{k} T_\ell^4$$

The important characteristic of this equation is that the difference between the hole and surface temperatures is directly proportional to the fourth power of the surface temperature.

Now Eq. (F-4) gives the relation between the true hole and surface temperatures and Eq. (F-2) gives the relation between the true and observed temperatures. Rewriting them in the prior nomenclature gives

$$T_{h_t} - T_{s_t} = \frac{a\ell\sigma\epsilon_s}{k} T_{s_t}^4 \tag{F-14}$$

$$T_{h_t} = T_{h_0} - T_{h_t} T_{h_o} \frac{\lambda}{C_2} \ln \epsilon_h \tag{F-15}$$

$$T_{s_t} = T_{s_o} - T_{s_t} T_{s_o} \frac{\lambda}{C_2} \ln \epsilon_s \tag{F-16}$$

Putting Eqs. (F-15) and (F-16) into Eq. (F-14) gives

$$T_{h_0} - T_{s_o} = T_{h_o}^2 \frac{\lambda}{C_2} \ln \epsilon_h - T_{s_o}^2 \frac{\lambda}{C_2} \ln \epsilon_s + \frac{a\ell\sigma\epsilon_s}{k} T_{s_t}^4 \tag{F-17}$$

where the approximations $T_{h_t} T_{h_o} \approx T_{h_o}^2$ and $T_{s_t} T_{s_o} \approx T_{s_o}^2$ have been used. The variable $T_{s_t}^4$ in the last term of Eq. (F-17) can be approximated in the following manner. Taking both sides of Eq. (F-16) to the fourth power:

$$T_{s_t}^4 = T_{s_o}^4 - 4\left(\frac{\lambda}{C_2} \ln \epsilon_s\right) T_{s_o}^5 + 6\left(\frac{\lambda}{C_2} \ln \epsilon_s\right)^2 T_{s_o}^6 -$$

$$- 4\left(\frac{\lambda}{C_2} \ln \epsilon_s\right)^3 T_{s_o}^7 + \left(\frac{\lambda}{C_2} \ln \epsilon_s\right)^4 T_{s_o}^8 \qquad \text{(F-18)}$$

Since $T_s \sim O(10^3)$, $\frac{\lambda}{C_2} \ln \epsilon_s \sim O(10^{-5})$, $\ell\sigma\epsilon_s/k \sim O(10^{-12})$ for $\epsilon_s \approx 1/2$, and $a \sim O(1)$, the last term of Eq. (A-17) is on the order of

$$\frac{a\ell\sigma\epsilon_s}{k} T_{s_t}^4 \approx O(1) + O(10^{-2}) + O(10^{-4}) +$$

$$+ O(10^{-6}) + O(10^{-8})$$

and the other two terms on the right-hand side of Eq. (F-17) are seen to be of $O(10)$. Hence a good approximation in Eq. (F-17) is $T_{s_t}^4 \approx T_{s_o}^4$. If it is also assumed that $T_{h_o}^2 \approx T_{s_o}^2$ then Eq. (F-17) becomes

$$T_{h_o} - T_{s_o} = T_{s_o}^2 \frac{\lambda}{C_2} \ln\left(\frac{\epsilon_h}{\epsilon_s}\right) + \frac{a\ell\sigma\epsilon_s}{k} T_{s_o}^4 \qquad \text{(F-18)}$$

Dividing by $T_{s_o}^2$

$$\frac{T_{h_o} - T_{s_o}}{T_{s_o}^2} = \frac{\lambda}{C_2} \ln\left(\frac{\epsilon_h}{\epsilon_s}\right) + \frac{a\ell\sigma\epsilon_s}{k} T_{s_o}^2 \qquad \text{(F-19)}$$

Then $(T_{h_o} - T_{s_o})/T_{s_o}^2$ versus $T_{s_o}^2$ should plot as a straight line of slope $\frac{a\ell\sigma\epsilon_s}{k}$ and intercept $\frac{\lambda}{C_2} \ln\left(\frac{\epsilon_h}{\epsilon_s}\right)$.

In practice, this relationship was used as follows. A series of hole and surface temperatures were measured for different values of the surface temperature. A typical set of results is shown in Fig. (F-2). The intercept

$$\frac{\lambda}{C_2} \ln\left(\frac{\epsilon_h}{\epsilon_s}\right)$$

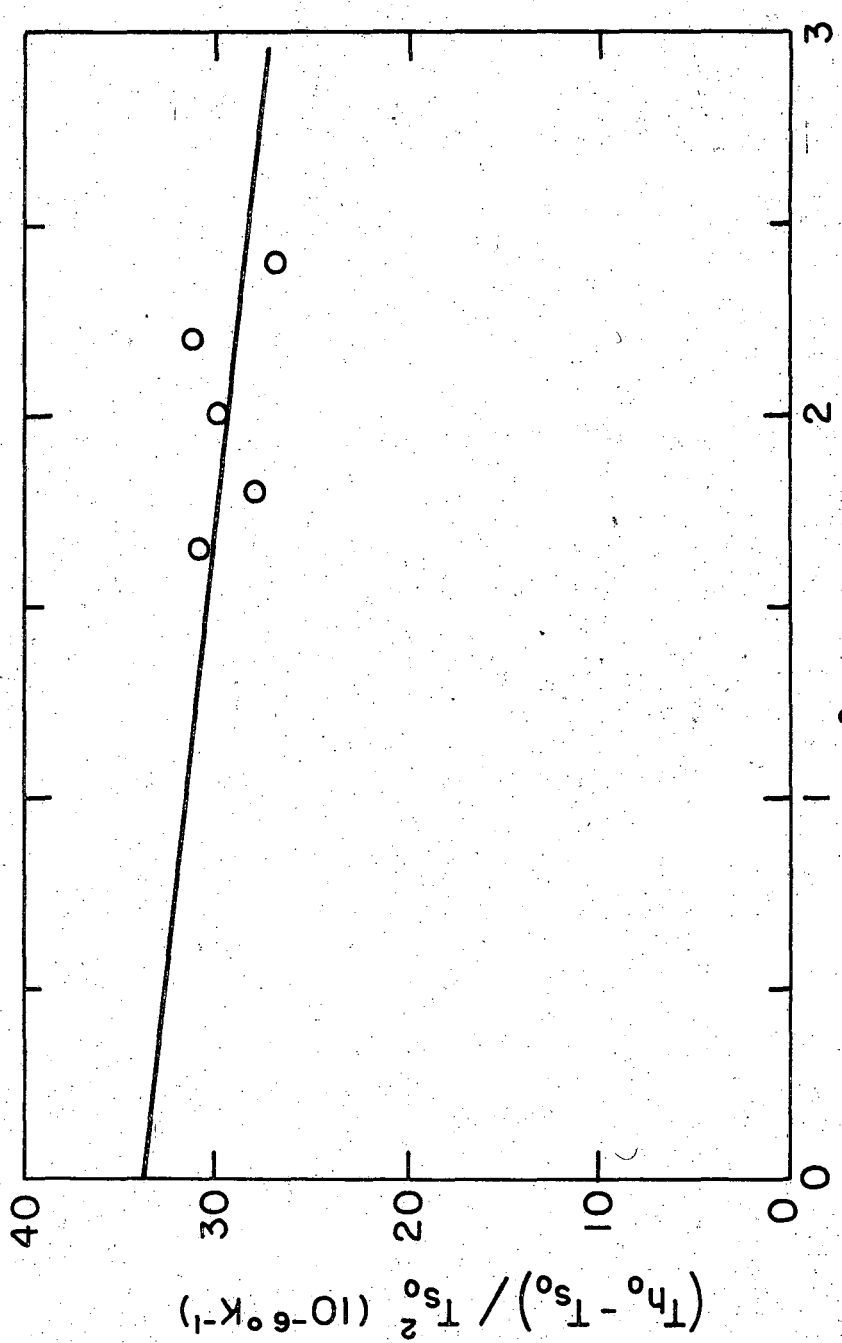

Fig. F-2

was computed by fitting the points by the least-squares method to a straight line. Knowing then the ratio of the surface and hole emissivities, the surface emissivity was determined from Fig. (F-1). The results for a set of seven different disks is shown in Table (F-1).

TABLE F-1

Disk No.	ϵ_s	ϵ_h	$\frac{a\ell\sigma}{k}\epsilon_s$ (10^{-12})
1	0.57	0.91	3.3
2	0.48	0.90	-2.5
3	0.35	0.85	-4.6
4	0.75	0.95	4.5
5	0.63	0.91	1.35
6	0.42	0.88	-2.2
7	0.65	0.89	-1.2

The average emissivity of the seven disks was found to be 0.55. The variance of the data was computed using the "student-t" distribution. For a 95% confidence limit, the emissivity of the surface was found to be 0.55 ± 0.11. This was the value used in correcting the surface temperatures in this experiment. It is felt that the variance in the emissivity is not real but is due to errors in the measurement. The reason for this is that the surfaces of the disks were very identical to each other both before and after the run and thus did not indicate an emissivity variation. Also, but less important, the data show much less scatter when plotted with a constant emissivity.

The data on the emissivity of chromium as given in Ref. 38 varies from 0.1 to 0.52 with 0.43 indicated to be the most likely value. This ranges comprises five points. From the scatter of the data it can be

assumed that an emissivity measurement is very difficult to make. The value computed in this experiment is located at the top of the range, i.e. 0.55 measured by us versus 0.52 at the top of the range in Ref. 43. However, the lower range of our measured value for 95% confidence, i.e. 0.44 = 0.55 - 0.11, is approximately equal to the most likely indicated value of 0.43. The agreement is probably about as close as can be expected for a system that was not specifically designed to measure emissivity.

APPENDIX G

PROPERTIES USED IN THE CALCULATION

The properties of argon were obtained from Ref. 39 and the properties of helium were obtained from Ref. 47. The diffusion coefficients of iron through argon and chromium through helium were calculated using the Lennard-Jones (6-12) potential.[17] The Lennard-Jones parameters were obtained from the bulk liquid metal properties at the melting point. The diffusion coefficients are plotted in Fig. G-1.

The surface tension and density of the bulk liquid metals were obtained from Refs. 1, 40 and 41. The values are plotted in Figs. G-2 and 3.

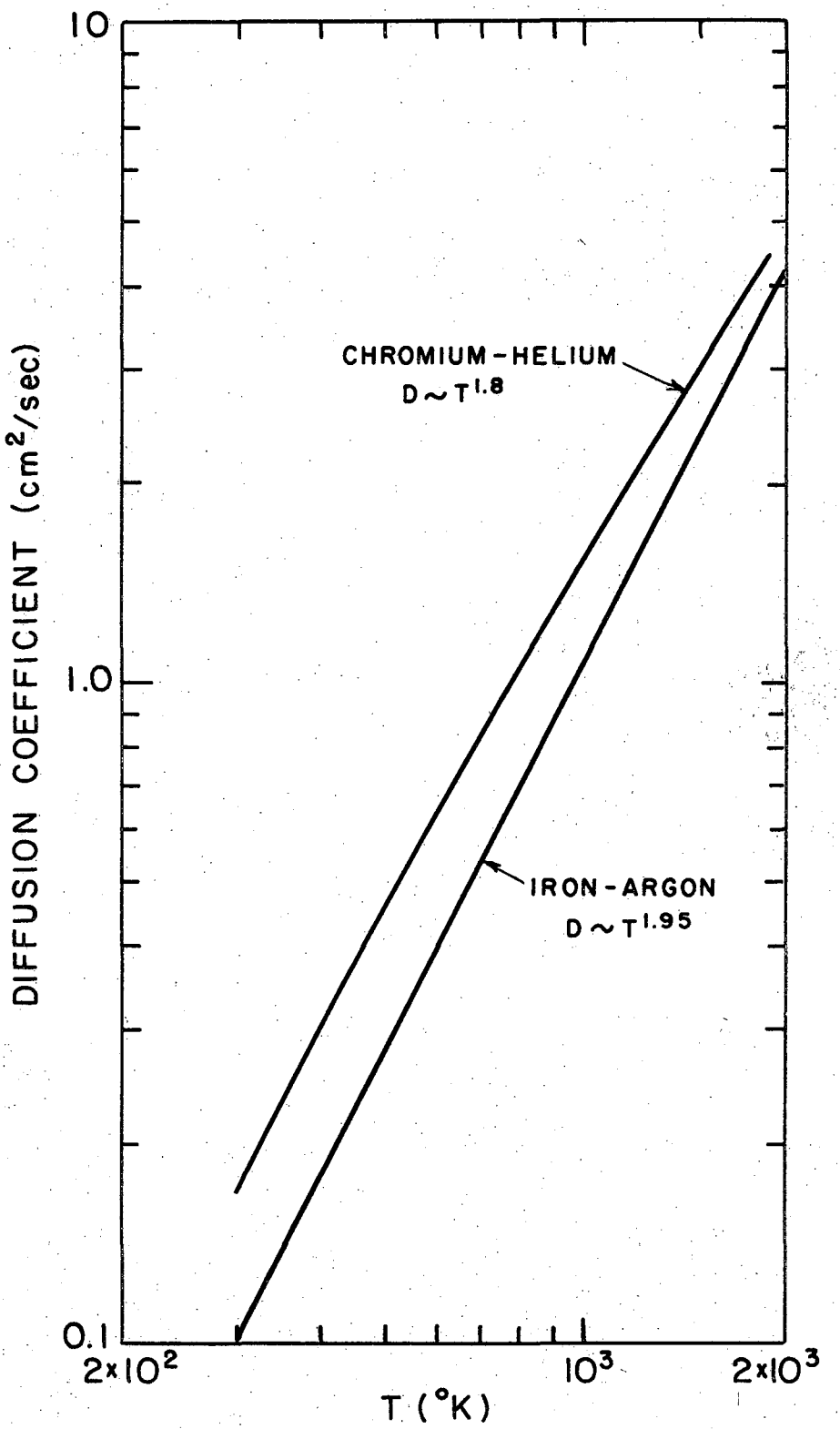
10
1.0
0.1
DIFFUSION COEFFICIENT (cm²/sec)
CHROMIUM-HELIUM
D ~ T^1.8
IRON-ARGON
D ~ T^1.95
2x10²
10³
2x10³
T (°K)

Fig. G-1

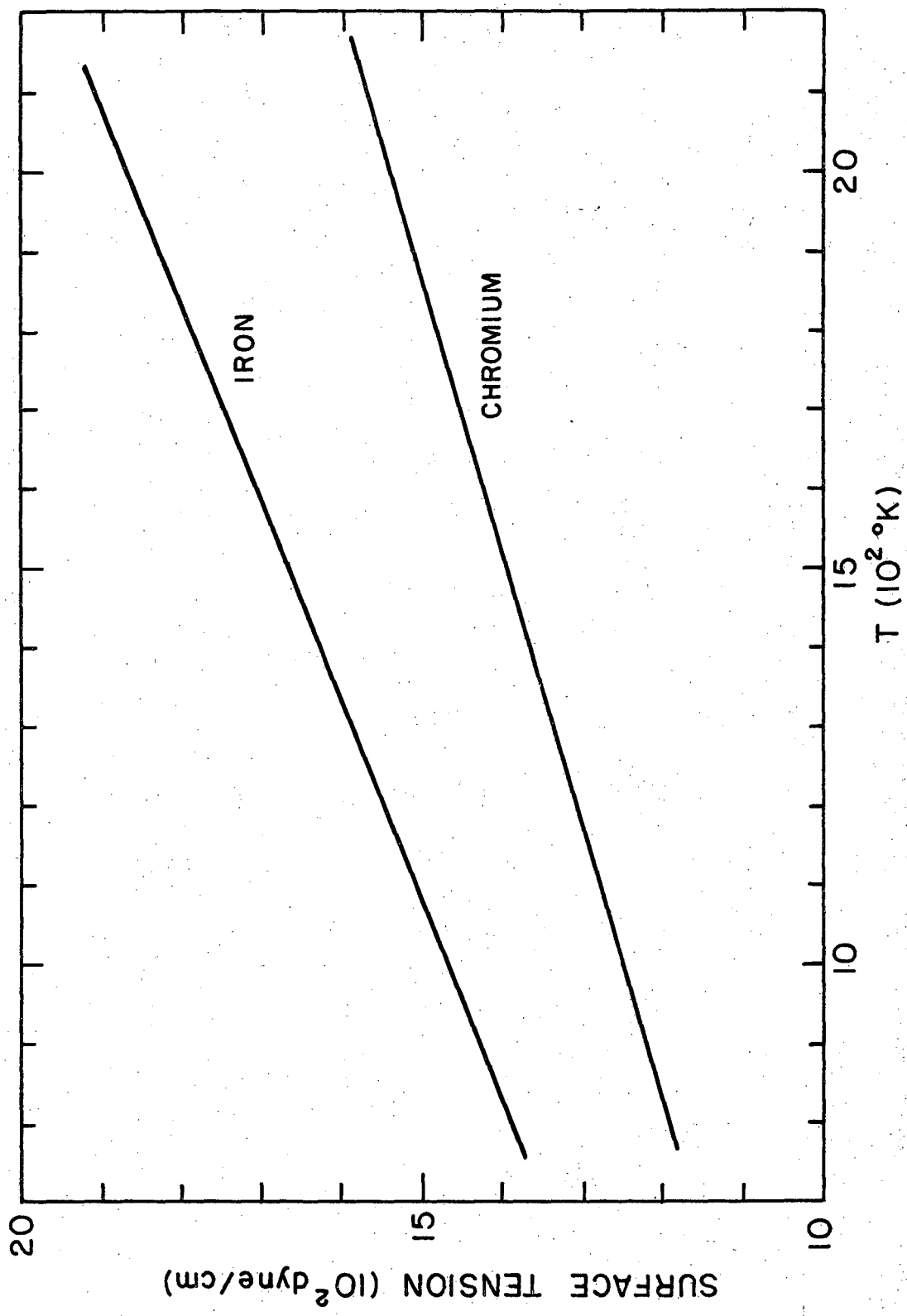
IRON
CHROMIUM
SURFACE TENSION (10^2 dyne/cm)
T (10^2 °K)
20
15
10
20
15
10

Fig. G-2

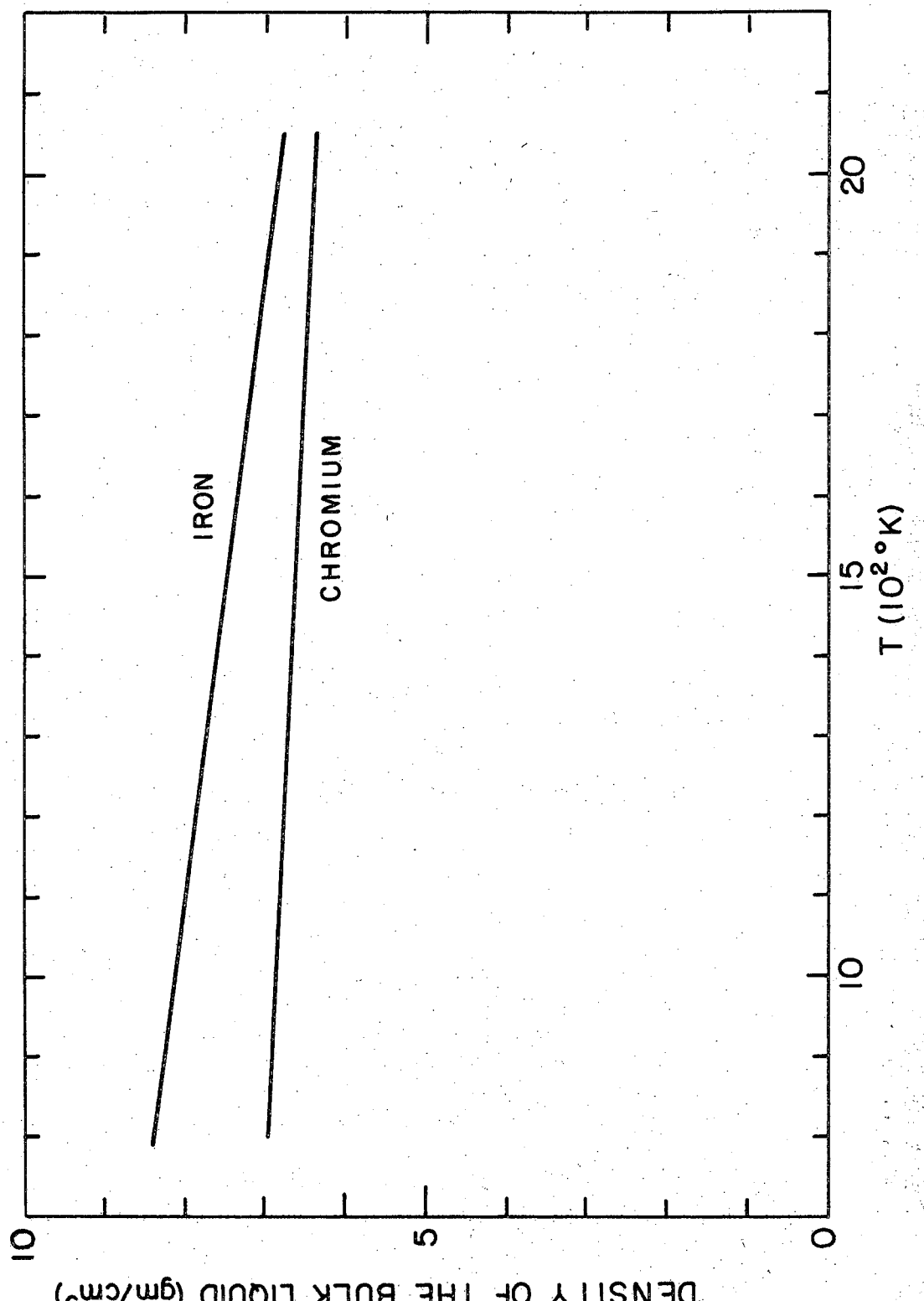
DENSITY OF THE BULK LIQUID (gm/cm³)
10
5
0
IRON
CHROMIUM
10
15
20
T (10² °K)

Fig. G-3

APPENDIX H

THE MACHINE PROGRAM

```
      PROGRAM CONTROL(INPUT,OUTPUT)                                    1
      COMMON /100/ V
      COMMON /150/ VL
      COMMON /200/ ALPHA, BETA
      COMMON /250/ Z
      COMMON /300/ VX
      COMMON /350/ YZ
      COMMON /400/ GB
      COMMON /450/ SQ
      COMMON /500/ GX, GX1
      COMMON /550/ EG
      COMMON /600/ NS, XS
      COMMON /700/ XN, SS
      COMMON /750/ T
      COMMON /800/ U
      COMMON /850/ GL, XNG
      COMMON /900/ U1, U2
      COMMON /950/ V1, V2, V3
      COMMON /975/ S
      COMMON /ITI/ IT
      COMMON /RHT/ RET
      DIMENSION VL(25,50)
      DIMENSION V(25,50)
      DIMENSION V1(25,50), V2(25,50), V3(25,50)
      DIMENSION XN(500), SS(500)
      DIMENSION ALPHA(50), BETA(50)
      DIMENSION VX(50)
      DIMENSION Z(50)
      DIMENSION GB(50)
      DIMENSION GX(50), GX1(50)
      DIMENSION XS(25)
      DIMENSION U(25), U1(25), U2(25)
      DIMENSION S(50)
      DIMENSION YZ(25,50)
      DIMENSION SQ(500)
      DIMENSION T(50)
      DIMENSION GL(50), XNG(50)
      DIMENSION EG(50)
      LOGICAL RET
      PRINT 1
    1 FORMAT(1H1)
      PRINT 4
    4 FORMAT(1H0)
      PRINT 9
    9 FORMAT(1H0 * $$$$$$$$$$$$$$$$$$$$$$$$$$$$$$$$$$$$$$$$$$$$$$$$$$$$ * )
      PRINT 10
   10 FORMAT(1H0 * THIS PROGRAM CALCULATES THE GRADIENT AT THE WALL * /
     $ *  WITH CONDENSATION IN THE BOUNDARY LAYER * )
      PRINT 11
   11 FORMAT(1H0 * $$$$$$$$$$$$$$$$$$$$$$$$$$$$$$$$$$$$$$$$$$$$$$$$$$$$ * )
      PRINT 4
      IT = 0
      CALL READIN
      CALL CONST
      CALL NGF
      CALL INITL
    5 CONTINUE
      PRINT 25
   25 FORMAT(1H1)
```

```
      PRINT 14
   14 FORMAT(1H0 * $$$$$$$$$$$$$$$$$$$$$$$$$$$$$$$$$$$$$$$$$$$$$$$$$$$$ * )
      PRINT 15, IT
   15 FORMAT(1H0 *           ITERATION NUMBER * I5)
      PRINT 14
      CALL DROP
   50 CONTINUE
      CALL MONO
      IF (RET) CALL RESET
      IF (RET) GO TO 50
      CALL TEST
      IT = IT + 1
      IF (IT .LE. 25) GO TO 5
      PRINT 20
   20 FORMAT(1H0 * THE PROCESS DID NOT CONVERGE * )
      CALL ABORT
      END


      SUBROUTINE READIN
      COMMON /AAA/ A
      COMMON /ABC/ BKTW, XL
      COMMON /ACP/ ATH, CP
      COMMON /BRB/ B
      COMMON /DCK/ DC, TK
      COMMON /GRP/ NGROUP
      COMMON /MAX/ XMAX
      COMMON /NOT/ GNOT
      COMMON /MMM/ MW
      COMMON /PPP/ HPRINT
      COMMON /PZP/ PV, PVW
      COMMON /QQQ/ QX, NA, OMEGA
      COMMON /RRR/ TINF, TW, PR
      COMMON /SIG/ SIGMA, DENS
      COMMON /SSS/ SC, SC8, SCP
      REAL MW
      DOUBLE PRECISION HPRINT
      READ 10, TW
      READ 10, TINF
      READ 10, OMEGA
      READ 10, SC
      READ 10, PR
      READ 20, PV
      READ 10, PVW
      READ 5, NGROUP
      READ 10, GNOT
      READ 15, HPRINT
      READ 10, XMAX
      READ 10, SIGMA
      READ 10, DENS
      READ 20, XL
      READ 10, MW
      READ 10, ATH
      READ 20, CP
      READ 10, DC
      READ 10, TK
    5 FORMAT(I5)
   10 FORMAT(F10.5)
   15 FORMAT(D20.5)
```

```
 20 FORMAT(E20.5)
    PRINT 1
  1 FORMAT(1H0 * /-/-/-/-/-/-/-/-/-/-/-/-/-/-/ * )
    PRINT 25
 25 FORMAT(1H0 *       THE INPUT DATA IS     * )
    PRINT 1
    PRINT 50, TW
 50 FORMAT(1H0 * THE TEMPERATURE AT THE WALL IS * E15.5)
    PRINT 55, TINF
 55 FORMAT(1H0 * THE TEMPERATURE AT INFINITY IS * E15.5)
    PRINT 60, OMEGA
 60 FORMAT(1H0 * THE ANGULAR VELOCITY IS * E15.5)
    PRINT 65, PR
 65 FORMAT(1H0 * PRANDTL NUMBER * E15.5)
    PRINT 70, SC
 70 FORMAT(1H0 * SCHMIDT NUMBER * E15.5)
    PRINT 75, PV
 75 FORMAT(1H0 * THE COEFFICIENT IN THE VAPOUR EQ IS * E15.5)
    PRINT 80, PVW
 80 FORMAT(1H0 * THE VAPOUR PRESSURE AT THE WALL IS * E15.5)
    PRINT 90, NGROUP
 90 FORMAT(1H0 * THE NUMBER OF GROUPS IS * I5)
    PRINT 100, GNOT
100 FORMAT(1H0 * THE VALUE OF GNOT IS * E15.5)
    PRINT 105, HPRINT
105 FORMAT(1H0 * THE VALUE OF HPRINT IS * D15.5)
    PRINT 110, XMAX
110 FORMAT(1H0 * THE VALUE OF XMAX IS * E15.5)
    PRINT 115, SIGMA
115 FORMAT(1H0 * THE SURFACE TENSION IS * F15.5)
    PRINT 120, DENS
120 FORMAT(1H0 * THE DENSITY IS * E15.5)
    PRINT 125, XL
125 FORMAT(1H0 * THE LATENT HEAT PER ATOM IS * E15.5)
    PRINT 130, MW
130 FORMAT(1H0 * THE MOLECULAR WEIGHT IS * E15.5)
    PRINT 135, ATH
135 FORMAT(1H0 * THE THERMAL ACCOMODATION COEFFICIENT IS * E15.5)
    PRINT 140, CP
140 FORMAT(1H0 * THE SPECIFIC HEAT PER ATOM IS * E15.5)
    PRINT 150, DC
150 FORMAT(1H0 * THE DIFFUSION COEFFICIENT IS * E15.5)
    PRINT 160, TK
160 FORMAT(1H0 * THE THERMAL CONDUCTIVITY IS * E15.5)
    RETURN
    END


    SUBROUTINE CONST
    COMMON /AAA/ A
    COMMON /ABC/ BKTW, XL
    COMMON /ACP/ ATH, CP
    COMMON /BBB/ BC
    COMMON /BRB/ B
    COMMON /CCC/ C1, C2
    COMMON /CZC/ CZ
    COMMON /DCK/ DC, TK
    COMMON /DHF/ DEF, KEF
    COMMON /KKK/ AC, KTW
```

```
      COMMON /MAM/ MA
      COMMON /MMM/ MW
      COMMON /PZP/ PV, PVW
      COMMON /QQQ/ QX, NA, OMEGA
      COMMON /RRR/ TINF, TW, PR
      COMMON /SIG/ SIGMA, DENS
      COMMON /SKT/ SMKTW
      COMMON /SSS/ SC, SC8, SCP
      COMMON /SUP/ PP
      COMMON /WWW/ TC, PR8
      COMMON /ZZZ/ CZ1, CZ2, CZ3, CZ4, CZ5, CZ6
      REAL NA
      REAL KTW
      REAL MA, K, MKTW
      REAL MW, NAV
      REAL KEF
      DATA X0 /3.53782/
      DATA HINF /-0.88447/
      DATA EMS /0.4/
      DATA SBC /5.67E-05/
      DATA K /1.38E-16/ , NAV /6.025E+23/
    2 FORMAT(1H1)
      PRINT 2
      PRINT 1
    1 FORMAT(1H0 * /-/-/-/-/-/-/-/-/-/-/-/-/-/-/-/-/-/-/-/ * )
      PRINT 5
    5 FORMAT(1H0 * THE PARAMETERS FROM CONST ARE *)
      PRINT 1
      A = HINF * SC
      SC8 = SQRT(SC / 8.0)
      SCX = SC8 * X0
      SCP = SQRT(2.0 * 3.1416 / SC)
      C1 = EXP( - SCX**2)
      C1 = C1 / A
      C1 = C1 - SCP * ERF(SCX)
      C1 = 1.0 / C1
      C2 = C1 * EXP( - SCX**2 )
      C2 = C2 * EXP( - A * X0)
      C2 = C2 / A
      KTW = K * TW
      TC = 1.0 - TINF / TW
      PR8 = SQRT(PR / 8.0)
      MA = MW / NAV
      MKTW = 2.0 * 3.1416 * MA * K * TW
      SMKTW = SQRT(MKTW)
      BC = PVW / SMKTW
      PP = PVW / PV
      AC = PV / SMKTW
      NA = NAV * DENS / MW
      B = 4.0 * 3.1416 * SIGMA * (3.0 / 4.0 / 3.1416 / NA)**0.66667
      QX = B / OMEGA / SIGMA
      BKTW = B / KTW
      CZ = 0.5
      CZ1 = BC
      CZ2 = AC
      CZ3 = 1.0 / KTW
      CZ4 = 2.0 * B / 3.0
      CZ5 = CP * ATH / SBC / EMS / TW**3
      CZ6 = XL / SBC / EMS / TW**4
```

```
      PRINT 10, A, SC8, SCX, SCP
      PRINT 11, C1, C2
      PRINT 12, KTW, TC, PR8
      PRINT 13, MA, MKTW, SMKTW
      PRINT 14, BC, PP, AC
      PRINT 15, NA, B, BKTW, QX
      PRINT 16, CZ1, CZ2, CZ3, CZ4, CZ5, CZ6
   10 FORMAT(1H0 * A = * E15.5, 12X, * SC8 = * E15.5 /
     $ *  SCX = * E15.5, 10X, * SCP = * E15.5)
   11 FORMAT(1H0 * C1 = * E15.5, 11X, * C2 = * E15.5)
   12 FORMAT(1H0 * KTW = * E15.5, 10X, * TC = * E15.5 /
     $ *  PR8 = * E15.5)
   13 FORMAT(1H0 * MA = * E15.5, 11X, * MKTW = * E15.5 /
     $ *  SMKTW = * E15.5)
   14 FORMAT(1H0 * BC = * E15.5, 11X, * PP = * E15.5 /
     $ *  AC = * E15.5)
   15 FORMAT(1H0 * NA = * E15.5, 11X, * B = * E15.5 /
     $ *  BKTW = * E15.5, 9X, * QX = * E15.5)
   16 FORMAT(1H0 * CZ1 = * E15.5, 10X, * CZ2 = * E15.5 /
     $ *  CZ3 = * E15.5, 10X, * CZ4 = * E15.5 /
     $ *  CZ5 = * E15.5, 10X, * CZ6 = * E15.5)
      DEF = SQRT(KTW / 2.0 / 3.1416 / MA) / DC
      DEF = DEF * (3.0 * MA / 4.0 / 3.1416 / DENS) ** 0.33333
      KEF = 1.0E+06 * CP * ATH / SMKTW / TK
      KEF = KEF * (3.0 * MA / 4.0 / 3.1416 / DENS) ** 0.33333
      PRINT 17, DEF, KEF
   17 FORMAT(1H0 * DEF = * E15.5, 10X, * KEF = * E15.5)
      RETURN
      END


      SUBROUTINE NGF
      COMMON /400/ GB
      COMMON /500/ GX, GX1
      COMMON /550/ EG
      COMMON /600/ NS, XS
      COMMON /850/ GL, XNG
      COMMON /GRP/ NGROUP
      COMMON /NGN/ NG
      COMMON /NOT/ GNOT
      COMMON /PPP/ HPRINT
      COMMON /SPN/ SPAN
      COMMON /SSS/ SC, SC8, SCP
      DIMENSION NG(50)
      DIMENSION GB(50)
      DIMENSION GX(50), GX1(50)
      DIMENSION XS(25)
      DIMENSION GL(50), XNG(50)
      DIMENSION EG(50)
      REAL NG
      PRINT 1
    1 FORMAT(1H0 * /-/-/-/-/-/-/-/-/-/-/ * )
      PRINT 2
    2 FORMAT(1H0 * THE DATA FROM NGF IS * )
      PRINT 1
      L = NGROUP
      ML = L - 1
      DO 20 I = 1,NGROUP
      READ 10, NG(I)
```

```
 10 FORMAT(E7.1)
 20 CONTINUE
    PRINT 15, (NG(I), I = 1,NGROUP)
 15 FORMAT(1H0 * THE NUMBER OF DROPS PER GROUP IS * / (4E15.5))
    GB(1) = GNOT + (NG(1) - 1.0) / 2.0
    DO 50 I = 2,NGROUP
    GB(I) = GB(I-1) + 1.0 + (NG(I-1) - 1.0) / 2.0 + (NG(I) - 1.0)
   $  / 2.0
 50 CONTINUE
    SPAN = GB(L) + (NG(L) - 1.0) / 2.0
    SPAN = SPAN - (GB(1) - (NG(1) - 1.0) / 2.0)
    DO 25 I = 1,NGROUP
    GX(I) = GEX(GB(I))
    GX1(I) = 1.0 / SQRT(GX(I))
 25 CONTINUE
    PRINT 3, (GB(I), I = 1,L)
  3 FORMAT(1H0 * THE GROUP MEAN VALUES OF G ARE * // (3E15.5))
    DO 100 I = 1,L
    GL(I) = ALOG(GB(I))
100 CONTINUE
    DO 200 I = 1,ML
    XNG(I) = GL(I+1) - GL(I)
200 CONTINUE
    EX = 1.0 / 6.0
    DO 75 I = 1,L
    EG(I) = SQRT(2.0 * 0.8930) * (6.0 / GX(I) / SC) ** EX
 75 CONTINUE
    PRINT 125, (EG(I), I = 1,L)
125 FORMAT(1H0 * THE COEFFICIENTS OF PERTURBATION ARE * // (3E15.5))
    RETURN
    END


    SUBROUTINE INITL
    COMMON /100/ V
    COMMON /150/ VL
    COMMON /200/ ALPHA, BETA
    COMMON /400/ GB
    COMMON /600/ NS, XS
    COMMON /800/ U
    COMMON /DDD/ DUDX
    COMMON /FST/ FIRST
    COMMON /GRP/ NGROUP
    COMMON /IXI/ IX
    COMMON /JJJ/ JN
    COMMON /LGL/ LG
    COMMON /LLL/ L
    COMMON /MAX/ XMAX
    COMMON /MLM/ ML
    COMMON /NGN/ NG
    COMMON /PPP/ HPRINT
    COMMON /PST/ POST
    COMMON /STR/ GSTAR
    DIMENSION U(25), XS(25)
    DIMENSION VL(25,50)
    DIMENSION GB(50)
    DIMENSION V(25,50)
    DIMENSION ALPHA(50), BETA(50)
    DIMENSION NG(50)
```

```
      DOUBLE PRECISION HPRINT                                          7
      LOGICAL SHIFT
      LOGICAL POST
      LOGICAL SHOW
      LOGICAL FIRST
      DATA ZET /1.0E-290/
      DATA SHIFT /.FALSE./
      DATA CE /0.5/
      DATA LG /3/
      REAL JN
      REAL NG
      POST = .FALSE.
      L = NGROUP
      ML = NGROUP - 1
      PRINT 1
    1 FORMAT(1H0 * /-/-/-/-/-/-/-/-/-/-/-/-/-/ * )
      PRINT 2
    2 FORMAT(1H0 * THE DATA FROM INITL IS * )
      PRINT 1
      X = 0.0
      I = 1
    5 CONTINUE
      XS(I) = X
      U(I) = UI(X)
      PRINT 10, X, U(I)
   10 FORMAT(2E15.5)
      NS = I
      I = I + 1
      X = X + SNGL(HPRINT)
      IF (X .GT. XMAX) GO TO 15
      GO TO 5
   15 CONTINUE
      DUDX = (U(2) - U(1)) / SNGL(HPRINT)
      PRINT 40, DUDX
   40 FORMAT(1H0 * THE VALUE OF DUDX IS * E15.5)
      READ 3, C
    3 FORMAT(F10.5)
      PRINT 4, C
    4 FORMAT(1H0 * C = * E15.5)
      SHOW = .FALSE.
      IF (C .LT. 0.0) SHOW = .TRUE.
      PRINT 8
    8 FORMAT(1H0)
      DO 35 I = 1,NS
      X = XS(I)
      IF (SHOW) READ 7, U(I)
    7 FORMAT(E7.1)
      IF ( .NOT. SHOW ) U(I) = U(I) * (1.0 - ERF(X / XMAX)) ** C
      PRINT 10, XS(I), U(I)
   35 CONTINUE
      DUDX = (U(2) - U(1)) / SNGL(HPRINT)
      PRINT 40, DUDX
      DO 900 I = 1,NS
      IF (U(I) .GT. 1.0E-03) GO TO 900
      GO TO 950
  900 CONTINUE
      GO TO 975
  950 CONTINUE
      XMAX = XS(I)
```

```
      NS = I
  975 CONTINUE
      X = 0.0
      IX = 1
      PRINT 60
   60 FORMAT(1H0)
      PRINT 75
   75 FORMAT(1H0 * THE INITIAL VALUES OF VX ARE * )
   20 CONTINUE
      CALL DIMEN(X)
      DO 150 I = 1,L
      G = GB(I)
      IF(G .LE. GSTAR) V(IX,I) = VXINF(X,G)
      IF (G .GT. GSTAR) V(IX,I) = JN / BETA(I)
  150 CONTINUE
  200 CONTINUE
      PRINT 90, X
   90 FORMAT(1H0 * X = * E15.5)
      PRINT 91, GSTAR, JN, (V(IX,I), I = 1,L)
   91 FORMAT(1H0 * GSTAR = * E15.5, 10X, * JN = * E15.5 // (7E15.5))
      X = X + SNGL(HPRINT)
      IX = IX + 1
      IF (X .GT. XMAX) GO TO 50
      GO TO 20
   50 CONTINUE
      FIRST = .FALSE.
      X = 0.0
      IX = 1
      PRINT 60
      PRINT 500
  500 FORMAT(1H0 * THE STARTING VALUES OF VX ARE * )
  520 CONTINUE
      CALL DIMEN(X)
      DO 550 I = 1,L
      IF (I .LE. LG) GO TO 550
      TQ = BETA(I-1) - ALPHA(I-1)
      TR = BETA(I) - ALPHA(I)
      TQ = ABS(TQ)
      TR = ABS(TR)
      V(IX,I) = TQ / (TR + CE * NG(I)) * V(IX,I-1)
  550 CONTINUE
      PRINT 590, X, (V(IX,I), I = 1,L)
  590 FORMAT(1H0 * X = * E15.5 // (7E15.5))
      X = X + SNGL(HPRINT)
      IX = IX + 1
      IF (X .GT. XMAX) GO TO 600
      GO TO 520
  600 CONTINUE
      RETURN
      END


      SUBROUTINE DROP
      COMMON /100/ V
      COMMON /200/ ALPHA, BETA
      COMMON /400/ GB
      COMMON /500/ GX, GX1
      COMMON /550/ EG
      COMMON /600/ NS, XS
```

```
      COMMON /700/ XN, SS
      COMMON /950/ V1, V2, V3
      COMMON /ACY/ ARCY
      COMMON /CIC/ IC
      COMMON /CQC/ CQ
      COMMON /GRP/ NGROUP
      COMMON /HPH/ HP
      COMMON /IPI/ IP
      COMMON /IXI/ IX
      COMMON /ITI/ IT
      COMMON /LLL/ L
      COMMON /MAX/ XMAX
      COMMON /MLM/ ML
      COMMON /NLN/ N
      COMMON /NOT/ GNOT
      COMMON /PPP/ HPRINT
      COMMON /PST/ POST
      COMMON /SET/ SETUP
      COMMON /SPR/ SWPR
      COMMON /SSS/ SC, SC8, SCP
      COMMON /YYY/ IM
      DIMENSION Y(100), F(100), T(800)
      DIMENSION ALPHA(50), BETA(50)
      DIMENSION XN(500), SS(500)
      DIMENSION XS(25)
      DIMENSION CQ(50)
      DIMENSION GB(50)
      DIMENSION V(25,50)
      DIMENSION V1(25,50), V2(25,50), V3(25,50)
      DIMENSION EG(50)
      DIMENSION GX(50), GX1(50)
      DOUBLE PRECISION T, HPRINT
      DOUBLE PRECISION HPDP
      DOUBLE PRECISION XDP
      LOGICAL SWPR
      LOGICAL POST
      LOGICAL PRINT
      LOGICAL ARCY
      LOGICAL SETUP
      DATA XI /0.0/
      DATA IP /2/
      DATA IS /1/
      DATA SETUP /.FALSE./
      EXTERNAL DERIV2
      ARCY = .FALSE.
      SWPR = .TRUE.
      POST = .FALSE.
      N = NGROUP
      HPDP = HPRINT / DBLE(FLOAT(IP))
      HP = SNGL(HPDP)
      SETUP = .FALSE.
      CALL SORT
      SETUP = .TRUE.
      PRINT 1
    1 FORMAT(1H0 * /-/-/-/-/-/-/-/-/-/-/-/-/-/-/-/-/-/-/-/-/-/-/-/-/-/-/-/-/ * )
      PRINT 5
    5 FORMAT(1H0 *              THE DATA FROM DROP IS                        * )
      PRINT 1
      DO 150 I = 1,NGROUP
```

```
      Y(I) = 0.0                                                        10
  150 CONTINUE
      IF (IT .NE. 0) GO TO 500
      DO 300 IX = 1,NS
      DO 200 IG = 1,L
      EZ = ERF(EG(IG) * SC8 * SQRT(GX(IG)) * XS(IX))
      V2(IX,IG) = VXI(GB(IG)) * (1.0 - EZ)
      V3(IX,IG) = EZ
  200 CONTINUE
  300 CONTINUE
  500 CONTINUE
      NC = 0
      IX = 1
      X = XI
      PRINT 6
    6 FORMAT(1H0)
      PRINT 100
  100 FORMAT(1H0 * $-$-$-$-$-$-$-$-$-$-$-$-$-$ * )
      PRINT 101, X
  101 FORMAT(1H0 * X IS NOW * E15.5)
      PRINT 100
      POST = .TRUE.
      SETUP = .TRUE.
      IC = NC + 1
      XDP = DBLE(XI)
      XN(IC) = SNGL(XDP)
      CALL DIMEN(X)
      CALL SRCDRP(X)
      CALL SORC(IC)
      POST = .FALSE.
      SETUP = .FALSE.
      CALL INTO(N,X,DERIV2,Y,F,T,HPDP)
   10 CONTINUE
      IF (SWPR) GO TO 75
      GO TO 575
   75 CONTINUE
      NL = MOD(NC,IP)
      IF (NL .NE. 0) GO TO 110
      DO 650 I = 1,L
      V1(IX,I) = Y(I) / CQ(I)
  650 CONTINUE
      PRINT 12
   12 FORMAT(1H0 * ============================== * )
      PRINT 14
   14 FORMAT(1H0 * THE VALUES OF VI(IX,I) ARE * )
      PRINT 12
      PRINT 15, X, (V1(IX,I), I = 1,L)
      IF (IT .GT. 0) GO TO 110
      PRINT 15, X, (V2(IX,I), I = 1,L)
      PRINT 15, X, (V3(IX,I), I = 1,L)
   15 FORMAT(1H0 * X = * E15.5 // (3E15.5))
  110 CONTINUE
      NC = NC + 1
      X = X + HP
      IF (X .GT. XMAX) GO TO 50
      IC = NC + 1
      XDP = XDP + HPDP
      XN(IC) = SNGL(XDP)
      SETUP = .TRUE.
```

```
      CALL DIMEN(X)
      CALL SRCDRP(X)
      CALL SORC(IC)
      SETUP = .FALSE.
   30 CONTINUE
      NL = MOD(NC,IP)
      IF (NL .NE. 0) GO TO 575
      IX = IX + 1
      PRINT 100
      PRINT 101, X
      PRINT 100
   25 CONTINUE
      POST = .TRUE.
      SETUP = .FALSE.
      CALL DIMEN(X)
      CALL SRCDRP(X)
      CALL SORC(IC)
      POST = .FALSE.
      SETUP = .TRUE.
      CALL SECOND(TIME)
      PRINT 990, TIME
  990 FORMAT(1H0 * THE CENTRAL PROCESSER TIME IS * F15.5)
  575 CONTINUE
      CALL INT(X, DERIV2, Y, F, T, SWPR)
      GO TO 10
   50 CONTINUE
      CALL SOLV
      PRINT 90
   90 FORMAT(1H0 * ================================ * )
      PRINT 95
   95 FORMAT(1H0 * THE MONOMER EQ SOURCE TERMS ARE * )
      PRINT 90
      SETUP = .FALSE.
      POST = .FALSE.
      IR = IC
      DO 1000 I = 1,IR,IS
      IC = I
      IX = IC / IP + 1
      X = XN(I)
      CALL DIMEN(X)
      CALL SRCDRP(X)
      CALL SORC(I)
      PRINT 925, XN(I), SS(I)
  925 FORMAT(2E15.5)
 1000 CONTINUE
      RETURN
      END


      SUBROUTINE MONO
      COMMON /100/ V
      COMMON /400/ GB
      COMMON /500/ GX, GX1
      COMMON /550/ EG
      COMMON /600/ NS, XS
      COMMON /800/ U
      COMMON /900/ U1, U2
      COMMON /950/ V1, V2, V3
      COMMON /ACY/ ARCY
```

```
      COMMON /DDD/ DUDX                                                  12
      COMMON /III/ IC
      COMMON /ITI/ IT
      COMMON /LGL/ LG
      COMMON /LLL/ L
      COMMON /MAX/ XMAX
      COMMON /NGN/ NG
      COMMON /PPP/ HPRINT
      COMMON /SRT/ START
      COMMON /SSS/ SC, SC8, SCP
      COMMON /YYY/ IM
      DIMENSION Y(2), F(2), T(26)
      DIMENSION U1(25), U2(25)
      DIMENSION U(25)
      DIMENSION GB(50)
      DIMENSION V(25,50)
      DIMENSION UZ(25)
      DIMENSION DVDX(50)
      DIMENSION NG(50)
      DIMENSION GX(50), GX1(50)
      DIMENSION XS(25)
      DIMENSION EG(50)
      DIMENSION V1(25,50), V2(25,50), V3(25,50)
      DOUBLE PRECISION T, HPRINT
      LOGICAL SWPR
      LOGICAL ARCY
      LOGICAL START
      REAL NG
      EXTERNAL DERIV1
      DATA ZIP /1.0E-03/
      DATA START /.TRUE./
      ARCY = .TRUE.
      IM = 1
      Y1 = 1.0
      Y2 = 0.0
      GO TO 9
    7 CONTINUE
      Y1 = 0.0
      Y2 = 1.0
    9 CONTINUE
      N = 2
      X = 0.0
      SWPR = .TRUE.
      IC = 0
      Y(1) = Y1
      Y(2) = Y2
      CALL INTO(N, X, DERIV1, Y, F, T, HPRINT)
   10 CONTINUE
      IF (SWPR) GO TO 15
      GO TO 25
   15 CONTINUE
      IC = IC + 1
      UZ(IC) = Y(1)
      X = X + SNGL(HPRINT)
      IF (X .GT. XMAX) GO TO 50
   25 CALL INT(X, DERIV1, Y, F, T, SWPR)
      GO TO 10
   50 CONTINUE
      X = 0.0
```

```
      PRINT 5                                                          /3
    5 FORMAT(1H0 * /-/-/-/-/-/-/-/-/-/-/-/-/-/ * )
      PRINT 6
    6 FORMAT(1H0 * THE DATA FROM MONO IS * )
      PRINT 5
      IF (IM .EQ. 2) GO TO 60
      DO 75 I = 1,IC
      U1(I) = UZ(I)
      PRINT 30, X, U1(I)
   30 FORMAT(2E15.5)
      X = X + SNGL(HPRINT)
   75 CONTINUE
      IM = 2
      GO TO 7
   60 CONTINUE
      X = 0.0
      DO 95 I = 1,IC
      U2(I) = UZ(I)
      PRINT 30, X, U2(I)
      X = X + SNGL(HPRINT)
   95 CONTINUE
  100 CONTINUE
      IF (START) CALL SOLN
      DUDX = (U(2) - U(1)) / SNGL(HPRINT)
      PRINT 20, DUDX
   20 FORMAT(1H0 * THE VALUE OF DUDX IS * E15.5)
      SUM = 0.0
      DO 150 I = 1,L
      DVDX(I) = 0.0
      IF (I .LE. LG) GO TO 150
      XNG = NG(I)
      DVDX(I) = XNG * SQRT(GX(I))
      DVDX(I) = DVDX(I) * (V(2,I) - V(1,I)) / SNGL(HPRINT)
      SUM = SUM + DVDX(I)
  150 CONTINUE
      PRINT 200, (DVDX(I), I = 1,L)
  200 FORMAT(1H0 * THE DVDX(I) ARE * / (4E15.5))
      PRINT 225, SUM
  225 FORMAT(1H0 * THE SUM OF THE DVDX(I) IS * E15.5)
      DUDX = DUDX + SUM
      PRINT 250, DUDX
  250 FORMAT(1H0 * THE NEW VALUE OF DUDX IS * E15.5)
      DO 400 I = 1,NS
      IF (I .EQ. NS) GO TO 700
      IF (U(I) .LT. ZIP) GO TO 600
  400 CONTINUE
  600 NS = I
      XMAX = XS(NS)
      IF (NS .LE. 2) CALL ABORT
  700 CONTINUE
      RETURN
      END


      SUBROUTINE RESET
      COMMON /CIC/ IC
      COMMON /450/ SQ
      COMMON /700/ XN, SS
      DIMENSION XN(500), SS(500)
```

```
      DIMENSION SQ(500)                                                 14
      DO 10 I = 1,IC
      SS(I) = 0.5 * (SS(I) + SQ(I))
   10 CONTINUE
      RETURN
      END

      SUBROUTINE TEST
      COMMON /CIC/ IC
      COMMON /DDD/ DUDX
      COMMON /DRG/ DRAG
      COMMON /ITI/ IT
      COMMON /SMS/ SUM
      COMMON /SLW/ SLOW
      COMMON /SRT/ START
      COMMON /TST/ XXX
      LOGICAL QUIT
      LOGICAL START
      DATA INQ /7/
      DATA EPSLN /1.0E-03/
      DATA TEN /1.0E-02/
      DATA QQQ /0.0/
      DATA TEXIT /250.0/
      DATA ND /20/
      DATA SUM /1.0/
      DATA XXX /0.0/
      DATA IJK /0/
      LOGICAL DRAG
      LOGICAL SLOW
      PRINT 1
    1 FORMAT(1H0 * ++++++++++++++++++++++++++++++++++ * )
      PRINT 5
    5 FORMAT(1H0 * THE DATA FROM SUBROUTINE TEST IS * )
      PRINT 1
      PRINT 50, SUM
   50 FORMAT(1H0 * SUM = * E15.5)
      XXX = SQRT(XXX) / FLOAT(IC)
      IF (IT .EQ. 0) XXX = 1.0
      PRINT 60, XXX
   60 FORMAT(1H0 * XXX = * E15.5)
      T = SUM
      QUIT = .FALSE.
      IF (IT .NE. 0) QQQ = ABS( (DUDX - QQQ) / QQQ )
      PRINT 75, QQQ
   75 FORMAT(1H0 * QQQ = * E15.5)
      IF (QQQ .GE. TEN) IJK = 0
      IF (QQQ .LT. TEN) IJK = IJK + 1
      IF ( .NOT. START) GO TO 100
      IF ((T .LT. EPSLN) .AND. (IT .GE. INQ)) QUIT = .TRUE.
      IF ( (QUIT) .AND. (XXX .LE. TEN) ) GO TO 15
  100 CONTINUE
      CALL SECOND(TIME)
      IF ( (IT .GE. ND) .OR. (TIME .GE. TEXIT) ) GO TO 15
      QQQ = DUDX
      IF (IJK .EQ. 5) GO TO 15
      RETURN
   15 CONTINUE
      PRINT 20
```

```
 20 FORMAT(1H0 * /-/-/-/-/-/-/-/-/-/-/-/-/-/-/-/-/-/ * )          15
    PRINT 25
 25 FORMAT(1H0 *          NORMAL EXIT          * )
    PRINT 20
    CALL EXIT
    END


    SUBROUTINE SORT
    COMMON /975/ S
    COMMON /CIC/ IC
    COMMON /CQC/ CQ
    COMMON /GRP/ NGROUP
    COMMON /HPH/ HP
    COMMON /IPI/ IP
    COMMON /ITI/ IT
    COMMON /IXI/ IX
    COMMON /MAX/ XMAX
    COMMON /NGN/ NG
    COMMON /PPP/ HPRINT
    COMMON /ROP/ ROPE
    DIMENSION CQ(50)
    DIMENSION AQ(50)
    DIMENSION NG(50)
    DIMENSION S(50)
    DIMENSION CQN(50)
    LOGICAL ROPE
    REAL NG
    DOUBLE PRECISION HPRINT
    DATA (CQ(I), I = 1,50) /50 * 1.0/
    PRINT 50
 50 FORMAT(1H0 * 0-0-0-0-0-0-0-0-0-0 * )
    PRINT 55
 55 FORMAT(1H0 * THE DATA FROM SORT IS * )
    PRINT 50
    L = NGROUP
    DO 20 I = 1,L
    AQ(I) = 0.0
    CQN(I) = CQ(I)
    CQ(I) = 1.0
 20 CONTINUE
    IC = 1
    IX = 1
    X = 0.0
  3 CONTINUE
    ROPE = .TRUE.
    CALL DIMEN(X)
    CALL SRCDRP(X)
    ROPE = .FALSE.
    DO 4 I = 1,L
    AQI = AQ(I)
    CQI = S(I)
    AQ(I) = AMAX1(AQI, CQI)
  4 CONTINUE
    X = X + SNGL(HPRINT)
    IC = IC + IP
    IX = IX + 1
    IF (X .GT. XMAX) GO TO 75
    GO TO 3
```

```
 75 CONTINUE                                                          16
    DO 150 I = 1,NGROUP
    IF (AQ(I) .EQ. 0.0) AQ(I) = 1.0E-290
    CQ(I) = 1.0 / AQ(I)
150 CONTINUE
    PRINT 2, (CQ(I), I = 1,L)
  2 FORMAT(1H0 * THE CQ(I) ARE * / (3E15.5))
    RETURN
    END


    FUNCTION UI(X)
    COMMON /AAA/ A
    COMMON /CCC/ C1, C2
    COMMON /SSS/ SC, SC8, SCP
    DATA X0 /3.53782/
    IF (X .GT. X0) GO TO 5
    UI = 1.0 + C1 * SCP * ERF(SC8 * X)
    RETURN
  5 UI = C2 * EXP( A * X)
    RETURN
    END


    SUBROUTINE SOLV
    COMMON /100/ V
    COMMON /150/ VL
    COMMON /400/ GB
    COMMON /500/ GX, GX1
    COMMON /950/ V1, V2, V3
    COMMON /AAA/ A
    COMMON /CRL/ CRAWL
    COMMON /DDD/ DUDX
    COMMON /DRG/ DRAG
    COMMON /GRP/ NGROUP
    COMMON /HNG/ HANG
    COMMON /IXI/ IX
    COMMON /ITI/ IT
    COMMON /LGL/ LG
    COMMON /MAX/ XMAX
    COMMON /MLM/ ML
    COMMON /PPP/ HPRINT
    COMMON /SLW/ SLOW
    COMMON /WHT/ WAIT
    DIMENSION VL(25,50)
    DIMENSION V(25,50)
    DIMENSION VS(25,50)
    DIMENSION V1(25,50), V2(25,50), V3(25,50)
    DIMENSION C(50)
    DIMENSION GB(50)
    DIMENSION GX(50), GX1(50)
    DIMENSION VV(50)
    DOUBLE PRECISION HPRINT
    LOGICAL SET
    LOGICAL NET
    LOGICAL SLOW
    LOGICAL DRAG
    LOGICAL CRAWL
    LOGICAL WAIT
```

```
      LOGICAL HANG                                                    17
      DATA SLOW /.TRUE./
      DATA DRAG /.TRUE./
      DATA CRAWL /.FALSE./
      DATA WAIT /.FALSE./
      DATA HANG /.FALSE./
      DATA ZET /1.0E-290/
      DATA EX /0.33333/
      DATA X0 /3.53782/
      CRAWL = .FALSE.
      IF (ABS(DUDX) .GT. 0.5) CRAWL = .TRUE.
      WAIT = .FALSE.
      IF (ABS(DUDX) .GT. 0.6) WAIT = .TRUE.
      HANG = .FALSE.
      IF (ABS(DUDX) .GT. 0.7) HANG = .TRUE.
      PRINT 10
   10 FORMAT(1H0 * ========================= * )
      PRINT 15
   15 FORMAT(1H0 * THE DATA FROM SOLV IS * )
      PRINT 10
      PRINT 190
  190 FORMAT(1H0 * THE CONSTANTS FROM SOLV ARE * )
      SET = .FALSE.
      NET = .FALSE.
      X = 0.0
      DO 100 I = 1,IX
      IF (I .EQ. 1) GO TO 95
      DO 90 IG = 1,NGROUP
      QN = V(I,IG)
      ZQ = V2(I,IG) - V1(IX,IG) * V3(I,IG) + V1(I,IG)
      IF (ZQ .LT. ZET) ZQ = ZET
      V(I,IG) = ZQ
   90 CONTINUE
   95 CONTINUE
      PRINT 150, X, (V(I,IG), IG = 1,NGROUP)
  150 FORMAT(1H0 * THE V(IX,IG) AT X = * E15.5 * ARE * / (4E15.5))
      X = X + SNGL(HPRINT)
  100 CONTINUE
      RETURN
      END


      SUBROUTINE DERIV2(X,Y,F)
      COMMON /200/ ALPHA, BETA
      COMMON /400/ GB
      COMMON /500/ GX, GX1
      COMMON /750/ T
      COMMON /975/ S
      COMMON /GRP/ NGROUP
      COMMON /LLL/ L
      COMMON /MLM/ ML
      COMMON /NGN/ NG
      COMMON /NLN/ N
      COMMON /PST/ POST
      COMMON /SPR/ SWPR
      COMMON /SSS/ SC, SC8, SCP
      COMMON /YYY/ IM
      DIMENSION Y(1), F(1)
      DIMENSION ALPHA(50), BETA(50)
```

```
      DIMENSION GB(50)                                                  18
      DIMENSION GX(50), GX1(50)
      DIMENSION S(50)
      DIMENSION NG(50)
      DIMENSION T(50)
      LOGICAL SWPR
      LOGICAL FLAG
      LOGICAL POST
      REAL NG
      IF (POST) FLAG = .TRUE.
      FLAG = .FALSE.
      IF (FLAG) 30, 75
   30 CONTINUE
      PRINT 45
   45 FORMAT(1HO * ========================== * )
      PRINT 50
   50 FORMAT(1HO * THE DATA FROM DERIV2 IS * )
      PRINT 45
   75 CONTINUE
      HX = H(X)
   90 FORMAT(5E15.5)
   95 FORMAT(1HO)
      DO 250 I = 1,NGROUP
      F(I) = S(I) / HX
      GO TO 250
  250 CONTINUE
      IF (FLAG) 260, 270
  260 CONTINUE
      PRINT 95
      PRINT 90, (S(I), I = 1,L)
      PRINT 95
      PRINT 90, (Y(I), I = 1,L)
      PRINT 95
      PRINT 90, (F(I), I = 1,L)
      PRINT 95
      L1 = L + 1
      PRINT 90, (F(I), I = L1,LI)
  270 CONTINUE
      RETURN
      END


      SUBROUTINE SRCDRP(X)
      COMMON /100/ V
      COMMON /150/ VL
      COMMON /200/ ALPHA, BETA
      COMMON /400/ GB
      COMMON /500/ GX, GX1
      COMMON /600/ NS, XS
      COMMON /750/ T
      COMMON /850/ GL, XNG
      COMMON /975/ S
      COMMON /ABT/ AT, BT, VT
      COMMON /CIC/ IC
      COMMON /CQC/ CQ
      COMMON /GRP/ NGROUP
      COMMON /HPH/ HP
      COMMON /ITI/ IT
      COMMON /IXI/ IX
```

```
      COMMON /JJJ/ JN
      COMMON /JQJ/ JQ
      COMMON /LGL/ LG
      COMMON /LLL/ L
      COMMON /MAX/ XMAX
      COMMON /MLM/ ML
      COMMON /NGN/ NG
      COMMON /PPP/ HPRINT
      COMMON /PST/ POST
      COMMON /ROP/ ROPE
      COMMON /SET/ SETUP
      COMMON /SJS/ SJ
      COMMON /SPN/ SPAN
      COMMON /SPR/ SWPR
      COMMON /STR/ GSTAR
      COMMON /YYY/ IM
      DIMENSION Y(50)
      DIMENSION GX(50), GX1(50)
      DIMENSION V(25,50)
      DIMENSION NG(50)
      DIMENSION ALPHA(50), BETA(50)
      DIMENSION VL(25,50)
      DIMENSION D(5,50)
      DIMENSION GB(50)
      DIMENSION CQ(50)
      DIMENSION XS(25)
      DIMENSION S(50)
      DIMENSION JQ(50)
      DIMENSION SZ(50,50)
      DIMENSION T(50)
      DIMENSION A(50), B(50)
      DIMENSION GL(50), XNG(50)
      DIMENSION SJ(50)
      DATA C /0.3/
      DATA SQ /0.0/
      REAL JN
      REAL JQ
      DOUBLE PRECISION HPRINT
      LOGICAL SWPR
      LOGICAL FLAG
      LOGICAL POST
      DATA ZET /1.0E-285/
      LOGICAL ROPE
      LOGICAL KEEL
      LOGICAL SETUP
      REAL NG
      FLAG = .FALSE.
      IF (POST) FLAG = .TRUE.
      IF (ROPE) FLAG = .TRUE.
      IQ = IFIX(X / SNGL(HPRINT)) + 1
      IF (IQ .GE. NS) IQ = NS - 1
      IR = IQ + 1
      X1 = (X - XS(IQ)) / SNGL(HPRINT)
      DO 10 I = 1,L
      F = V(IQ,I) + X1 * (V(IR,I) - V(IQ,I))
      IF (F .LE. ZET) F = ZET
      FA = ALPHA(I) * F
      FB = BETA(I) * F
      IF (FA .LT. ZET) FA = ZET
```

```
      IF (FB .LT. ZET) FB = ZET                                          22
      A(I) = ALOG(FA)
      B(I) = ALOG(FB)
      Y(I) = ALOG(F)
   10 CONTINUE
      DO 150 I = 1,ML
      G1 = GB(I) + (NG(I) - 1.0) / 2.0
      G2 = GB(I+1) - (NG(I+1) - 1.0) / 2.0
      G1 = ALOG(G1)
      G2 = ALOG(G2)
      BQ = B(I) + (G1 - GL(I)) / XNG(I) * (B(I+1) - B(I))
      AQ = A(I) + (G2 - GL(I)) / XNG(I) * (A(I+1) - A(I))
      AQ = EXP(AQ)
      BQ = EXP(BQ)
      JQ(I) = BQ - AQ
      IF ( ABS(JQ(I)) .LE. ZET) JQ(I) = 0.0
  150 CONTINUE
      JQ(L) = 0.0
      IL = IC
      S(1) = JN / BETA(1)
      S(1) = C * S(1)
      SJ(1) = S(1)
      IF (IT .NE. 0) S(1) = 0.5 * (S(1) + SZ(IL,1))
      IF (IT .NE. 0) S(1) = 0.5 * (S(1) + SZ(IL,1))
      IF (IT .NE. 0) S(1) = 0.5 * (S(1) + SZ(IL,1))
      IF (SETUP) SZ(IL,1) = S(1)
      DO 250 I = 2,ML
      IF (I .GE. LG) GO TO 50
      S(I) = JN / BETA(I)
      S(I) = C * S(I)
      SJ(I) = (JQ(I-1) - JQ(I)) / NG(I)
      IF (IT .NE. 0) S(I) = 0.5 * (S(I) + SZ(IL,I))
      IF (IT .NE. 0) S(I) = 0.5 * (S(I) + SZ(IL,I))
      IF (IT .NE. 0) S(I) = 0.5 * (S(I) + SZ(IL,I))
      IF (SETUP) SZ(IL,I) = S(I)
      GO TO 250
   50 CONTINUE
      S(I) = (JQ(I-1) - JQ(I)) / NG(I)
      SJ(I) = S(I)
      IF (IT .NE. 0) S(I) = 0.5 * (S(I) + SZ(IL,I))
      IF (IT .NE. 0) S(I) = 0.5 * (S(I) + SZ(IL,I))
      IF (IT .NE. 0) S(I) = 0.5 * (S(I) + SZ(IL,I))
      IF (SETUP) SZ(IL,I) = S(I)
  250 CONTINUE
      S(L) = (JQ(L-1) - JQ(L)) / NG(L)
      SJ(L) = S(L)
      IF (IT .NE. 0) S(L) = 0.5 * (S(L) + SZ(IL,L))
      IF (IT .NE. 0) S(L) = 0.5 * (S(L) + SZ(IL,L))
      IF (IT .NE. 0) S(L) = 0.5 * (S(L) + SZ(IL,L))
      IF (SETUP) SZ(IL,L) = S(L)
      IF ( .NOT. FLAG) GO TO 300
      PRINT 75, (S(I), I = 1,L)
   75 FORMAT(1H0 * THE GROUP SOURCES ARE * /(7E15.5))
      IF (ROPE) GO TO 300
      PRINT 175, (JQ(I), I = 1,L)
  175 FORMAT(1H0 * JQ(I) * / (7E15.5))
      PRINT 400, (A(I), I = 1,L)
  400 FORMAT(1H0 * THE A(I) ARE * / (7E15.5))
      PRINT 450, (B(I), I = 1,L)
```

```
450 FORMAT(1HO * THE B(I) ARE * / (7E15.5))                    21
300 CONTINUE
    DO 200 I = 1,L
    S(I) = CQ(I) * S(I)
200 CONTINUE
    RETURN
    END


    SUBROUTINE DIMEN(X)
    COMMON /200/ ALPHA, BETA
    COMMON /350/ YZ
    COMMON /400/ GB
    COMMON /500/ GX, GX1
    COMMON /600/ NS, XS
    COMMON /ABT/ AT, BT, VT
    COMMON /BBB/ BC
    COMMON /BRB/ B
    COMMON /FFF/ FLAG
    COMMON /FST/ FIRST
    COMMON /GRP/ NGROUP
    COMMON /IXI/ IX
    COMMON /ITI/ IT
    COMMON /JJJ/ JN
    COMMON /JQJ/ JQ
    COMMON /PPP/ HPRINT
    COMMON /PST/ POST
    COMMON /QQQ/ QX, NA, OMEGA
    COMMON /SPR/ SWPR
    COMMON /WZW/ W1, W2, W3, W4
    COMMON /ZZZ/ CZ1, CZ2, CZ3, CZ4, CZ5, CZ6
    DIMENSION ALPHA(50), BETA(50)
    DIMENSION GB(50)
    DIMENSION GX(50), GX1(50)
    DIMENSION JQ(50)
    DIMENSION XS(25)
    DIMENSION YZ(25,50)
    REAL JN
    REAL JQ
    LOGICAL SWPR
    LOGICAL FLAG
    LOGICAL POST
    LOGICAL FIRST
    DOUBLE PRECISION HPRINT
    DATA FIRST / .TRUE. /
    FLAG = .FALSE.
    IF (POST) FLAG = .TRUE.
    W1 = WX(X)
    CALL JZERO(X)
    DO 25 I = 1,NGROUP
    IF (FIRST) GO TO 500
    YT = YZ(IX,I) + (X - XS(IX)) * (YZ(IX+1,I) - YZ(IX,I))
   $  / SNGL(HPRINT)
    GO TO 550
500 CONTINUE
    YT = W1
    YT = ZERO(X,YT,I)
    YZ(IX,I) = YT
550 CONTINUE
```

```
      ALP = ALPHA1(X,YT,I)                                          22
      BTA = BETA1(X,YT,I)
      BETA(I) = QX * GX(I) * BTA
      ALPHA(I) = QX * GX(I) * ALP
   25 CONTINUE
      IF (POST) FLAG = .TRUE.
      IF (FLAG) GO TO 50
      RETURN
   50 CONTINUE
      PRINT 1
    1 FORMAT(1H0 * /-/-/-/-/-/-/-/-/-/-/-/ * )
      PRINT 5
    5 FORMAT(1H0 * THE DATA FROM DIMEN IS * )
      PRINT 1
      PRINT 10, X
   10 FORMAT(1H0 * X = * E15.5)
      PRINT 75, JN
   75 FORMAT(1H0, 15X, * JN = * E15.5)
      PRINT 15, (BETA(I), I = 1,NGROUP)
   15 FORMAT(1H0 * BETA(I) * / (7E15.5))
      IF (IT .NE. 0) GO TO 150
      PRINT 90, W1
   90 FORMAT(1H0 * THE GAS TEMPERATURE IS * E15.5)
      PRINT 100, (YZ(IX,I), I = 1,NGROUP)
  100 FORMAT(1H0 * THE DROP TEMPERATURES ARE * /(7E15.5))
      PRINT 20, (ALPHA(I), I = 1,NGROUP)
   20 FORMAT(1H0 * ALPHA(I) * / (7E15.5))
  150 CONTINUE
      RETURN
      END


      SUBROUTINE JZERO(X)
      COMMON /ABC/ BKTW, XL
      COMMON /JJJ/ JN
      COMMON /KKK/ AC, KTW
      COMMON /MAM/ MA
      COMMON /QQQ/ QX, NA, OMEGA
      COMMON /SIG/ SIGMA, DENS
      COMMON /STR/ GSTAR
      COMMON /WZW/ W1, W2, W3, W4
      REAL KTW
      REAL NA
      REAL JN
      REAL MA
      DATA H /6.63E-27/
      IF (X .GT. 0.0) GO TO 5
    1 CONTINUE
      JN = 0.0
      GSTAR = 1.0E+290
      RETURN
    5 CONTINUE
      I = 1
      YT = W1
      BTA = BETA1(X,YT,I)
      S = SUPSAT(X)
      IF (S .LE. 1.0) GO TO 1
      WL = H / SQRT(2.0 * 3.1416 * MA * KTW * W1)
      GSTAR = (2.0 / 3.0 * BKTW / W1 / ALOG(S))**3
```

```
      GZ = GEX(GSTAR)
      GZ = - 1.0 / 3.0 * BKTW / W1 * GZ
      USTAR = UX(X) * EXP(GZ)
      JN = 2.0 * BTA / OMEGA / NA * SQRT(SIGMA / KTW / W1) * USTAR
      RETURN
      END

      SUBROUTINE DERIV1(X, Y, F)
      COMMON /SSS/ SC, SC8, SCP
      COMMON /YYY/ IM
      DIMENSION Y(2), F(2)
      F(1) = Y(2)
      GO TO (1,5) IM
    1 CONTINUE
      F(2) = SC * (H(X) * Y(2) - Y(1) * QX(X) / UX(X))
      RETURN
    5 CONTINUE
      F(2) = SC * (H(X) * Y(2) - Y(1) * QX(X) / UX(X))
      RETURN
      END

      FUNCTION QX(X)
      COMMON /CIC/ IC
      COMMON /700/ XN, SS
      DIMENSION XN(500), SS(500)
      DATA MM /5/
      Z = X
      CALL LAGINT(IC, XN, SS, MM, K, Z, F)
      QX = F
      IF (K .EQ. 0) GO TO 10
      RETURN
   10 PRINT 20
   20 FORMAT(1H0, * THE TABLE IN LAGINT HAS BEEN EXCEEDED *)
      CALL ABORT
      RETURN
      END

      SUBROUTINE SOLN
      COMMON /800/ U
      COMMON /900/ U1, U2
      COMMON /AAA/ A
      COMMON /CRL/ CRAWL
      COMMON /DDD/ DUDX
      COMMON /DRG/ DRAG
      COMMON /HNG/ HANG
      COMMON /III/ IC
      COMMON /ITI/ IT
      COMMON /MAX/ XMAX
      COMMON /PPP/ HPRINT
      COMMON /RHT/ RET
      COMMON /SMS/ SUM
      COMMON /SLW/ SLOW
      COMMON /WHT/ WAIT
      DIMENSION U1(25), U2(25), U(25)
      DIMENSION US(25)
      DOUBLE PRECISION HPRINT
```

```
      LOGICAL SLOW
      LOGICAL DRAG
      LOGICAL CRAWL
      LOGICAL WAIT
      LOGICAL HANG
      LOGICAL RET
      DATA ZER /1.0E-06/
      DATA X0 /3.53782/
      PRINT 1
    1 FORMAT(1H0 * /-/-/-/-/-/-/-/-/-/-/-/-/ * )
      PRINT 2
    2 FORMAT(1H0 * THE DATA FROM SUBROUTINE SOLN IS * )
      PRINT 1
      IF (XMAX .LT. X0) GO TO 75
      S1 = 137.0 * U1(IC) - 300.0 * U1(IC-1) + 300.0 * U1(IC-2)
     $ - 200.0 * U1(IC-3) + 75.0 * U1(IC-4) - 12.0 * U1(IC-5)
      S1 = S1 / 60.0 / SNGL(HPRINT)
      S1 = S1 - A * U1(IC)
      S2 = 137.0 * U2(IC) - 300.0 * U2(IC-1) + 300.0 * U2(IC-2)
     $ -200.0 * U2(IC-3) + 75.0 * U2(IC-4) - 12.0 * U2(IC-5)
      S2 = S2 / 60.0 / SNGL(HPRINT)
      S2 = S2 - A * U2(IC)
      C2 = - S1 / S2
      GO TO 100
   75 CONTINUE
      C2 = - U1(IC) / U2(IC)
  100 CONTINUE
      RET = .FALSE.
      DO 10 I = 1,IC
      Q = U(I)
      US(I) = U(I)
      U(I) = U1(I) + C2 * U2(I)
      IF (U(I) .LT. ZER) U(I) = ZER
      IF (U(I) .LE. 0.0) RET = .TRUE.
   10 CONTINUE
      PRINT 50, RET
   50 FORMAT(1H0 * RET = * L5)
      X = 0.0
      SUM = 0.0
      DO 40 I = 1,IC
      PRINT 15, X, U(I)
   15 FORMAT(2E15.5)
      Q = US(I)
      SUM = SUM + ( (U(I) - Q) / Q ) ** 2
      X = X + SNGL(HPRINT)
   40 CONTINUE
      SUM = SQRT(SUM) / FLOAT(IC)
      RETURN
      END


      FUNCTION UX(X)
      COMMON /600/ NS, XS
      COMMON /800/ U
      DIMENSION XS(25), U(25)
      MM = 3
    1 CONTINUE
      Z = X
      CALL LAGINT(NS, XS, U, MM, K, Z, F)
```

```
      IF (K .EQ. 0) GO TO 10                                          25
      IF (F .LT. 0.0) GO TO 5
      UX = F
      RETURN
    5 CONTINUE
      IF (MM .EQ. 1) CALL ABORT
      MM = 1
      GO TO 1
   10 PRINT 20
   20 FORMAT(1H0 * THE TABLE IN LAGINT IS EXCEEDED * )
      CALL ABORT
      RETURN
      END


      SUBROUTINE SORC(IX)
      COMMON /400/ GB
      COMMON /450/ SQ
      COMMON /600/ NS, XS
      COMMON /700/ XN, SS
      COMMON /975/ S
      COMMON /CQC/ CQ
      COMMON /DDD/ DUDX
      COMMON /GRP/ NGROUP
      COMMON /HNG/ HANG
      COMMON /ITI/ IT
      COMMON /JQJ/ JQ
      COMMON /LGL/ LG
      COMMON /LLL/ L
      COMMON /NGN/ NG
      COMMON /PST/ POST
      COMMON /SJS/ SJ
      COMMON /TST/ XXX
      COMMON /WHT/ WAIT
      DIMENSION XN(500), SS(500)
      DIMENSION S(50)
      DIMENSION SV(50)
      DIMENSION CQ(50)
      DIMENSION NG(50)
      DIMENSION GB(50)
      DIMENSION SQ(500)
      DIMENSION JQ(50)
      DIMENSION SJ(50)
      DIMENSION XS(25)
      LOGICAL POST
      LOGICAL WAIT
      LOGICAL HANG
      REAL NG
      DATA LV /2/
      DATA ZEN /1.0E-25/
      IF ( (POST) .AND. (IX .NE. 1) ) GO TO 20
      SUM = 0.0
      DO 5 I = 1,L
      SV(I) = GB(I) * NG(I) * SJ(I)
      IF (I .LE. LV) SV(I) = 0.0
      SUM = SUM + SV(I)
    5 CONTINUE
      IF (ABS(SUM) .EQ. 0.0) SUM = 1.0E-290
      SM = - SUM
```

```
      IF (IT .EQ. 0) SS(IX) = SM                                        26
      IF (IT .EQ. 0) GO TO 10
      IF (IX .EQ. 1) XXX = 0.0
      ABC = SS(IX)
      SQ(IX) = ABC
      SS(IX) = SM
      IF (ABS(SM) .LT. ZEN) GO TO 10
      XXX = XXX + ( (SS(IX) - ABC) / SS(IX) ) ** 2
   10 CONTINUE
      IF (.NOT. POST) RETURN
   20 CONTINUE
      PRINT 1, SS(IX)
    1 FORMAT(1H0 * THE MONOMER EQUATION SOURCE TERM IS * E15.5)
      PRINT 15, (SV(I), I = 1,L)
   15 FORMAT(1H0 * THE CONTRIBUTIONS FROM THE GROUPS ARE * / (7E15.5))
      RETURN
      END

      FUNCTION BETA1(X,YT,I)
      COMMON /WZW/ W1, W2, W3, W4
      COMMON /BBB/ BC
      COMMON /DHF/ DEF, KEF
      COMMON /500/ GX, GX1
      DIMENSION GX(50), GX1(50)
      B = BC * UX(X) / SQRT(YT)
      AB = W1 + SQRT(GX(I)) * KEF * SQRT(0.5 * (W1 + YT)) * YT
      AB = AB / (1.0 + SQRT(GX(I)) * KEF * SQRT(0.5 * (W1 + YT)))
      BETA1 = B / (1.0 + SQRT(GX(I)) * DEF * SQRT(AB))
      RETURN
      END

      FUNCTION VXI(G)
      COMMON / ABC/ BKTW , XL
      GX = GEX(G)
      VXI = EXP( - BKTW * GX)
      RETURN
      END

      FUNCTION ALPHA1(X, YT, I)
      COMMON /500/ GX, GX1
      COMMON /ABC/ BKTW, XL
      COMMON /BRB/ B
      COMMON /DHF/ DEF, KEF
      COMMON /KKK/ AC, KTW
      COMMON /WZW/ W1, W2, W3, W4
      DIMENSION GX(50), GX1(50)
      REAL KTW
      IF (I .NE. 0) GJ = GX1(I)
      A1 = 1.0 / KTW / YT
      A2 = 0.66667 * B * GJ - XL
      AL = AC * SQRT(1.0 / YT)
      A = AL * EXP(A1 * A2)
      ALPHA1 = A / (1.0 + SQRT(GX(I)) * DEF * SQRT(0.5 * (W1 + YT)))
      RETURN
      END
```

27

```
      FUNCTION ZERO(X,YT,I)
      COMMON /500/ GX, GX1
      COMMON /ABC/ BKTW, XL
      COMMON /BBB/ BC
      COMMON /CZC/ CZ
      COMMON /FFF/ FLAG
      COMMON /ITI/ IT
      COMMON /PST/ POST
      COMMON /SPR/ SWPR
      COMMON /TTT/ BTA
      COMMON /WZW/ W1, W2, W3, W4
      COMMON /ZZZ/ CZ1, CZ2, CZ3, CZ4, CZ5, CZ6
      DIMENSION GX(50), GX1(50)
      DIMENSION E(2)
      DATA EPSLN /1.0E-05/
      DATA E(1) /1.0E-05/, E(2) /0.0/
      LOGICAL SWPR
      LOGICAL FLAG
      LOGICAL MAST
      LOGICAL POLE
      LOGICAL POST
      EXTERNAL PX
      IF (POST) MAST = .TRUE.
      MAST = .FALSE.
      IF (POST) POLE = .TRUE.
      POLE = .FALSE.
      IF (MAST) GO TO 50
      IF (FLAG) 50, 75
   50 CONTINUE
      IF (IT .NE. 0) GO TO 75
      PRINT 1
    1 FORMAT(1H0 * /-/-/-/-/-/-/-/-/-/-/-/-/-/-/ *)
      PRINT 2
    2 FORMAT(1H0 * THE DATA FROM ZERO IS * )
      PRINT 1
      FLAG = .FALSE.
   75 CONTINUE
      N = 0
      TEST = 0.0
      IF (I .NE. 0) XGX = GX1(I)
      W2 = CZ3 * (CZ4 * XGX - XL)
      IF (MAST) PRINT 10, N, YT, TEST, W1
   10 FORMAT(I10, 4E15.5)
    5 CONTINUE
      W4 = BETA1(X,YT,I)
      P = PX(YT,I)
      DP = DPX(YT,I)
      YT0 = YT
      YT = YT0 - P / DP
      TEST = (YT - YT0 ) / YT0
      TEST = ABS(TEST)
      N = N + 1
      IF (MAST) PRINT 10, N, YT, TEST, W1
      IF (N .GT. 20) GO TO 40
      IF ( TEST .LT. EPSLN ) GO TO 25
      GO TO 5
   40 CONTINUE
      CALL ZET(Z,YT0,YT,E,PX)
```

```
      IF (Z .EQ. 0.0) GO TO 15                                          29
      YT = Z
      GO TO 25
   15 PRINT 20
   20 FORMAT(1H0 * ZERO HAS FAILED TO CONVERGE * )
      CALL ABORT
   25 ZERO = YT
      IF (IT .NE. 0) RETURN
      IF (POST .AND. (.NOT. MAST)) POLE = .TRUE.
      IF (POLE) PRINT 10, N, YT, TEST, W1
      RETURN
      END


      FUNCTION PX(YT,I)
      COMMON /ALA/ ALPHA
      COMMON /CZC/ CZ
      COMMON /DHF/ DEF, KEF
      COMMON /SKT/ SMKTW
      COMMON /WZW/ W1, W2, W3, W4
      COMMON /ZZZ/ CZ1, CZ2, CZ3, CZ4, CZ5, CZ6
      COMMON /500/ GX, GX1
      REAL KEF
      DIMENSION GX(50), GX1(50)
      AZ = W2 / YT
      ALPHA = CZ2 / SQRT(YT)
      ALPHA = ALPHA * EXP(AZ)
      ALPHA = ALPHA / (1.0 + SQRT(GX(I)) * DEF * SQRT(0.5 * (W1 + YT)))
      AB = W1 + SQRT(GX(I)) * KEF * SQRT(0.5 * (W1 + YT)) * YT
      AB = AB / (1.0 + SQRT(GX(I)) * KEF * SQRT(0.5 * (W1 + YT)))
      BETGS = 1.0E+06 / SMKTW / SQRT(AB)
      BETGS = BETGS / (1.0 + SQRT(GX(I)) * KEF / SQRT(AB))
      W3 = CZ5 * BETGS
      P = YT**4
      P = P + W3 * (YT - W1)
      P = P - CZ + CZ6 * (ALPHA - W4)
      PX = P
      RETURN
      END


      FUNCTION DPX(YT,I)
      COMMON /ALA/ ALPHA
      COMMON /DHF/ DEF, KEF
      COMMON /WZW/ W1, W2, W3, W4
      COMMON /ZZZ/ CZ1, CZ2, CZ3, CZ4, CZ5, CZ6
      COMMON /500/ GX, GX1
      DIMENSION GX(50), GX1(50)
      AZ = W2 / YT
      DALPHA = - ALPHA / YT
      DALPHA = DALPHA * (0.5 + AZ)
      DP = 4.0 * YT**3
      DP = DP + W3
      DP = DP + CZ6 * DALPHA
      DPX = DP
      RETURN
      END
```

```
      FUNCTION ANOT(X)                                                  29
      COMMON /WZW/ W1, W2, W3, W4
      COMMON /QQQ/ QX, NA, OMEGA
      I = 0
      W1 = WX(X)
      YT = W1
      ALPHA = ALPHA1(X,YT,I)
      ANOT = QX * G1 * ALPHA
      RETURN
      END

      FUNCTION BNOT(X)
      COMMON /WZW/ W1, W2, W3, W4
      COMMON /QQQ/ QX, NA, OMEGA
      I = 0
      W1 = WX(X)
      YT = W1
      BETA = BETA1(X,YT,I)
      BNOT = QX * G1 * BETA
      RETURN
      END

      FUNCTION WX(X)
      COMMON /WWW/ TC, PR8
      WX = 1.0 - TC * ERF(PR8 * X)
      RETURN
      END

      FUNCTION SUPSAT(X)
      COMMON /ABC/ BKTW, XL
      COMMON /KKK/ AC, KTW
      COMMON /SUP/ PP
      REAL KTW
      W1 = WX(X)
      SUPSAT = UX(X) * EXP(XL / KTW * (1.0 / W1 - 1.0))
      RETURN
      END

      FUNCTION VXNOT(X)
      COMMON /ABC/ BKTW, XL
      VXNOT = VXINF(X,G0)
      RETURN
      END

      FUNCTION VXINF(X,G)
      COMMON /ABC/ BKTW, XL
      COMMON /KKK/ AC, KTW
      COMMON /MAM/ MA
      COMMON /QQQ/ QX, NA, OMEGA
      COMMON /STR/ GSTAR
      COMMON /WZW/ W1, W2, W3, W4
      REAL MA
      REAL NA
      REAL KTW
```

```
      DATA H /6.63E-27/                                                  30
      IF (X .NE. 0.0) GO TO 5
      GSTAR = 1.0E+290
      VXINF = VXEQ(X,G)
      RETURN
    5 CONTINUE
      WL = H / SQRT(2.0 * 3.1416 * MA * KTW * W1)
      S = SUPSAT(X)
      GSTAR = 2.0 / 3.0 * BKTW / W1 / ALOG(S)
      GSTAR = GSTAR**3
      CHI = 1.0 / 9.0 * BKTW / W1 / GSTAR ** 1.33333
   10 CONTINUE
      Z = SQRT(CHI) * (G - GSTAR)
      IF (Z .GT. 3.0) GO TO 25
      GO TO 15
   25 CONTINUE
      GX = GEX(G)
      V = G * ALOG(S) - CHI * (G - GSTAR) ** 2 - BKTW * GX / W1
      V = EXP(V)
      V = 0.5 * UX(X) * V / SQRT(3.1416 * CHI) / (G - GSTAR)
      GO TO 20
   15 CONTINUE
      V = VXEQ(X,G)
      ZA = ABS(Z)
      IF (Z .LT. 0.0) E = - ERF(ZA)
      IF (Z .GE. 0.0) E = ERF(ZA)
      V = 0.5 * V * (1.0 - E)
   20 CONTINUE
      VXINF = V
      RETURN
      END

      FUNCTION VXEQ(X, G)
      COMMON /ABC/ BKTW, XL
      COMMON /KKK/ AC, KTW
      COMMON /MAM/ MA
      COMMON /QQQ/ QX, NA, OMEGA
      COMMON /WZW/ W1, W2, W3, W4
      REAL MA
      REAL NA
      REAL KTW
      DATA H /6.63E-27/
      S = SUPSAT(X)
      WL = H / SQRT(2.0 * 3.1416 * MA * KTW * W1)
      V = G * ALOG(S)
      GX = GEX(G)
      V = V - BKTW * GX / W1
      VXEQ = UX(X) * EXP(V)
      RETURN
      END

      FUNCTION GEX(G)
      GEX = G**0.66667
      RETURN
      END
```

```
      FUNCTION H(X)
      DATA X0 / 3.53782 /
      DATA HINF / -0.88447 /
      DATA EPS /1.0E-06/
      IF (X .GT. X0) GO TO 10
      H = - EPS - 0.25 * X
      RETURN
   10 H = HINF
      RETURN
      END

      FUNCTION DHDX(X)
      DATA X0 /3.53782/
      IF (X .GT. X0) GO TO 5
      DHDX = - 0.25
      RETURN
    5 DHDX = 0.0
      RETURN
      END

      SUBROUTINE ZET(Z,A1,B1,ER,F)
      DIMENSION ER(1)                                                    ZER00002
      A=A1                                                               ZER00003
      B=B1                                                               ZER00004
      RE=ABS(ER(1))                                                      ZER00005
      AE=ABS(ER(2))                                                      ZER00006
      FA=F(A)                                                            ZER00007
      FB=F(B)                                                            ZER00008
      IF ((FA*FB .LT. 0.0) .AND. (AMAX1(RE,AE) .GT. 0.0)) GO TO 70       ZER00009
      H=0.0                                                              ZER00010
      GO TO 110                                                          ZER00011
   70 C=A                                                                ZER00012
      FC=FA                                                              ZER00013
      S=C                                                                ZER00014
      FS=FC                                                              ZER00015
C                                                                        ZER00016
   10 CONTINUE                                                           ZER00017
      H=0.5*(B+C)                                                        ZER00018
      T=ABS(H*RE)+AE                                                     ZER00019
      IF(ABS(H-B) .LE. T) GO TO 110                                      ZER00020
      IF (ABS(FB) .LE. ABS(FC)) GO TO 15                                 ZER00021
      Y=B                                                                ZER00022
      FY=FB                                                              ZER00023
      G=B                                                                ZER00024
      FG=FB                                                              ZER00025
      S=C                                                                ZER00026
      FS=FC                                                              ZER00027
      GO TO 20                                                           ZER00028
   15 Y=S                                                                ZER00029
      FY=FS                                                              ZER00030
      G=C                                                                ZER00031
      FG=FC                                                              ZER00032
      S=B                                                                ZER00033
      FS=FB                                                              ZER00034
   20 CONTINUE                                                           ZER00035
      IF (FY .NE. FS) GO TO 21                                           ZER00036
      B=H                                                                ZER00037
```

```
      GO TO 29                                                          ZER00038
   21 CONTINUE                                                          ZER00039
      E=(S*FY-Y*FS)/(FY-FS)                                             ZER00040
      IF (ABS(E-S) .LE. T) E=S+SIGN(T,G-S)                              ZER00041
      IF ((E-H)*(S-E) .LT. 0.0) GO TO 28                                ZER00042
      B=E                                                               ZER00043
      GO TO 29                                                          ZER00044
   28 B=H                                                               ZER00045
   29 FB=F(B)                                                           ZER00046
   30 CONTINUE                                                          ZER00047
      IF (FG*FB .LT. 0.0) GO TO 35                                      ZER00048
      C=S                                                               ZER00049
      FC=FS                                                             ZER00050
      GO TO 10                                                          ZER00051
   35 CONTINUE                                                          ZER00052
      C=G                                                               ZER00053
      FC=FG                                                             ZER00054
      GO TO 10                                                          ZER00055
  110 Z=H                                                               ZER00056
      RETURN                                                            ZER00057
      END

      FUNCTION ERF(X)
C
C  ERF=2/SQRT(PI)*INTEGRAL OF EXP(-T*T) FROM 0 TO X.
C  USING AN APPROXIMATION DUE TO HASTINGS  GOOD TO SEVEN SI
C  USING AN APPROXIMATION DUE TO HASTINGS. ABSOLUTE ERROR ABOUT 3E-7
C
      DIMENSION A(6)
      DATA A/.0000430638,.0002765672,.0001520143,.0092705272,.0422820123
     1,.0705230784 /
      T=A(1)*X
      DO 10 I=2,6
      T=(T+A(I))*X
   10 CONTINUE
      T=1./(T+1.)
      ERF=1.-T**16
      RETURN
      END

      SUBROUTINE LAGINT( N, A, F, M, K, X, Y )
      DIMENSION A(1), F(1)
C  DETERMINE INDEX OF TABLE VALUE NEAREST THE INTERPOLATE.
      CALL BAINS( A, N, X, I )
      IF( I.EQ.0 ) GO TO 10
      IF( X.EQ.A(I) ) GO TO 9
C  DETERMINE INDEX OF THE FIRST POINT TO BE USED IN THE INTERPOLATION.
      J = MIN0( MAX0( I - M/2, 1 ), N - M )
      IF( M.EQ.1.AND.I.LE.N-1.AND.X.LT.A(I) ) J = J - 1
      CALL LAGRNG( A(J), F(J), M, X, Y )
   10 K = I
      RETURN
    9 Y = F(I)
      GO TO 10
      END
$IBFTC LAGRNG
      SUBROUTINE LAGRNG( A, F, M, X, Y )
```

```
      DIMENSION A(11), F(11), DA(11), D(11,11)                          JJ
C**94
      DATA (D(I),I=1,121,12) / 11*1.0 /
C**94
   15 L = M + 1
C  FORM TABLES.
      FN = 1.
      DO 1 KK = 1, L
      DA(KK) = A(KK) - X
      IF( DA(KK).EQ.0.0 ) GO TO 7
      FN = FN*DA(KK)
    1 CONTINUE
      KK = 1
      LL = 2
    2 DO 3 JJ = LL, L
      D(KK,JJ) = DA(KK) - DA(JJ)
    3 D(JJ,KK) = -D(KK,JJ)
      KK = KK + 1
      LL = KK + 1
      IF( LL.LE.L ) GO TO 2
C  COMPUTE INTERPOLATED VALUE.
      Y = 0.
      DO 6 KK = 1, L
      FD = 1.
      DO 5 JJ = 1, L
    5 FD = FD*D(JJ,KK)
    6 Y = Y + ( FN*F(KK) )/( DA(KK)*FD )
      RETURN
    7 Y = F(KK)
      RETURN
      END
$IBFTC BAINS
      SUBROUTINE BAINS( SLIST, MM, Z, K )
      DIMENSION SLIST(1)
C     SLIST=TABLE, WHICH MUST BE MONOTONICALLY INCREASING
C     M= NUMBER OF ENTRIES IN SLIST
C     Z=VALUE TO BE FOUND IN TABLE
C     K=SUBSCRIPT OF VALUE IN TABLE NEAREST TO Z
C     PROGRAM RETURNS K = 0 IF Z IF OFF TABLE.
      M=MM
      L1=1
      L2=M
      K=1
      IF(Z-SLIST(1)) 1,15,3
    3 K=M
      IF(SLIST(M)-Z) 1,15,9
    9 K=M/2
      IF(Z-SLIST(K)) 20, 15, 29
   20 L2=K
      GO TO 23
   29 L1=K
   23 IF(L2-L1-1) 1,14,25
   25 M=L1+L2
      GO TO 9
   14 IF(2.*Z-SLIST(L1)-SLIST(L2)) 30,15,31
   30 K=L1
      GO TO 15
   31 K=L2
      GO TO 15
```

```
    1 K = 0                                                                  34
   15 RETURN
      END


      FORTRAN IV SUBROUTINE INTO(NO,X,DERI ,Y,F,T,HPRO)                      ZAM 0001
      COMMON /ACY/ ARCY
      COMMON /INTC/ IPMX,AREF,EMAX,SSSR,HFAC,SWAM,SWEX                       ZAM 0002
      COMMON /INTP/ HPR,XX,N,EUB,ELB,IP,IT,NRKS,SWIN                         ZAM 0003
      COMMON /YYY/ IM
      DIMENSION Y(1),F(1),T(8,1)                                             ZAM 0004
      LOGICAL SWAM,SWEX,SWIN                                                 ZAM 0005
      LOGICAL ARCY
      INTEGER HFAC                                                           ZAM 0006
      DOUBLE PRECISION T,HPRO,HPR,XX                                         ZAM 0007
      DATA IPMX,AREF,EMAX,SSSR,HFAC,SWAM,SWEX                                ZAM 0008
     $    /1024,1.0,1.0E-6,100.0,2,.TRUE.,.TRUE./                            ZAM 0009
C                                                                            ZAM 0010
      IPMX = 2 ** 45
      IF (ARCY) EMAX = 1.0E-05
      IF (.NOT. ARCY) EMAX = 1.0E-02
      HPR=HPRO                                                               ZAM 0011
      XX=DBLE(X)                                                             ZAM 0012
      N=NO                                                                   ZAM 0013
      EUB=EMAX                                                               ZAM 0014
      ELB=EMAX/SSSR                                                          ZAM 0015
      IP=1                                                                   ZAM 0016
      IT=0                                                                   ZAM 0017
      NRKS=0                                                                 ZAM 0018
      SWIN=SWEX                                                              ZAM 0019
      CALL DERI (X,Y,F)                                                      ZAM 0020
      DO 9 I=1,N                                                             ZAM 0021
      T(5,I)=DBLE(Y(I))                                                      ZAM 0022
    9 CONTINUE                                                               ZAM 0023
      RETURN                                                                 ZAM 0024
      END                                                                    ZAM 0025
       SUBROUTINE INT(X,DERI ,Y,F,T,SWPR                                     ZAM 0026
     X )                                                                     ZAM 0027
      COMMON /INTC/ IPMX,AREF,EMAX,SSSR,HFAC,SWAM,SWEX                       ZAM 0028
      COMMON /INTP/ HPR,XX,N,EUB,ELB,IP,IT,NRKS,SWIN                         ZAM 0029
C                                                                            ZAM 0030
       DIMENSION Y(1),F(1),T(8,1)                                            ZAM 0031
      LOGICAL SWAM,SWEX,SWIN                                                 ZAM 0032
      LOGICAL SWPR                                                           ZAM 0033
      INTEGER HFAC                                                           ZAM 0034
       DOUBLE PRECISION T,HPR,XX                                             ZAM 0035
       DOUBLE PRECISION D,H                                                  ZAM 0036
 6000  FORMAT (36H0 CANNOT DECREASE H BECAUSE OF HMIN.    ,1PE16.8,I20)     ZAM 0037
C                                                                            ZAM 0038
 1     CONTINUE                                                              ZAM 0039
       SWPR=.FALSE.                                                          ZAM 0040
       TEST=0.0                                                              ZAM 0041
       H=HPR/DBLE(FLOAT(IP*24))                                              ZAM 0042
       IF ((NRKS .LT. 3) .OR. (.NOT. SWAM)) GO TO 200                        ZAM 0043
C                                                                            ZAM 0044
C      ADAMS-MOULTON STEP.                                                   ZAM 0045
 100   CONTINUE                                                              ZAM 0046
       DO 109 I=1,N                                                          ZAM 0047
       D=DBLE(F(I))                                                          ZAM 0048
```

```
      T(4,I)=D                                                          ZAM 0049
      Y(I)=SNGL(T(5,I)+H*(                                              ZAM 0050
     X 55.0D0*D-59.0D0*T(3,I)+37.0D0*T(2,I)- 9.0D0*T(1,I) ))            ZAM 0051
  109 CONTINUE                                                          ZAM 0052
      X=SNGL(XX+24.0D0*H)                                               ZAM 0053
      CALL DERI (X,Y,F)                                                 ZAM 0054
      DO 119 I=1,N                                                      ZAM 0055
      D=DBLE(F(I))                                                      ZAM 0056
      D=(     T(5,I)+H*(                                                ZAM 0057
     X  9.0D0*D+19.0D0*T(4,I)- 5.0D0*T(3,I)+       T(2,I) ))           ZAM 0058
      T(6,I)=D                                                          ZAM 0059
      E=ABS(SNGL(D)-Y(I))/14.0                                          ZAM 0060
      TEST=AMAX1(E/AMAX1(AREF,ABS(SNGL(D))),TEST)                       ZAM 0061
  119 CONTINUE                                                          ZAM 0062
C                                                                       ZAM 0063
      GO TO 300                                                         ZAM 0064
C                                                                       ZAM 0065
C     ZONNEVELD STEP.                                                   ZAM 0066
  200 CONTINUE                                                          ZAM 0067
      DO 209 I=1,N                                                      ZAM 0068
      D=DBLE(F(I))                                                      ZAM 0069
      T(4,I)=D                                                          ZAM 0070
C     1                                                                 ZAM 0071
      Y(I)=SNGL(T(5,I)+H*(                                              ZAM 0072
     X 12.0D0*D                                          ))             ZAM 0073
  209 CONTINUE                                                          ZAM 0074
      X=SNGL(XX+12.0D0*H)                                               ZAM 0075
      CALL DERI (X,Y,F)                                                 ZAM 0076
      DO 219 I=1,N                                                      ZAM 0077
      D=DBLE(F(I))                                                      ZAM 0078
      T(6,I)=D                                                          ZAM 0079
C     2                                                                 ZAM 0080
      Y(I)=SNGL(T(5,I)+H*(                                              ZAM 0081
     X 12.0D0*D                                          ))             ZAM 0082
  219 CONTINUE                                                          ZAM 0083
      CALL DERI (X,Y,F)                                                 ZAM 0084
      DO 229 I=1,N                                                      ZAM 0085
      D=DBLE(F(I))                                                      ZAM 0086
      T(7,I)=D                                                          ZAM 0087
C     3                                                                 ZAM 0088
      Y(I)=SNGL(T(5,I)+H*(                                              ZAM 0089
     X 24.0D0*D                                          ))             ZAM 0090
  229 CONTINUE                                                          ZAM 0091
      X=SNGL(XX+24.0D0*H)                                               ZAM 0092
      CALL DERI (X,Y,F)                                                 ZAM 0093
      DO 239 I=1,N                                                      ZAM 0094
      D=DBLE(F(I))                                                      ZAM 0095
      T(8,I)=D                                                          ZAM 0096
C     4                                                                 ZAM 0097
      Y(I)=SNGL(T(5,I)+H*(                                              ZAM 0098
     X 3.75D0*T(4,I)+5.25D0*T(6,I)+9.75D0*T(7,I)-0.75D0*D ))            ZAM 0099
  239 CONTINUE                                                          ZAM 0100
      X=SNGL(XX+18.0D0*H)                                               ZAM 0101
      CALL DERI (X,Y,F)                                                 ZAM 0102
      DO 249 I=1,N                                                      ZAM 0103
      D=DBLE(F(I))                                                      ZAM 0104
      E=ABS(SNGL(H*(                                                    ZAM 0105
     X -16.0D0*T(4,I)+48.0D0*T(6,I)+48.0D0*T(7,I)+48.0D0*T(8,I)         ZAM 0106
     X -128.0D0*D   )))                                                 ZAM 0107
```

REFERENCES

1. Turkdogen, E. T., "Theory of Enhancement of Diffusion-Limited Vaporization Rates by Convection-Condensation Process. Part I - Theoretical," Trans. AIME, 230, 740 (1964).

2. Becker, R. and W. Doring, "Kinetische Behandlung der Keimbildung in ubersattigten Dampfen," Ann. Phys., Folge 5, Band 24, p. 719 (1935); or NASA Tech. Memo. 1374.

3. Frenkel, J., Kinetic Theory of Liquids, Clarendon Press, Oxford, 1946, Chapter 7.

4. Farley, F. M. J., "The Theory of the Condensation of a Supersaturated Ion-Free Vapor," Proc. Roy. Soc., A, 212, 530 (1952).

5. Barnard, A. J., "The Theory of Condensation of Supersaturated Vapors in the Absence of Ions," Proc. Roy. Soc. A, 220, 132 (1953).

6. Zeldovich, J. B., "On the Theory of New Phase Formation; Cavitation," Acta Physicochimica, U.R.S.S., 18, 1 (1943).

7. Katz, J. L. and B. J. Ostermier, "Diffusion Cloud-Chamber Investigation of Homogeneous Nucleation," J. Chem. Phys. 47, 2, 478 (1967).

8. Nucleation Phenomena, American Chemical Society Publication, Washington, D. C. (1966).

9. Turkdogan, E. T. and K. C. Mills, "The Theory of Enhancement of Diffusion-Limited Vaporization Rates by a Convection-Condensation Process. Part II - Experimental," Trans. AIME, 230 750 (1964).

10. Rosner, D. E., "Enhancement of Diffusion-Limited Vaporization Rates by Condensation Within the Thermal Boundary Layer," Int. J. Heat and Mass Transfer, 10, 1267 (1967).

11. Elenbaas, W., Philips Research Reports, 22 1 (1967).

12. Epstein, M. and D. E. Rosner, "Enhancement of Diffusion-Limited Vaporization Rates by Condensation Within the Thermal Boundary Layer." Unpublished manuscript.

13. Wegener, P. P. and A. A. Pouring, "Experiments on Condensation of Water Vapor by Homogeneous Nucleation in Nozzles," Phys. of Fluids, 7, [3], 352 (1964).

14. Wegener, P. P. and L. M. Mack, "Condensation in Supersonic and Hypersonic Wind Tunnels," Adv. Appl. Mech. 5, 307 (1958).

15. Schlichting, H., Boundary Layer Theory, 4th ed., McGraw Hill Book Company, New York, 1960, p. 85.

16. Dorfman, L. A., "Hydrodynamic Resistance and the Heat Loss of Rotating Solids," Oliver and Boyd, Edinburg and London, (1963); translated from Russian.

17. Bird, R., W. E. Stewart, and E. N. Lightfoot, Transport Phenomena, John Wiley and Sons, Inc., New York, 1960.

18. Friedlander, S. K., "Particle Diffusion in Low-Speed Flows," J. Colloid Interfac. Sci. 23, 157 (1967).

19. Wakeshima, H., J. Phys. Soc. Japan, 9, 400 (1954).

20. Mason, B. J., Proc. Phys. Soc. London, B64, 773 (1951).

21. Feder, J., J. C. Russell, J. Lothe, and G. M. Pound, "Homogeneous Nucleation and Growth of Droplets in Vapors," Adv. Physics, 15, 111 (1966).

22. Lothe, J. and G. M. Pound, Reconsideration of Nucleation Theory," J. Chem. Phys. 36, [8], 2080 (1962).

23. Reiss, H. and J. L. Katz, "Resolution of the Translation-Rotation Paradox in the Theory of Irreversible Condensation," J. Chem. Phys. 46, [7] 2496 (1967).

24. Lothe, J. and G. M. Pound, "Concentration of Clusters in Nucleation and the Classical Phase Integral," J. Chem. Phys. 48, 1849 (1968).

25. Courtney, W. G., "Non-Steady-State Nucleation," J. Chem. Phys. 36, 2009 (1962).

26. Kantrowitz, A., "Nucleation in Very Rapid Vapor Expansions, " J. Chem. Phys. 19, 1097 (1951).

27. Von Karman, Th., "Uber laminare und turbulent Reibung," Zeit. ange. Mathe. und Mech. 1, 244 (1921); or NACA Tech. Memo. 1092.

28. Cochran, W. G., "The Flow Due to a Rotating Disk," Proc. Cambridge Phil. Soc. 30, 365 (1934).

29. Millsaps, K. and K. Pohlhausen, "Heat Transfer from a Rotating Disk to Fluids of Any Prandtl Number," J. Heat Transfer, 810, 249 (1959).

30. Sparrow, E. M. and J. L. Gregg, "Heat Transfer from a Rotating Disk to Fluids of Any Prandtl Number," J. Heat Transfer, 810, 249 (1959).

31. Kays, W. M., Convective Heat and Mass Transfer, McGraw Hill Book Company, New York, 1966, p . 264.

32. Olander, D. R., "Surface Chemical Kinetics and Gas Phase Diffusion in the Germanium-Iodine Reaction," Ind. and Eng. Chem. Fund. 6, 178 (1967).

33. Hills, A. W. D. and J. Szekely, Chem. Eng. Sci. 19, 79 (1964).

34. Levich, V. G., Physiochemical Hydrodynamics, Prentice-Hall Inc. New Jersey, 1966, (Transaction from Russian).

35. Schofill, J. UCRL-19029, Ph.D. Thesis, to be published.

36. Sparrow, E. M. and L. U. Albers, "Apparent Emissivity and Heat Transfer in Long Cylindrical Hole," J. Heat Transfer, 82C, 253 (1960).

37. Hills, A. D. W. and J. Szekely, "A Note on the Enhancement of Diffusion Limited Vaporization Rates by Condensation within the Thermal Boundary Layer," Int. J. Heat and Mass Transfer, 12

111 (1969).

38. Nucleation Phenomena, American Chemical Society Publication, Washington, D.C. (1966).

39. Hilsenrath, J. et al., "Table of Thermal Properties of Gases," NBS Circular 564 (1955).

40. Grosse, A. V., "The Relationship Between Surface Tension and Energy of Liquid Metals and Their Heat of Vaporization at the Melting Point", Jour. of Inorg. Nucl. Chem., 26, 1349 (1964).

41. Gross, A. V., "High Temperature Research", Science, 140, 791 (1963).

42. Nesmeyamov, A. N., Vapor Pressure of the Chemical Elements, Elsevier Publishing Company, New York (1963).

43. Goldsmith, A, T. E. Waterman, and H. J. Hirschhorn, Handbook of Thermophysical Properties of Solid Materials, Vol. 1, Elements, Pergamon Press, New York (1961).

44. Hirschfadder, J. O., C. F. Curtiss, and R. B. Bird, Molecular Theory of Gases and Liquids, John Wiley and Sons, New York (1954).

45. Ames, W. F., Nonlinear Ordinary Differential Equations in Transport Processes, Mathematics in Science and Engineering Series, Vol. 42, Academic Press, New York (1968).

46. Kastkowski, H. J. and R. D. Lee, "Theory and Methods of Optical Pyrometry", National Bureau of Standards Monograph 41, U.S. Government Printing Office, (1962).

47. Rosner, D. E. and M. Epstein, "Condensation-Enhanced Vaporization Rates in Nonisothermal Systems", Trans of the AIME, 242, p. 2355 (1968).

48. Hultgren, R., R. L. Orr, P. D. Anderson, and K. K. Kelley, Selected Values of Thermodynamic Properties of Metals and Alloys; John Wiley (1963).

49. Elenbaas, W., "Rate of Evaporation and Heat Dissipation of a Heated Filament in a Gaseous Atmosphere," 22 5 (1967).

TECHNICAL INFORMATION DIVISION
LAWRENCE RADIATION LABORATORY
UNIVERSITY OF CALIFORNIA
BERKELEY, CALIFORNIA 94720